

UC Santa Barbara

UC Santa Barbara Electronic Theses and Dissertations

Title

Late Holocene Environmental History of UC Santa Barbara, Campus Lagoon

Permalink

<https://escholarship.org/uc/item/2wg033xs>

Author

Owings, Ryan

Publication Date

2023

Peer reviewed|Thesis/dissertation

UNIVERSITY OF CALIFORNIA

Santa Barbara

Late Holocene Environmental History of UC Santa Barbara, Campus Lagoon

A Thesis submitted in partial satisfaction of the
requirements for the degree Master of Science
in Earth Science

by

Ryan W. Owings

Committee in Charge:

Professor Alexander Simms, Chair

Professor Gen Li

Professor Lorraine Lisiecki

December 2023

The thesis of Ryan W. Owings is approved.

Lorraine Lisiecki

Gen Li

Alexander Simms, Committee Chair

October 2023

Late Holocene Environmental History of UC Santa Barbara, Campus Lagoon

Copyright © 2023

by

Ryan W. Owings

ACKNOWLEDGEMENTS

This study would not have been possible without assistance from many individuals across the University of California, friends, and family members. Thank you to my principal advisor, Alexander Simms, for introducing me to sedimentology and guiding me throughout this Master's project during the second year of my graduate education at UC Santa Barbara. I would also like to thank the members of my committee, Gen Li and Lorraine Lisiecki, for their assistance in geochemical interpretation and feedback. Technical help from Devin Rand regarding the creation of radiocarbon age-depth models is greatly appreciated. Assistance from Matt Rioux, Gareth Seward, Miguel Zepeda-Rosales, and Christie Yorke at UC Santa Barbara regarding EPMA / SEM, XRD, and CN stable isotope analysis is greatly appreciated. Many thanks to John Southon at UC Irvine for assistance regarding radiocarbon age dating. Calcite $\delta^{18}\text{O}$ and $\delta^{13}\text{C}$ isotope analysis by Wenbo Yang at UC Berkeley is greatly appreciated. Thank you to my lab mates, Elisa Medri and Emily Huffman, and Jose Valera for their assistance in the field. I would also like to thank Lisa Stratton for granting field access to UCSB Campus Lagoon and providing background knowledge regarding anthropogenic history of the lagoon. Lastly, I would like to thank Ed Keller for introducing me to Santa Barbara geology and assisting me throughout my first year at UC Santa Barbara. Additional funding support was provided by the Southern / Statewide California Earthquake Center (SCEC). SCEC is funded by both the National Science Foundation (NSF) and United States Geological Survey (USGS).

ABSTRACT

Late Holocene Environmental History of UC Santa Barbara, Campus Lagoon

by

Ryan W. Owings

Heightened storm activity, drought, and large earthquakes have the potential to impact daily life in Southern California and transform its coastal landscape. To better understand the nature and frequency of these events, the stratigraphy and seismic architecture of University of California, Santa Barbara (UCSB), Campus Lagoon (referred to as Campus Lagoon hereafter), a flooded river valley incised into a marine isotope stage (MIS) 3 marine terrace near Santa Barbara, California, was examined. The valley fill provides a record of late Holocene environmental change for the Santa Barbara region as well as a potential archive of coseismic uplift within the western Santa Barbara Fold Belt (SBFB). Nine sediment cores and 2.70 km of high-resolution seismic data from Campus Lagoon were examined. From the collected sediment cores, six sedimentary facies were identified. These facies span three broad depositional environments including intertidal, estuarine, and lower supratidal environments. The oldest deposits sampled in this study were coarse-grained gray sand facies (GS). Radiocarbon ages of the GS facies suggest deposition started at least ~5 ka and lasted until at least ~4 ka. The clayey silt with shell fragments facies (CS-SF) is found interbedded with the GS facies from ~4.5 ka and ~3.7 ka. Clayey silts with and without evaporites, respectively referred to as CS-E and CS facies, occur throughout the lagoon and typically reside atop the GS facies. Gypsum lamina occurs throughout Campus Lagoon between ~3.2 ka and ~0.6 ka. The CS-E and CS facies are atop the GS facies and are occasionally interbedded with packages of sandy silt facies (SASL), which lack coarse pebbles, rip-up

clasts, and shell fragments. The GS facies is typically also found in the stratigraphic top of sediment cores in the southeast region of the lagoon. Deposition of the upper beds of the GS facies occurs starting ~0.8 ka and ~0.7 ka in the southeast region of Campus Lagoon. The upper GS facies laterally grades into the SASL facies in the central region of the lagoon. The SASL facies was concurrently deposited with the GS facies starting ~0.6 ka and is interpreted to represent the distal sands associated with the GS facies. A laminated sandy silt facies (LSS) farther inland was concurrently deposited with the GS and SASL facies ~0.6 ka. The LSS facies is interpreted to be terrestrial input from sheetwash in the northwest region of Campus Lagoon based on its geographic location, lack of marine signatures, finer sediment grain size, and higher charcoal and wood fragment abundance.

Deposition of the GS facies between at least ~5 ka and until at least ~4 ka is interpreted to represent the onset of heightened El Niño Southern Oscillation (ENSO), which contributed to the migration of sands within the Santa Barbara littoral cell from the west to the east. The CS-E and CS facies represent evaporative mudflat environments, which are interpreted as responses to periods of late Holocene aridity, specifically the Late Holocene Dry Period (LHDP) and Medieval Climate Anomaly (MCA). The return of the GS facies, as well as deposition of the SASL and LSS facies, between ~0.7 ka and ~0.6 ka coincides with the onset of stormy conditions associated with the Little Ice Age (LIA).

In addition to providing information related to paleoclimate, coastal depositional environments have the potential to preserve tectonic events and document changes in relative sea level (RSL). Two separate downward shifts in overlapping seismic reflections observed within the southeast region of Campus Lagoon suggest at least two potentially rapid falls in RSL between ~3.7 ka and ~0.6 ka. Seismic unit (SU) 1 consists of the GS facies and is

overlain by the CS-E / CS facies. SU 2 onlaps SU 1 at a lower elevation, suggesting a possible transition from an intertidal zone to a lower supratidal mudflat environment. A second possibly abrupt RSL fall is observed between SU 3 and SU 4 in which SU 4 onlaps SU 3 at a lower elevation. Possible RSL falls may have been triggered by large magnitude earthquakes that uplifted the lagoon. As RSL fell due to potential coseismic uplift of the land surface, marine water circulation between the ocean and lagoon may have been hindered and possibly exposed the middle and back regions of Campus Lagoon to drought-like conditions associated with the LHDP and MCA during the late Holocene.

TABLE OF CONTENTS

1. INTRODUCTION	1
2. BACKGROUND	3
2.1 Geologic Setting of Campus Lagoon	3
2.2 Southern California Hydroclimate	6
2.3 Sea-Level Since the Last Glacial Maximum	8
3. METHODS	9
4. RESULTS	12
4.1 Campus Lagoon Seismic Survey	12
4.2 Sediment Core Facies Description	13
4.3 Chronology of Sediment Cores from Campus Lagoon	15
4.4 Mineralogical, Elemental, and Isotopic Data	17
5. DISCUSSION	18
5.1 Campus Lagoon Sediment Core Facies Interpretation	18
5.1a GS Interpretation	18
5.1b CS-E and CS Facies Interpretation	18
5.1c CS-SF Facies Interpretation	19
5.1d SASL Facies Interpretation	19
5.1e LSS Facies Interpretation	20

5.2 Seismic Stratigraphic Analysis	21
5.3 Campus Lagoon Sediment Core Facies Historical Interpretation	22
<i>5.3a Mid-to-Late Holocene ENSO Intensification</i>	22
<i>5.3b Late Holocene Aridity and Possible Coseismic Uplift</i>	25
<i>5.3c Return to Late Holocene Stormy Conditions</i>	32
6. CONCLUSION	33
7. WORKS CITED	36
8. FIGURES.....	45
9. APPENDIX	71

1. INTRODUCTION

Climate variability and large earthquakes have the potential to upend daily life in Southern California and transform the coastline. In the aftermath of the 2017 Thomas Fire in the nearby Santa Ynez Mountains, fire-linked debris flows following intense rainstorms inundated the community of Montecito, California on January 9th, 2018, which claimed the lives of 23 individuals, damaged hundreds of homes, and disrupted regional transportation along Highway 101 (Goto et al., 2021). In addition, Santa Barbara, California has experienced damaging earthquakes within the past century that highlight their safety hazard to the +132,000 people who reside within the Carpinteria, Goleta, and Santa Barbara regions (population estimate provided by Santa Barbara South Coast Chamber of Commerce, 2023). For example, a M_w 6.8 earthquake in 1925 destroyed downtown Santa Barbara, killed 13 individuals, and caused \$8 million in damage (SCEDC, 2013). Adjusting for inflation and expansion of coastal communities within the past century, an earthquake of similar magnitude in Santa Barbara today could cause ~\$142 million in damages and would likely cause more loss of life than the 1925 earthquake due to an increase in population density (financial estimate provided by U.S. Bureau of Labor Statistics, 2023). Societal disruptions, damage, and casualties from both climate and tectonic related phenomena prompts the need to further investigate both the climate variability and active tectonics of the Santa Barbara area.

Sedimentary archives can provide information on the occurrence, frequency, and impacts of past climate change and earthquakes. Although the Santa Barbara Basin (SBB) provides some of the most detailed records of past climate in Southern California, few studies have examined environmental changes within the coastal zone. Thus, little is known

regarding how climate variability and past earthquakes have impacted the coast. Campus Lagoon is located on the University of California, Santa Barbara (UCSB) campus (N 34.408479° W119.846909°) and resides on a marine terrace located on the upthrown side of the Western More Ranch fault to the north (Figure 1) and the upthrown side of the north-dipping reverse Pitas Point-North Channel fault system (Dibblee, 1966; Morel et al., 2021). The lagoon's geographic location on the upthrown sides of these faults along with the presence of uplifted marine terraces in the Santa Barbara area makes the lagoon an ideal candidate for investigating potential coseismic uplift of the land surface in the western SBFB region. In addition, Ejarque et al. (2015) notes the presence of evaporite deposits between ~2.4 ka and ~0.9 ka within Dune Pond, a swale pond adjacent to the UCSB campus. King et al. (2019) also document mud facies with gypsum lamina within Batiquitos Lagoon and Buena Vista Lagoon near San Diego, California. Correlating the timing of possible evaporite deposits in Campus Lagoon with Dune Pond, Batiquitos Lagoon, and Buena Vista Lagoon may strengthen evidence of late Holocene drought that impacted the Santa Barbara coastal plain and possibly the Southern California coast.

The objectives of this research study are to: 1) understand how late Holocene climate variability in the Santa Barbara region influenced its coastline and 2) assess the possibility of coseismic uplift in the western SBFB. I hypothesize Campus Lagoon may contain evidence of late Holocene environmental change, such as drought and storm deposits, that impacted the Santa Barbara coastline. In addition, I hypothesize that Campus Lagoon contains evidence of RSL fall, which may be linked to coseismic uplift during past, large earthquakes.

2. BACKGROUND

2.1 Geologic Setting of Campus Lagoon

Campus Lagoon is a flooded river valley incised into the UCSB / Isla Vista marine terrace and consists of paleo-channels that extend to the southeast and south (Figure 2) (Keller & Keller, 2011; Gurrola et al., 2014). The first emergent marine terrace that hosts the UCSB campus stretches between Devereux Slough and Goleta Slough (Gurrola et al., 2014). Incision into the marine terrace likely occurred during the last glacial maximum (LGM) as global sea level fell between 130-134 m lower than the present (Lambeck et al., 2014). Marine terraces along the coast of Santa Barbara typically consist of paleo wave-cut platforms covered with marine sediments (Gurrola et al., 2014; Rockwell et al., 2016). Sea cliffs are present at the coastal edge of the paleo wave-cut platform and reside above the modern wave-cut platform. The late Pleistocene marine terraces within the SBFB are interpreted to be uplifted and preserved on flanks of anticlines (Gurrola et al., 2014). As part of the Santa Barbara Fold Belt (SBFB), the Santa Ynez Mountains to the north of Campus Lagoon are subjected to crustal compression due to compression within the restraining bend of the right-lateral San Andreas fault. The SBFB and Santa Ynez Mountains are the westernmost components of the larger Transverse Ranges, which is an east-west striking fold and thrust belt (Jackson & Yeats, 1982; Rockwell et al., 2016).

The SBFB experiences an array of tectonic behaviors, such as subsidence and uplift. Within Carpinteria Slough, California, blue-gray sands with intertidal and subtidal bivalves sharply overlie muds with geochemical signatures suggestive of terrestrial influence (Reynolds et al., 2022). Sea-level indicators, lateral continuity of a sharp contact across sediment cores, and the deposition of coarse-grained sands atop fine-grained muds suggest an

abrupt RSL rise of 1.3 ± 1.1 m occurring ~ 1 ka because of possible coseismic subsidence (Reynolds et al., 2022). In addition, emergent marine terraces along the coast of Santa Barbara are geomorphic indicators of paleo-sea level and tectonic uplift (Keller et al., 2000). Gurrola et al. (2014) determined rates of coastal uplift with the aid of radiometric dating techniques including radiocarbon, uranium-series, and optically stimulated luminescence dating. The first emergent marine terrace within the western SBFB has an age of 45 ka, which suggests an uplift rate of ~ 2 m/ky (Gurrola et al., 2014). Uplift determined by Gurrola et al. (2014), however, assumes long term average rates and does not include potential coseismic uplift. A small wave-cut platform at the southernmost edge of the UCSB campus, referred to as Campus Point, suggests potential coseismic uplift along this section of the Santa Barbara coastline (Figure 3). The platform resides ~ 2 m above the present sea-level and may have been uplifted due to a large magnitude earthquake, but efforts to constrain the age of the uplifted wave-cut platform have been thwarted by the lack of datable material (Gurrola et al., 2014). This consequently leads to the following question: does uplift associated with the Santa Barbara region occur gradually or instantaneously during discrete earthquake events?

Coseismic uplift occurs during large magnitude earthquakes along tectonically active margins throughout the world (e.g. Stiros et al., 1992; Carver et al., 1994). A M_w 7.1 earthquake struck Cape Mendocino in Northern California in 1992, uplifted ~ 24 km of the coastline, and fostered a maximum uplift of 1.4 ± 0.2 m during the earthquake (Carver et al., 1994). Carver et al. (1994) notes that raised late Holocene marine terraces were the result of paleo-earthquakes with similar magnitude to the 1992 Cape Mendocino earthquake. Using the study of Wells and Coppersmith (1994) as a reference to uplift in response to earthquake

magnitude, Gurrola et al. (2014) notes the small wave-cut platform at Campus Point may have been uplifted by an earthquake of magnitude 7.0. Evidence of coseismic uplift to the east of the SBFB, specifically near Ventura, California, is supported by a study of uplifted Holocene marine terraces from Rockwell et al. (2016), but how far west along the SBFB this type of behavior persists is unknown. The deposits within Campus Lagoon may provide insight related to possible coseismic uplift in the western SBFB.

In addition to Gurrola et al. (2014), studies related to coastal uplift have been conducted by Rockwell et al. (1992) and Morel et al. (2021) in the western SBFB. Both authors interpret coastal uplift along this section of coastline to be driven by the blind, north-dipping reverse Pitas Point-North Channel fault system and / or the south-dipping left-reverse Santa Ynez fault (Morel et al., 2021). Rockwell et al. (1992) suggests the first emergent marine terrace between Point Conception and Gaviota, California correlates to MIS 5a while the other higher terraces correspond to MIS 5c, 5e, 7, and 9. Alternatively, Morel et al. (2021) suggest that the western SBFB, specifically from Point Conception to Isla Vista, California, have uplift rates between 0.8 ± 0.3 and 1.8 ± 0.4 m/ky, and the first emergent marine terrace correlates to MIS 3, which complements the interpretations of Gurrola et al. (2014). Rates of uplift determined by Morel et al. (2021) are more than 5 times greater than previously determined by Rockwell et al. (1992), consequently heightening the seismic hazard within the western SBFB.

Research conducted by Rockwell et al. (2016) found that four Holocene marine terraces between Ventura and Carpinteria, California are the result of coseismic uplift related to large magnitude earthquakes that occurred at 6.7 ka, 4.4 ka, 2.09 ka, and 0.95 ka. The discrete earthquake events uplifted the land surface between 7-12 m during individual

earthquakes and are interpreted to result from slip along the Pitas Point fault system (Rockwell et al., 2016). Compiled data from Morel et al. (2021), Gurrola et al. (2014), and Rockwell et al. (2016) demonstrate that coastal uplift generally decreases from east to west in the Ventura and SBFB regions. These studies show the active rock uplift exhibited on the coastal plain of the SBFB as well as the potential for coseismic uplift associated with large magnitude earthquakes in the Santa Barbara region.

2.2 Southern California Hydroclimate

During the mid-to-late Holocene, Southern California climate oscillated between periods of wet and dry conditions (Figure 4). Current understanding of Southern California hydroclimate variability is largely based on lake records and offshore marine sediment cores. Sediment cores from Lake Elsinore, California (Kirby et al., 2004, 2007, 2010) provide high-resolution records of terrestrial climate throughout the Holocene for inland regions of Southern California. For instance, Kirby et al. (2010) used sand beds within sediment cores as a proxy record for hydrologic variability. Sand beds suggest an increase in runoff associated with heightened storm activity that increases the grain size carried by a stream. Conversely, a decrease in runoff during periods of lower storm frequency decreases the grain size carried by a stream. During the mid-to-late Holocene, seven periods of wet climate were observed in sediment cores from Lake Elsinore from 6.9 ka to 6.3 ka, 4.5 ka to 4.1 ka, 3.7 ka to 3.5 ka, 3.3 ka to 3.2 ka, 1.5 ka to 1.3 ka, 1.2 ka to 1.0 ka, and 0.6 ka to 0.1 ka (Kirby et al., 2010). Using alternating organic rich and carbonate rich sediments within a sediment core from Lower Bear Lake in the mountains of San Bernardino, California, Kirby et al. (2012) provides a hydroclimate reconstruction of large pluvial events (PE), which occur from 9.1 ka to 8.2 ka (PE-V), 7 ka to 6.4 ka (PE-IV), 3.3 ka to 3 ka (PE-III), 0.8 ka to 0.7 ka (PE-II), and

0.5 ka to 0.4 ka (PE-I). Kirby et al. (2015) utilized variations in grain size within an 8.4 m sediment core from Silver Lake, California as a proxy for hydroclimate variations within the Mojave Desert region of Southern California and suggests arid conditions between 7.4 ka and 4.2 ka and a return to wetter conditions thereafter. Between 0.7 ka and 0.2 ka, the Little Ice Age (LIA) led to the expansion of glaciers globally and stormy conditions in California, which led to lake level rise at Mono Lake near Owens valley and Cronise Lakes in the Mojave Desert (Barbour et al., 2007).

Studies by Kirby et al. (2014) at Zaca Lake near Santa Barbara, California and studies by Friddell et al. (2003) and Du et al. (2018) in the Santa Barbara Basin (SBB) provides further insight into Southern California hydroclimate. Sand layers within sediment cores collected from Zaca Lake occur between 0.5 ka and 0.45 ka and are interpreted to represent periods of higher discharge capable of carrying coarse-grained sediments into the lake (Kirby et al., 2014). In addition to periods of storm activity, sediment cores from Zaca Lake reveal two notable dry intervals within the past 3 ka. Low sand accumulation noted by Kirby et al. (2014) suggests the driest period within the Zaca Lake record occurred between 2.5 ka and 2 ka, which also corresponds to the timing of drought-like conditions in the Great Basin between 2.8 ka and 1.8 ka documented by Mensing et al. (2013). Hydrogen isotope data from plant leaf wax (δD_{wax}) demonstrates a second period of late Holocene aridity between 1.5 ka and 0.9 ka (Kirby et al., 2014). Gray flood layers within sediment cores collected by Du et al. (2018) occur during periods of wetter climate documented within lake records from Southern California. Approximately 75 gray layers were deposited within the SBB over the last 9 ka and are interpreted to be from increased runoff in Southern California that delivered sediment to the SBB (Du et al., 2018). Du et al. (2018) suggests that frequency and magnitude of the

floods coincided with lake records in Southern California with high precipitation events occurring between 9 ka and 8.5 ka, 7.3 ka and 6.6 ka, 5.5 ka and 3 ka, and 0.8 ka and 0.4 ka. In addition, Du et al. (2018) observed an absence of gray layers between ~1 ka and 0.65 ka, which coincides with drier conditions recorded in tree-ring records in the western United States by Cook et al. (2004). Moreover, Friddell et al. (2003) utilized decadal resolved planktonic foraminiferal $\delta^{18}\text{O}$ records from the SBB to show climate variability during the mid-Holocene and proposes ENSO intensification between 5.2 ka and 3.6 ka followed by a decline in ENSO conditions thereafter.

2.3 Sea-Level Since the Last Glacial Maximum

The melting of ice sheets following the last glacial maximum (LGM) around 21 ka caused barostatic sea-level to rise between 130-134 m (Austermann et al., 2013; Lambeck et al., 2014). Reynolds and Simms (2015) provide a late Quaternary RSL reconstruction for Southern California corrected for tectonic uplift and suggest rapid sea-level rise from 15 ka and decelerates to the present mean sea level between 8 ka and 6 ka. The average rate of sea-level rise for the Southern California region starting ~4 ka and through the late Holocene is 0.8 ± 0.3 mm/year (Reynolds & Simms, 2015). This RSL rise was largely due to the collapse of a peripheral forebulge following the LGM (Reynolds & Simms, 2015).

Along active margins, vertical movements, such as coseismic uplift and subsidence, are an important cause of RSL variability (Nelson, 1992). During the 1960 Chilean and 1964 Alaskan earthquakes, hundreds of square kilometers of land subsided anywhere between 0.5 m and 2.5 m (Nelson, 1992). Nelson et al. (1996, 1998) and Shennan et al. (2016) proposed criteria that document paleoseismic events based on subduction zone-related earthquakes. These criteria include sharp contacts between sedimentary facies, evidence of RSL change,

and evidence of synchronous change across multiple sediment cores, which were ultimately applied to other tectonic settings, such as fault-bounded estuaries along the coast near Carpinteria, California (Reynolds et al., 2022). Within regions protected from tidal action, abrupt boundaries are likely caused by sudden and erosive events (Nelson, 1992).

Onlapping patterns as seen in seismic surveys also provide valuable information regarding RSL variability. A rise in RSL is indicated by landward onlap of littoral deposits, while a fall in RSL is indicated by the seaward progradation of coastal deposits (Vail et al., 1977). In contrast, a rapid fall in RSL is indicated by a downward shift in coastal onlap from the highest position in one sequence to the lowest position of an overlying sequence (Vail et al., 1977). With regards to the Santa Barbara area, sudden coastal uplift may foster a rapid fall in RSL, which would consequently lead to a downward shift in onlap within seismic profiles. Deposition of clays and silts atop coarse-grained sands within regions that experience RSL fall may suggest a possible environmental transition driven by coseismic uplift of the land surface.

3. METHODS

An Edgetech 216s portable sub-bottom profiling system attached to a raft with two pontoons was used to gather 2.70 km of seismic data from Campus Lagoon (Figure 5). A frequency sweep between 2.0 kHz and 16.0 kHz was utilized during the survey. A seismic velocity of 1500 m/s was used to correlate velocity to depth. Four new vibracores as well as five existing vibracores were taken from the lagoon and range in length between 1.2 m and 3.2 m. Once sediment cores were extracted from the lagoon, the cores were cut vertically along their long axis with a mechanical saw, photographed, and described at the UCSB

Sedimentological Lab. Descriptions of the sediment cores included sedimentary structures, sedimentary grain size, and organic content.

Grain size analysis was conducted on the sediment cores every 3 cm to 10 cm to help distinguish sedimentary facies. Sections of the sediment core that consist largely of coarse-grained sands were sampled at 10 cm intervals, while finer grained sands, silts, and clays were sampled at intervals between 3 cm and 5 cm. Each sample underwent hydrogen peroxide (H₂O₂) pretreatment to dissolve organic material and hydrochloric acid (HCl) pretreatment to dissolve carbonate bearing materials. Following pretreatment, grain size analysis was performed using a CILAS 1190 laser-particle size analyzer at the UCSB Sedimentological Lab following the methods of Sperazza et al. (2004).

To determine whether a ~3 cm carbonate bed in sediment core CL22-01 was a product of subaerial exposure, it was sampled at 3 mm intervals and underwent geochemical analysis to deduce elemental chemistry, mineralogy, and stable isotopic ($\delta^{18}\text{O}$ and $\delta^{13}\text{C}$) signatures. Carbonate samples from CL22-01 were sent to the UCSB Materials Research Laboratory (MRL) and underwent x-ray diffraction (XRD) by a Panalytical Empyrean Powder Diffractometer to determine whether the carbonate was composed of calcite or aragonite. Samples from the carbonate bed within CL22-01 were analyzed at the UCSB Department of Earth Science by scanning electron microscopy (SEM) to obtain images related to crystal morphology and electron probe microanalysis (EPMA) to acquire elemental composition and determine whether the carbonate had a high or low magnesium content. SEM analysis was performed with a FEI Quanta 400F field emission source (FEG) SEM, and EPMA analysis was performed with a Cameca SX-100 with five wavelength spectrometers, energy dispersive x-ray spectroscopy (EDS), and cathodoluminescence (CL) detector. Mg/Ca

ratios, mol percent (mol%) Mg, and weight ratio with respect to Mg were calculated using EPMA results. Carbonate samples were powdered and sent to the Center for Stable Isotope Biogeochemistry at the University of California, Berkeley campus to measure the $\delta^{18}\text{O}$ and $\delta^{13}\text{C}$ signatures and determine the presence of possible subaerial exposure conditions. The $\delta^{18}\text{O}$ and $\delta^{13}\text{C}$ of the carbonate samples were measured using a MultiCarb system with a GV IsoPrime mass spectrometer in Dual Inlet. Carbonate shear strength was tested using a Humboldt H-4212MH pocket shear vane. Evaporite deposits in CL22-01, CL22-03, and CL14-01 also underwent SEM and EDS analysis to determine whether gypsum was present in the southeast, central, and northwest regions of Campus Lagoon, respectively.

Carbon and nitrogen isotopic signatures ($\delta^{13}\text{C}$ and $\delta^{15}\text{N}$) and nitrogen and carbon weight percent (wt%) measurements were conducted on bulk sediment samples at depths between 211 cm and 272 cm within CL22-03 to deduce possible pedogenic processes as a function of depth across a sharp contact between the GS, CS, and CS-E facies. Samples were pretreated with HCl prior to analysis to remove carbonates. Organic carbon analysis was conducted at the UCSB Marine Science Institute Analytical Laboratory using a Thermo-Finnigan MAT Delta+ Advantage.

In total, forty-seven samples consisting of charcoal, shells, and wood fragments from sediment cores in Campus Lagoon were used within this study to document the timing of environmental changes. Twenty-six new samples were collected from Campus Lagoon for this study and underwent radiocarbon age dating at the W.M. Keck Carbon Cycle AMS facility at the University of California, Irvine (UCI) campus. One radiocarbon age collected by Roman (2014), one radiocarbon age from Simms et al. (2016), and nineteen radiocarbon ages from Osleger (2018) were used in this study to complement the twenty-six new

radiocarbon ages gathered in this study and provide constraints on the timing of environmental changes in Campus Lagoon. In addition, four shells collected from sediment cores from a previous study (King et al., 2019) in Batiqitos Lagoon (BQL11-1) and Buena Vista Lagoon (BVL11-2) in San Diego, California also underwent radiocarbon age dating at the W.M. Keck Carbon Cycle AMS facility at UCI to determine the timing of evaporite formation within BQL11-1 and BVL11-2. This was to assess whether late Holocene aridity extended beyond the Santa Barbara coastal plain to other locations farther south along the Southern California coast.

Radiocarbon ages were calibrated using INTCAL20.14C from the Radiocarbon Calibration Program CALIB REV8.2 (Stuiver & Reimer, 1993). A reservoir age of 217 ± 129 ^{14}C year based on the study by Holmquist et al. (2015) for Southern California estuaries was applied to radiocarbon ages derived from shell and carbonate material from Campus Lagoon, Batiqitos Lagoon, and Buena Vista Lagoon. In addition, a reservoir age of 171 ± 154 ^{14}C year based on the study by Holmquist et al. (2015) was applied to a single *C. californica* shell from CL13-02 at 180 cm. A Bayesian age-depth model was created for sediment cores with more than one radiocarbon age date using the software package Bayesian Inference Gaussian Process Regression and Multiproxy Alignment of Continuous Signals (BIGMACS) from Lee et al. (2023).

4. RESULTS

4.1 Campus Lagoon Seismic Survey

Two seismic facies and six seismic units are present within the seismic profiles collected from Campus Lagoon (Figure 6A and 6C). Seismic facies (SF) 1 consists of low

amplitude chaotic reflections (Figure 6A). SF 1 is best developed near the lagoon surface but occurs throughout the seismic profile (Figure 6A). SF 2 is defined by continuous, high amplitude, and parallel reflections (Figure 6A). Examples of SF 2 occur throughout the seismic profile and are best developed in the southeast region of Campus Lagoon, such as those between Navigation Markers 21 and 22 (Figure 6B). Six seismic units were identified and separated from each other by prominent reflections. These units from bottom to top are SU 1, SU 2, SU 3, SU 4, SU 5, and SU 6 (Figure 6B and 6C). Seismic unit (SU) 2 onlaps SU 1 and shows a basinward shift in onlap from a higher to a lower elevation. SU 4 onlaps SU 3 at a lower elevation and similarly shows a basinward shift in onlap. Based on the seismic profile, the elevation difference between the highest elevation of SU 1 and the point of onlap with SU 2 is ~0.7 m. The elevation difference between the highest elevation of SU 3 and the point of onlap with SU 4 is ~1.5 m. SU 5 and SU 6 overlie the older seismic units within Campus Lagoon.

4.2 Sediment Core Facies Description

Sediment cores from Campus Lagoon contain six sedimentary facies (Figures 7 and 8), which include a coarse-grained gray sand (GS), clayey silt interbedded with gypsum and calcite (CS-E), clayey silt (CS), clayey silts with shell fragments (CS-SF), sandy silt (SASL), and a fine-grained laminated sandy silt (LSS).

The gray sand facies (GS) has a mean grain size of 174 μm and typically contains pebbles, rip-up clasts, and shell fragments (Figure 7A). Wood fragments and organic material are sparse within the GS facies. A partially fragmented *Leukoma staminea* shell was found within the GS facies of CL22-02 and is among the only identifiable shells collected from Campus Lagoon in this study. The GS facies is found at the base of sediment cores

throughout the lagoon, atop the CS and CS-SF facies within CL16-02 and CL22-03, and at the stratigraphic top of sediment cores located near the mouth of Campus Lagoon in the southeast (Figure 9).

The clayey silt with evaporite facies (CS-E) has a mean grain size of 11 μm and is composed of a clayey silt interbedded with gypsum lamina and calcite (Figure 7B). The CS-E facies is found within sediment cores in the northwest, central, and southeast regions of Campus Lagoon (Figure 9). EDS and visual observation suggests the presence of gypsum lamina within the CS-E facies of sediment cores CL14-01, CL16-01, CL22-01, and CL22-03 (Figures 10 and 11). An indurated, cemented carbonate bed was found within the CS-E facies in CL22-01 (Figure 12A). The stratigraphic top of the carbonate in CL22-01 has a higher degree of induration relative to the bottom of the carbonate. The stratigraphic top of the cemented carbonate bed within CL22-01 has a shear strength of $\sim 8.25 \text{ kg/cm}^2$, and the stratigraphic bottom of the carbonate bed has a shear strength of $\sim 3.31 \text{ kg/cm}^2$ (Figure 12A). SEM images show a combination of fibrous and possible microcrystalline morphology (Figure 12B). Diatoms are occasionally encrusted within the carbonate bed (Figure 12C).

The clayey silt facies (CS) has an average grain size of 14 μm and consists of clayey silt that lacks evaporite deposits, pebbles, rip-up clasts, and shell fragments (Figure 7C). The CS facies within CL22-03 is bioturbated and contains sand filled burrows. The CS facies also commonly overlies the GS facies and is observed in all sediment cores throughout Campus Lagoon except for CL22-01 and CL23-02 (Figure 9). Ostracod microfossils are commonly present within the CS facies and have also been found in the CS-E facies of CL22-01 (Figure 12D).

The clayey silts with shell fragments facies (CS-SF) has an average grain size of 10 μm and consists of fragmented shell material within a clayey silt matrix (Figure 8A). The CS-SF occurs solely within the northwest and central regions of Campus Lagoon, specifically within CL16-01 at a depth between 195 cm and 205 cm and CL16-02 at a depth between 260 cm and 265 cm (Figure 9).

The sandy silt facies (SASL) has an average grain size of 44 μm and consists of fine-grained sandy silt (Figure 8B). SASL lacks pebbles, rip-up clasts, sedimentary structures, and shell fragments that characterize the GS facies (Figure 8B). Organic material, such as charcoal and wood, is rare. The SASL facies varies from brown to gray in color and occurs as discrete beds within the CS-E / CS facies of CL13-01, CL22-02, and CL22-03 (Figure 9). The SASL facies also occurs within the upper 143 cm of CL22-03 and is interbedded with the coarser grained sands of the GS facies (Figure 9).

Laminated sandy silt facies (LSS) is observed in sediment core CL14-01 and consists of laminations and more organic material, such as wood fragments and charcoal, relative to other facies in Campus Lagoon (Figure 8C). The LSS facies lacks pebbles, rip-up clasts, and shell fragments (Figure 8C). The LSS facies is only observed in the northwest region of Campus Lagoon (Figure 9).

4.3 Chronology of Sediment Cores from Campus Lagoon

Forty-seven charcoal, shell, and wood fragments collected across all sediment cores from Campus Lagoon from this study, Roman (2014), Simms et al. (2016), and Osleger (2018) were used to help constrain the timing of stratigraphic changes within Campus Lagoon (Tables 1 and 2). Following calibration, ages range from ~ 26 ka to ~ 0.1 ka, with most occurring between ~ 5.1 ka and ~ 0.6 ka. Four radiocarbon ages of shells collected from

cores taken in Batiquitos Lagoon and Buena Vista Lagoon in San Diego, California used within this study have ages that range between ~3.6 ka to ~1.1 ka (Table 2). Uncalibrated radiocarbon ages from this study, Roman (2014), Simms et al. (2016), and Osleger (2018) were used to construct age-depth models for sediment cores in Campus Lagoon and Batiquitos Lagoon (Figures 13-15). Radiocarbon ages were then calibrated and used to create age-depth models with BIGMACS. BIGMACS utilizes sediment accumulation rates based on ocean sediment cores, thus uncertainties with regards to age-depth models reported by BIGMACS within this study may be slightly larger than what is reported.

A radiocarbon age from CL13-01 at 138 cm depth yielded an age of 25859 ± 116 calibrated years before present (cal BP) and is interpreted to be reworked based on ages collected from similar depths within Campus Lagoon. Due to its old age, the CL13-01 age-depth model does not include the radiocarbon age from CL13-01 at 138 cm. Radiocarbon ages from CL14-01 at 17 cm, CL14-01 at 59 cm, and CL14-01 at 75 cm yielded ages of 654 ± 92 cal BP, 17089 ± 228 cal BP, and 13163 ± 140 cal BP, respectively. These ages are also interpreted to be reworked based on ages collected at similar depths within Campus Lagoon. Radiocarbon ages from CL16-01 at 100 cm, CL16-01 at 115 cm, and CL16-01 at 237 cm yield calibrated ages of 4686 ± 132 cal BP, 8816 ± 648 cal BP, and 13913 ± 122 cal BP, respectively. These ages are also interpreted to be reworked based on ages collected at similar depths in Campus Lagoon. Radiocarbon ages from CL16-02 at 160 cm and CL16-02 at 243 cm yielded calibrated ages 7507 ± 75 cal BP and 25115 ± 188 cal BP, respectively. These ages occur outside the interpreted deposition of the GS facies starting at least ~5 ka and are considered to be reworked. Radiocarbon ages from CL22-03 at 169 cm, CL22-03 at 269 cm, and CL22-03 at 275 cm yielded calibrated ages of 3930 ± 80 cal BP, 8879 ± 120 cal

BP, and 8265 ± 75 cal BP, respectively. These are interpreted to be reworked based on other ages at similar depths collected from Campus Lagoon. The ages from CL22-03 at 269 cm and CL22-03 at 275 cm were not included in the age-depth model due to their ability to skew the age-depth distribution and provide a possibly inaccurate age-depth relationship. An age-depth model for BVL11-2 and CL23-02 were not included in this study due to an insufficient quantity of radiocarbon ages to produce an age-depth model.

4.4 Mineralogical, Elemental, and Isotopic Data

XRD data suggests the carbonate bed from CL22-01 is composed of calcite (Figure 16). The mol% of the calcite bed ranges from 9.56 mol% Mg to 15.18 mol% Mg (Table 3 and Figure 17), which is within the range of high-magnesium calcite (Harris et al., 1985; Lenders et al., 2012; Gregg et al., 2015; Ries et al., 2016; Goetschl et al., 2021; Purgstaller et al., 2021). The MgCO_3 weight ratio ranges from 7.28 wt% to 10.62 wt% (Table 3 and Figure 17), which is within the range of high-magnesium calcite as classified by Boggs (2012). The $\delta^{18}\text{O}$ values of the calcite range between 0.93‰ Vienna Pee Dee Belemnite (VPDB) and 1.64‰ VPDB, while $\delta^{13}\text{C}$ values of the calcite range between -16.24‰ VPDB and -15.11‰ VPDB (Table 3 and Figure 17). The $\delta^{13}\text{C}$ values from bulk sediment samples between 211 cm and 272 cm within CL22-03 range from -22.36‰ Pee Dee Belemnite (PDB) to -17.94‰ PDB, while the $\delta^{15}\text{N}$ values range from 4.36‰ PDB to 8.74‰ PDB (Table 4 and Figure 18). Carbon wt% values between 211 cm and 272 cm within CL22-03 range from 0.1 wt% to 1.92 wt%, while nitrogen wt% values range from 0.01 wt% to 0.17 wt% (Table 4 and Figure 18). Organic carbon data shows low $\delta^{13}\text{C}$ and $\delta^{15}\text{N}$ in the bioturbated CS facies, GS facies, and CS-E facies of CL22-03 (Table 4 and Figure 18). Carbon wt% between the bioturbated CS facies and GS facies decreases and is followed by a gradual increase through the GS facies

and into the SASL facies (Figure 18). This gradual increase is followed by a slight decrease in carbon weight percent and an increase during the transition to the CS-E facies (Figure 18).

5. DISCUSSION

5.1 Campus Lagoon Sediment Core Facies Interpretation

5.1a GS Interpretation

The GS facies consist of coarse-grained sand, pebbles, rip-up clasts, and shell fragments. A partially fragmented *Leukoma staminea*, commonly referred to as the Pacific littleneck clam, is present in the GS facies of CL22-02 and can be found in mid-intertidal zones as far north as the Aleutian Islands, Alaska and as far south as Baja California (Washington Department of Fish & Wildlife, 2023). Based on studies by Meyers et al. (1994), carbon and nitrogen atomic ratios (C/N) and $\delta^{13}\text{C}$ values within the GS facies of CL22-03 suggest marine algae influence, which suggests deposition in a marine environment. Based on its relatively coarse grain size and these listed properties, the GS facies is interpreted to be deposited within a high-energy intertidal environment, such as a washover fan.

5.1b CS-E and CS Facies Interpretation

The CS-E and CS facies consist of clayey silt with and without evaporite deposits, respectively. The CS facies in CL22-03 between 264 cm and 290 cm contains sand filled burrows. The average $\delta^{13}\text{C}$ value of the calcite in CL22-01 is -15.9‰ VPDB, which correlates to $\delta^{13}\text{C}$ values of C4 land plants (Kohn and Cerling, 2002; Hood-Nowotny and Knols, 2007; Basu et al., 2015; Kirkels et al., 2022), suggesting possible plant influence on

calcite formation in the southeast region of Campus Lagoon. The presence of gypsum throughout the lagoon, calcite, and possible C4 plant influence suggests an environment characterized by limited connection with the open-ocean. The lack of coarse-grained sands, pebbles, rip-up clasts, and shell fragments within the CS-E and CS facies supports an interpretation of a low-energy depositional environment with limited circulation with the open-ocean. Based on its grain size and these listed properties, the CS-E and CS facies are interpreted to represent a mudflat, specifically a sabkha environment prone to evaporation as a result of limited connection with the open-ocean.

5.1c CS-SF Facies Interpretation

The CS-SF facies (CS-SF) consists of fragmented shells within a clayey silt matrix. The CS-SF facies correlates with the timing of a bioturbated CS facies within CL22-03, which has atomic C/N ratios and $\delta^{13}\text{C}$ values suggestive of marine algae influence. The lack of coarse-grained sands, pebbles, and rip-up clasts suggests the depositional environment was not within a high energy zone. Based on the grain size, presence of shell fragments, and correlation with a bioturbated CS facies in CL22-03, the CS-SF facies is interpreted to be a quiet, shallow water central basin region of a lagoon.

5.1d SASL Facies Interpretation

The SASL facies has a brown-gray color and lacks pebbles, shell fragments, and rip-up clasts. It is often interbedded within the CS-E and CS facies. The SASL facies is found in the upper 143 cm of CL22-03. Deposits of the SASL facies are finely skewed. Radiocarbon ages suggest that the upper SASL facies in CL22-03 was concurrently deposited with the GS facies in CL22-02 starting ~0.6 ka. Based on the smaller grain size relative to the GS facies

and lack of pebbles, shell fragments, and rip-up clasts, the upper SASL facies is interpreted to represent the distal sands of the GS facies where coarser sediment was deposited closer to the coastline, and finer grained sediments associated with the SASL facies was deposited farther away from the coastline. Based on the fine skewness in the grain size distribution curves, the SASL facies that interbed the CS-E and CS facies may represent a distal overwash characterized by the settling of finer grained sediments farther away from the coastline.

5.1e LSS Facies Interpretation

The LSS facies is solely observed in the northwest region of Campus Lagoon within sediment core CL14-01 and contains more wood and charcoal fragments than the other sedimentary facies discussed in this study. The LSS facies lacks pebbles, rip-up clasts, and shell fragments, which distinguishes it from the GS facies. The beige-brown color of the LSS facies suggests more oxidation in contrast to the gray GS facies. The LSS facies also occurs farther inland and has a finer grain size than the GS and SASL facies. The incorporation of old radiocarbon ages within the LSS facies suggests older material washing into the lagoon from the terrestrial landscape. Radiocarbon ages suggest the LSS facies was deposited starting ~0.6 ka, which is concurrent with the deposition of the GS and SASL facies in CL22-02 and CL22-03, respectively. Based upon these observations and its geographic location towards the northwest region of Campus Lagoon, the LSS facies is interpreted to represent sheetwash from the terrestrial landscape.

5.2 Seismic Stratigraphic Analysis

Sediment cores that sample the chaotic seismic facies of SF 1 contain sand beds of the GS facies. Mitchum et al. (1977) also interprets chaotic seismic reflections to represent deposition in a high-energy setting. Based on these correlations and observations, SF 1 is interpreted to represent coarse sands of the GS facies. Cores that sample SF 2 contain fine-grained sediment of the CS-E and CS facies. SF 2 is interpreted to represent the low-energy deposits of a central basin lagoon and evaporative mudflat environments with limited ocean connection.

Seismic profiles from Campus Lagoon show basinward shifts in onlap between seismic unit (SU) 2 and SU 4. Within Campus Lagoon, SU 2 onlaps SU 1 at a lower elevation (Figure 19). Based on the study by Vail et al. (1977) and seismic profiles from the lagoon, this basinward shift in onlap from a higher to a lower elevation may represent a rapid fall in RSL of ~0.7 m. Following the possible regression, sea-levels are interpreted to have risen given how SU 1 and SU 2 are overlain by SU 3 (Figure 19). Between SU 3 and SU 4, a second basinward shift in onlap occurs in which SU 4 onlaps against SU 3 at a lower elevation (Figure 19). Based on the study by Vail et al. (1977) and seismic profiles from the lagoon, the shift in onlap to a lower elevation may also represent a second potentially rapid fall in RSL of ~1.5 m. SU 5 through SU 6 overlie SU 4, which suggests a resumption of sediment deposition associated with rising sea-levels (Figure 20). The timing of the basinward shifts in onlap within Campus Lagoon can only be loosely constrained. SU 2 and SU 4 overlie SU 1, which has an upper age of ~3.7 ka. SU 2 and SU 4 reside below SU 5, which has an age of ~0.6 ka. An alternative explanation for the onlapping seismic units are large influxes of sediment from inundation caused by a storm, tsunami, or slope failure from

the sides of the lagoon. The presence of uplifted marine terraces within this region and instances of coseismic uplift near Ventura, California by Rockwell et al. (2016) provide support for coseismic uplift during large earthquakes.

5.3 Campus Lagoon Sediment Core Facies Historical Interpretation

5.3a Mid-to-Late Holocene ENSO Intensification

Heightened wave action within the Santa Barbara Channel could be a possible driver for deposition of the GS facies. Deposition of the GS facies within Campus Lagoon occurs at least ~5 ka and lasts through at least ~4 ka. This time period marks the timing of ENSO intensification and the loss of perennial beach sands along the western Santa Barbara coast (Masters, 2006). This intensification was documented by the absence of the Pismo clam, *Tivela stultorum*, which acts as a proxy record for sand accretion within the littoral cells of Southern California (Masters, 2006). Sand beaches culminated along the western Santa Barbara coast between 6 ka and 5 ka, but *Tivela*-dated sites become rare between 5 ka and 4 ka along the western Santa Barbara coast (Masters, 2006). The absence of *Tivela*-dated sites between 5 ka and 4 ka coincides with the onset of ENSO intensification recorded in the sediments of Laguna Pallcacocha in Ecuador (Moy et al., 2002). Geoarchaeological and paleontological evidence from Peru by Sandweiss et al. (1996) also suggests the presence of mid-Holocene ENSO intensification starting ~5 ka. Marine sediment cores off the coast of Peru also suggest ENSO intensification and higher frequency of ENSO related flood events starting ~5 ka (Rein et al., 2005). Friddell et al. (2003) used planktonic foraminiferal $\delta^{18}\text{O}$ records from the Santa Barbara Basin (SBB) to show climate variability during the mid-Holocene. High $\Delta\delta^{18}\text{O}$ between 5.2 ka and 3.6 ka were observed, which suggest that Pacific

Decadal Oscillation (PDO) was within a warm phase and ENSO was intensified during this time (Friddell et al., 2003). A study by Woodroffe et al. (2003) documents $\delta^{18}\text{O}$ signatures of fossil coral microatolls from Christmas Island within the central Pacific that suggest less intense variations in ENSO sea-surface temperature and precipitation between 3.8 ka and 2.8 ka, which helps support the interpretation of declining ENSO intensification after 4 ka. ENSO variability based on uranium-thorium (U-Th) dated fossil corals from the central tropical Pacific by Cobb et al. (2013) suggests the strength of ENSO related storms was low ~ 5 ka and started to increase in strength after ~ 4 ka. These studies ultimately show uncertainties surrounding the exact timing of ENSO intensification but generally showcase mid-Holocene ENSO intensification and variability.

Based on a number of studies in the Pacific and from the work of Masters (2006), ENSO intensification is interpreted to have occurred in the Santa Barbara region ~ 5 ka, which increased sediment supply to the Santa Barbara littoral cell and led to beach progradation as small estuaries filled beyond valley headlands (Masters, 2006). Masters (2006) suggests that El Niño storms generated high waves within the Santa Barbara Channel, causing the exposed western beaches to erode, disrupt the *Tivela* fishery between 5 ka and 4 ka, and transport sediment from the west to the east (Masters, 2006). Thus, as sandbars were removed from the mouth of Campus Lagoon during heightened wave action and ENSO related storm conditions, the GS facies in Campus Lagoon was deposited.

Estuaries and lagoons along the Santa Barbara Channel, such as Campus Lagoon, are possible repositories for the sediments reworked from the beaches and transported eastward between 5 ka and 4 ka. A study by Nelson (2018) shows that sands similar to the GS facies also appear to the west of Campus Lagoon in Devereux Slough. The stratigraphic top of the

well-sorted sand facies in Devereux Slough dates to ~3.8 ka, which is within error of the stratigraphic top of the GS facies in Campus Lagoon. The presence of the well-sorted sands in Devereux Slough illustrates that the GS facies is not unique to Campus Lagoon but also found in other nearby estuaries and lagoons. As ENSO increased sediment supply to the Santa Barbara littoral cell, heightened wave action eroded beaches and transported sediment from the west to the east, which led to the trapping of sands, such as the GS facies within Campus Lagoon from at least ~5 ka and until ~4 ka and the well-sorted sand facies found in Devereux Slough ~3.8 ka.

Studies by Kirby et al. (2010, 2012, 2014) and Du et al. (2018) also document periods of heightened storm activity at the same time as deposition of the GS facies in Campus Lagoon and the well-sorted sand facies within Devereux Slough. Kirby et al. (2010) used percent sand accumulation as a proxy for water discharge in Lake Elsinore, California, which records wet climates between 4.5 ka and 4.1 ka. In addition, the frequency and magnitude of flood deposited gray layers within sediment cores collected from the SBB by Du et al. (2018) increased during periods of flooding documented by lake records from Kirby et al. (2010, 2012, 2014). Du et al. (2018) suggests a period of increased precipitation between 5.5 ka and 3 ka, which overlaps the timing of deposition associated with the GS facies in Campus Lagoon. Deposition of the GS facies concurrently with flood deposits in terrestrial and marine sediment cores during a period of heightened ENSO starting ~5 ka and lasting until at least ~4 ka suggests that as stormy conditions delivered overland flow and flood deposits to lakes and the SBB, heightened wave action in the Santa Barbara Channel contributed to the deposition of the GS facies in Campus Lagoon and the well-sorted sand facies to Devereux Slough.

5.3b Late Holocene Aridity and Possible Coseismic Uplift

The calcite bed within CL22-01 was initially interpreted to be caused by either subaerial exposure following coseismic uplift or desiccation in response to regional aridity. Subaerial exposure is a catalyst for pedogenesis and may contribute to the formation of caliche facies that may consist of well-cemented, low-magnesian calcite deposits (Esteban & Klappa, 1983). A worldwide compilation of pedogenic carbonates by Zhou and Chafetz (2010) found that the $\delta^{18}\text{O}$ and $\delta^{13}\text{C}$ isotopic signatures range between -7‰ VPDB to -2‰ VPDB and -9‰ VPDB to -1‰ VPDB, respectively. The $\delta^{18}\text{O}$ values of the calcite bed in CL22-01 range between 0.93‰ VPDB and 1.64‰ VPDB, while $\delta^{13}\text{C}$ values range between -16.24‰ VPDB and -15.11‰ VPDB. The $\delta^{18}\text{O}$ and $\delta^{13}\text{C}$ signatures from the calcite bed of CL22-01 occur outside the range of pedogenic carbonates compiled by Zhou and Chafetz (2010), suggesting calcite formation within Campus Lagoon occurred in response to processes other than pedogenesis.

Electron probe microanalysis (EPMA) and $\delta^{18}\text{O}$ and $\delta^{13}\text{C}$ isotopic signatures of the calcite suggests calcite cementation could be attributed to factors, such as sulfate reducing bacteria (SRB), brine induced diagenesis, or a combination of both rather than subaerial exposure (Figure 21). Based on the diagenetic relationships under Reis et al. (2019), calcite samples from CL22-01 plot between the diagenetic trends related to SRB and brine induced diagenesis. EPMA analysis suggests the calcite bed in CL22-01 is composed of high-Mg calcite, which can be found in hypersaline, marine, or sabkha environments (Folk, 1974). In addition, SRB is important in the cycling of carbon in marine and hypersaline regions and was found to have a role in high-Mg calcite precipitation under laboratory conditions (Paul et al., 2017). The presence of SRB influences carbonate precipitation and produces increasingly

negative $\delta^{13}\text{C}$ values (Reis et al., 2019). SRB utilizes sulfate to decompose organic matter and release ^{12}C enriched CO_2 (Reis et al., 2019). ^{12}C depleted CO_2 is ultimately incorporated into carbonate cement (Reis et al., 2019). In agreement with the high-Mg calcite in CL22-01, studies by Irwin and Curtis (1977) and Machel (2004) show SRB is a factor in carbonate precipitation, which produces $\delta^{13}\text{C}$ values between -10‰ VPDB and -25‰ VPDB, similar to the $\delta^{13}\text{C}$ values found within the calcite bed of CL22-01. Based on radiocarbon ages, EPMA analysis, and stable isotopic analysis ($\delta^{18}\text{O}$ and $\delta^{13}\text{C}$), the indurated high-Mg calcite bed within CL22-01 is interpreted to be a product of late-Holocene aridity within an evaporative mudflat environment that occurred at least ~ 0.8 ka ago.

The formation of gypsum deposits throughout Campus Lagoon further supports limited connection with the open-ocean and desiccation during periods of late Holocene aridity. Gypsum is indicative of a stagnant marine environment with poor circulation of marine waters. Within Campus Lagoon, sediment cores CL14-01 and CL16-01 provide the largest temporal span of evaporite formation. Gypsum lamina within CL14-01 dates between ~ 3.2 ka and ~ 1.2 ka, while gypsum lamina within CL16-01 occurs between ~ 3.6 ka and ~ 2.5 ka. Gypsum lamina in CL22-03 occurs between ~ 2.3 ka and ~ 2.0 ka and between ~ 1.4 ka and ~ 0.6 ka. Gypsum and carbonate precipitation occurs within CL22-01 prior to ~ 0.9 ka. The temporal continuity of the evaporite deposits within Campus Lagoon indicates widespread evaporative conditions within the lagoon. Adjacent to the UCSB campus, gypsum sands within Dune Pond occur between ~ 2.4 ka and ~ 0.9 ka, which coincides with evaporite formation within Campus Lagoon (Ejarque et al., 2015). Du et al. (2018) notes large pluvial events within the SBB between 3 ka and 2 ka, which occur during the time of arid conditions documented within Campus Lagoon and Ejarque et al. (2015). The similar

timing of gypsum deposits in Campus Lagoon and Dune Pond suggests the possibility that evaporite formation in the Santa Barbara coastal plain is influenced by similar climate forcings. Although evaporite deposits suggest arid conditions, the study by Du et al. (2018) suggests the possibility that arid conditions were punctuated by periods of increased storm activity that delivered runoff to the SBB.

Studies by King et al. (2019) in San Diego, California found mud facies with gypsum lamina within sediment cores BVL11-2 from Buena Vista Lagoon and BQL11-1 from Batiquitos Lagoon. Sediment cores of King et al. (2019) were revisited in this study, and shells were collected for radiocarbon age dating from BVL11-2 and BQL11-1. Radiocarbon ages collected from BVL11-2 in this study suggest the stratigraphic top of the mud with gypsum lamina facies in BVL11-2 dates to ~1.1 ka. Radiocarbon ages from BQL11-1 also suggest drought-like conditions between ~3.2 ka and ~1.2 ka. These new radiocarbon ages from evaporites within the sediment cores of King et al. (2019) are similar in age with gypsum deposits within Campus Lagoon and suggest that evaporite deposition extended beyond the Santa Barbara area and possibly impacted coastal environments as far south as San Diego, California.

Climate studies near the Santa Barbara region by Kirby et al. (2014) at Zaca Lake, California and Heusser et al. (2015) in the SBB show periods of heightened aridity within the last 2.5 ka that coincide with arid conditions documented in Campus Lagoon, Batiquitos Lagoon, and Buena Vista Lagoon. Kirby et al. (2014) used percent sand totals and hydrogen isotope data from plant leaf wax (δD_{wax}) as a proxy for hydroclimate variability. Low sand accumulation in Zaca Lake between ~2.5 ka and ~2.0 ka suggests low runoff and less precipitation, while high δD_{wax} values demonstrate arid conditions between 1.5 ka and 0.9 ka

(Kirby et al., 2014). The study by Kirby et al. (2014) suggests the timing of dry conditions in Zaca Lake coincides with the timing of evaporite formation in Campus Lagoon. In addition, Heusser et al. (2015) used pollen variations between *Quercus* and chaparral within a sediment core collected from the SBB to assess vegetation response to climate over the past 1.1 ka and similarly shows periods of increased aridity. *Quercus* pollen is associated with cool and mesic conditions within Southern California, while chaparral pollen is interpreted to represent warm and xeric environments (Heusser et al., 2015). Between 1.1 ka and ~0.9 ka and at ~0.7 ka, sediments within the SBB were characterized by xeric vegetation, which suggests the dominance of arid conditions in Southern California during these time periods (Heusser et al., 2015). The timing of evaporite formation in Campus Lagoon, Batiqitos Lagoon, and Buena Vista Lagoon is similar to periods of heightened aridity documented by Kirby et al. (2014) and Heusser et al. (2015), suggesting that evaporite deposits found within this study may reflect drought-like conditions that impacted the Southern California coast.

The timing of evaporite formation in coastal California environments, such as Campus Lagoon, Batiqitos Lagoon, and Buena Vista Lagoon, as well as other hydroclimate proxies from lake and marine sediment cores in the Southern California region, is interpreted to relate to two periods of prolonged drought that extended farther into the continental United States. Mensing et al. (2013) provides evidence of multi-century arid conditions for the first of these notable dry periods between 2.8 ka and 1.8 ka, referred to as the Late Holocene Dry Period (LHDP), using pollen, mollusks, diatoms, and sediments from Stonehouse Meadow within Spring Valley, Nevada. During this time, Mensing et al. (2013) documented a decrease of sedge meadow, trees, and shrubs and an increase in grasses, herbs, and total inorganic carbon. Using the study by Castelli et al. (2000), Mensing et al. (2013) argues that

a decline in sedges and increase in grass between 2.8 and 1.8 ka within Stonehouse Meadow suggests extended lowering of the water table and evidence of late Holocene drying. In addition, lake level records from Mono Lake, a closed-basin lake in Eastern California, suggest an extreme low stand occurring at 1.8 ka, which occurs during a time of arid conditions suggested by evaporites in sediment cores from Campus Lagoon and Batiquitos Lagoon (Stine, 1990).

The second period of drought conditions found in other terrestrial and offshore climate studies is the Medieval Climate Anomaly (MCA), which occurred between ~1 ka and ~0.65 ka (Masson-Delmotte et al., 2013). A study by Hiner et al. (2016) used sand accumulation, total organic matter content, and $\delta^{18}\text{O}$ of gastropods within sediment cores as proxy records for hydroclimate variability along the Central California coast for the past 1.4 ka. Low sand accumulation and higher total organic matter within sediment cores were interpreted to represent low runoff and the expansion of the littoral zone, respectively. Hiner et al. (2016) notes that peak MCA conditions occurred between ~0.9 ka and ~0.7 ka, which similarly coincides with the timing of evaporite formation in Campus Lagoon. Within Zaca Lake, California, Kirby et al. (2014) notes the presence of drought-like conditions between ~1.5 ka and ~0.9 ka, which also coincide with the MCA and timing of evaporites in Campus Lagoon. The timing of evaporite formation in Campus Lagoon complements hydroclimate studies by Hiner et al. (2016) and Kirby et al. (2014), suggesting that drought-like conditions associated with the MCA extended from the Central California coast to the Southern California coast.

Evaporite deposits that occur during the MCA within Campus Lagoon also coincide with arid conditions documented by climate studies conducted farther within the mainland

United States. Cook et al. (2004) used tree-ring records to reconstruct annual changes in climate variability over the North American continent within the past 1.2 ka and identified periods of heightened aridity between 1 ka and 0.6 ka. The drought reconstruction used by Cook et al. (2004) consists of a Palmer Drought Severity Index (PDSI), which is used to measure wet and arid conditions over the United States (Cook et al., 2004). The PDSI reconstruction was produced on a 286-point grid system that covered most of North America (Cook et al., 2004). The four driest epochs identified by Cook et al. (2004) occurred at ~1 ka, ~0.9 ka, ~0.8 ka, and ~0.7 ka. Radiocarbon ages of submerged tree trunks in Tenaya Lake within Yosemite National Park and Mono Lake, California by Stine (1994) also occur during the MCA and complement both Masson-Delmotte et al. (2013) and Cook et al. (2004). The submerged trees within Tenaya Lake occur at ~0.9 ka and ~0.6 ka, which suggests the lowering of lake levels during this time period (Stine, 1994). Ring counts associated with tree stumps from Mono Lake suggest that inland California regions endured two distinct droughts from before ~1 ka to ~0.8 ka and from before ~0.7 ka to ~0.6 ka (Stine, 1994). Studies by Heusser et al. (2015) also document an increase in xeric vegetation within sediment cores from the SBB during this time, suggesting arid conditions associated with the MCA. Regional hydroclimate studies by Cook et al. (2004), Stine (1994), and Heusser et al. (2015) suggest drought conditions associated with the MCA, which also coincides with gypsum formation within Campus Lagoon.

Local and regional hydroclimate studies pertaining to the timeframe of the LHDP and MCA coincide with the timing of evaporite formation in Campus Lagoon, while the timing of the LHDP coincides with the timing of gypsum formation in Batiquitos Lagoon and possibly Buena Vista Lagoon. This suggests that as arid conditions impacted inland regions

within the western United States, drought-like conditions also extended to coastal settings, such as Santa Barbara and San Diego, California. Desiccation of Campus Lagoon was facilitated by late Holocene aridity, but separation of the lagoon from the ocean to permit evaporite formation within a mudflat environment may have been influenced by other factors, such as sandbar formation at the mouth of the lagoon or possible coseismic uplift. Aerial photographs of Campus Lagoon from 1928 shows desiccation of the southeast and southern regions of the lagoon (Figure 22). Closure of the lagoon from the open-ocean by a natural barrier, such as a sandbar, could produce an evaporative mudflat susceptible to late-Holocene aridity.

Vail et al. (1977) suggest that downward shifts in onlap may represent possibly abrupt falls in RSL. Onlapping seismic reflections in the southeast region of Campus Lagoon suggest that evaporite formation may be attributed to possible coseismic uplift. The onlapping pattern between SU 1 and SU 2 coincides with the transition from the GS facies to the CS / CS-E facies, indicating a possible environmental transition from an intertidal zone to an evaporative sabkha environment. A possible cause of this transition from an intertidal region to a lower supratidal, evaporative sabkha is coseismic uplift of the land surface. As possible coseismic uplift occurred, separation between the lagoon and ocean would ensue and subsequently expose the lagoon to arid conditions during the late Holocene and facilitate evaporite formation. This interpretation is favored due to onlapping seismic reflections suggestive of possibly rapid RSL fall in Campus Lagoon and the occurrence of gypsum lamina only in coastal settings that experience land surface uplift. Seismic reflections within Campus Lagoon can be traced across the subsurface.

Radiocarbon ages of seismic reflections above and below the regions of onlap in the southeast area of Campus Lagoon provide loosely constrained ages of the onlapping seismic reflections suggestive of possible RSL fall. The timing of the possibly abrupt falls in RSL are interpreted to have occurred between ~ 3.7 ka and ~ 0.6 ka. Rockwell et al. (2016) argues that coseismic uplift events occurred in the Ventura, California region at 2.09 ka and 0.95 ka, which overlaps with the timing of the onlapping patterns in Campus Lagoon. Faults capable of causing coseismic uplift of the Campus Lagoon vicinity may possibly pertain to the Western More Ranch fault to the north and the offshore, north-dipping reverse Pitas Point-North Channel fault system.

Gypsum occurs in Campus Lagoon, Dune Pond, Batiquitos Lagoon, and Buena Vista Lagoon, all of which are experiencing tectonic uplift. Gypsum deposits have not yet been found in fault bounded estuaries, such as those in Goleta Slough and Carpinteria Slough (King et al., 2019). King et al. (2019) proposed that evaporites found in uplifted incised valley fills could be due to slower rates of accommodation whereas estuaries experiencing subsidence do not fill their accommodation enough to produce a mudflat environment. Although Batiquitos Lagoon and Buena Vista Lagoon do not undergo coseismic uplift, slower rates of accommodation in Campus Lagoon due to possible coseismic uplift may be a contributing factor to evaporite formation.

5.3c Return to Late Holocene Stormy Conditions

Radiocarbon ages and grain size analysis suggest the return of the GS facies in Campus Lagoon relates to stormy conditions associated with the Little Ice Age (LIA). Masson-Delmotte et al. (2013) suggest that the onset of the LIA occurs ~ 0.5 ka. A study by Hiner et al. (2016) at Abbott Lake in the Santa Lucia Range of Monterey County, California

used variations in sand content, percent total organic matter, and $\delta^{18}\text{O}$ of gastropods, specifically *G. parvus*, to provide insight into past hydrologic variability within the past 1.4 ka along the Central California Coast. Hiner et al. (2016) used sand deposits as a proxy record for runoff and notes the transition to the LIA occurs in Abbott Lake starting ~0.68 ka. The transition from the MCA to the LIA was interrupted by dry conditions between 0.59 ka and 0.51 ka, and a return to wet conditions associated with the LIA occurred starting ~0.5 ka (Hiner et al., 2016). In conjunction with their studies at Abbott Lake, Hiner et al. (2016) highlights that studies by Kirby et al. (2010) at Lake Elsinore and Kirby et al. (2014) at Zaca Lake show a transition out of dry conditions associated with the MCA and into stormy conditions related to the LIA between 0.7 ka and 0.6 ka. This transition from the MCA to LIA also occurs during the same time period as the transition from the CS-E / CS facies to the GS / SASL facies in Campus Lagoon. The timing of the LIA suggested by Hiner et al. (2016) also coincides with an increase in frequency of flood deposited gray layers in the stratigraphic record of the SBB between 0.8 ka and 0.4 ka (Du et al., 2018). Cook et al. (2004) also notes an abrupt change in the Drought Area Index (DAI) to less arid conditions ~0.6 ka. Together, these studies (Cook et al., 2004; Heusser et al., 2015; Hiner et al., 2016; Du et al., 2018) provide regional evidence of a return to more stormy conditions at the same time as the onset of deposition of the GS, SASL, and LSS facies in Campus Lagoon. The return to stormy conditions associated with the transition to the LIA between ~0.7 ka and ~0.6 ka left a tangible record in the sediments of Campus Lagoon.

6. CONCLUSION

The stratigraphic record of Campus Lagoon suggests that the Santa Barbara region is susceptible to coastal change in response to heightened storm activity, sustained drought-like

conditions, and possible seismic deformation. Nine sediment cores and a seismic survey from Campus Lagoon document how mid-to-late Holocene environmental change and possible coseismic uplift in the western Santa Barbara Fold Belt (SBFB) region impacted the Santa Barbara coast. Sediment cores contain coarse-grained gray sand facies (GS) deposited during ENSO intensification and heightened wave action in the Santa Barbara Channel starting at least ~5 ka and lasting until at least ~4 ka. Gypsum lamina throughout Campus Lagoon correlates with the timing of gypsum deposits found in Batiquitos Lagoon and Buena Vista Lagoon in San Diego, California. The timing of evaporite deposition in Campus Lagoon, Batiquitos Lagoon, and Buena Vista Lagoon occurred during periods of sustained late Holocene aridity, specifically the Late Holocene Dry Period (LHDP) and Medieval Climate Anomaly (MCA). Arid conditions documented by sediment cores from Campus Lagoon, Batiquitos Lagoon, and Buena Vista Lagoon are complemented by studies from lake records and both terrestrial and offshore marine sediment cores. Deposition of the GS facies, sandy silt facies (SASL), and laminated sandy silt facies (LSS) starting between ~0.7 ka and ~0.6 ka suggests a possible transition from late Holocene aridity to stormy conditions associated with the Little Ice Age (LIA). This study shows how wet climate conditions associated with ENSO and the LIA along with sustained arid conditions associated with the LHDP and MCA impacted the Southern California coastline.

In addition to climate variability, seismic profiles of Campus Lagoon show two basinward shifts in onlap, which suggest two possibly abrupt falls in RSL between ~3.7 ka and ~0.6 ka due to coseismic uplift of the land surface. Seismic unit (SU) 2 onlaps SU 1 at a lower elevation, while SU 4 onlaps SU 3 at a lower elevation. Onlapping patterns coincide with the transition from the GS to CS-E / CS facies, suggesting that coseismic uplift of the

land surface could be a possible factor promoting the transition from an intertidal zone to a lower supratidal, evaporative mudflat susceptible to late Holocene aridity. If onlapping geometries are a product of rapid RSL fall in response to coseismic uplift of the land surface, large magnitude earthquakes could be another hazard for the Santa Barbara coast and may be a factor contributing to marine terrace development in the western SBFB.

7. WORKS CITED

1. Austermann, Mitrovica, J. X., Latychev, K., & Milne, G. A. (2013). Barbados-based estimate of ice volume at Last Glacial Maximum affected by subducted plate. *Nature Geoscience*, 6(7), 553–557. <https://doi.org/10.1038/ngeo1859>
2. Barbour, Keeler-Wolf, T., & Schoenherr, A. A. (2007). Terrestrial vegetation of California (3rd ed.). *University of California Press*.
3. Basu, Agrawal, S., Sanyal, P., Mahato, P., Kumar, S., & Sarkar, A. (2015). Carbon isotopic ratios of modern C3-C4 plants from the Gangetic Plain, India and its implications to paleovegetational reconstruction. *Palaeogeography, Palaeoclimatology, Palaeoecology*, 440, 22–. <https://doi.org/10.1016/j.palaeo.2015.08.012>
4. Boggs. (2012). Principles of sedimentology and stratigraphy (5th ed.). *Pearson Prentice Hall*.
5. Carver, Jayko, A. S., Valentine, D. W., & Li, W. H. (1994). Coastal uplift associated with the 1992 Cape Mendocino earthquake, Northern California. *Geology* (Boulder), 22(3), 195–198. [https://doi.org/10.1130/0091-7613\(1994\)0222.3.CO;2](https://doi.org/10.1130/0091-7613(1994)0222.3.CO;2)
6. Castelli, Chambers, J. C., & Tausch, R. J. (2000). SOIL-PLANT RELATIONS ALONG A SOIL-WATER GRADIENT IN GREAT BASIN RIPARIAN MEADOWS. *Wetlands (Wilmington, N.C.)*, 20(2), 251–266. [https://doi.org/10.1672/0277-5212\(2000\)020\[0251:SPRAAS\]2.0.CO;2](https://doi.org/10.1672/0277-5212(2000)020[0251:SPRAAS]2.0.CO;2)
7. Cobb, Westphal, N., Sayani, H. R., Watson, J. T., Di Lorenzo, E., Cheng, H., Edwards, R. L., & Charles, C. D. (2013). Highly Variable El Niño—Southern Oscillation Throughout the Holocene. *Science (American Association for the Advancement of Science)*, 339(6115), 67–70. <https://doi.org/10.1126/science.1228246>
8. Cook, Woodhouse, C. ., Eakin, C. ., Meko, D. ., & Stahle, D. . (2004). Long-term aridity changes in the western United States. *Science (American Association for the Advancement of Science)*, 306(5698), 1015–1018. <https://doi.org/10.1126/science.1102586>
9. Dibblee, T. W. 1966. Geology of the Central Santa Ynez Mountains, Santa Barbara County, California. *California Division of Mines and Geology Bulletin* 186: 1-99.
10. Du, Hendy, I., & Schimmelmann, A. (2018). A 9000-year flood history for Southern California: A revised stratigraphy of varved sediments in Santa Barbara Basin. *Marine Geology*, 397, 29–42. <https://doi.org/10.1016/j.margeo.2017.11.014>
11. Ejarque, Anderson, R. S., Simms, A. R., & Gentry, B. J. (2015). Prehistoric fires and the shaping of colonial transported landscapes in southern California: A

- paleoenvironmental study at Dune Pond, Santa Barbara County. *Quaternary Science Reviews*, 112, 181–196. <https://doi.org/10.1016/j.quascirev.2015.01.017>
12. Esteban, & Klappa, C. F. 1983. “Subaerial Exposure Environment”, Carbonate Depositional Environments, Scholle, Bebout, D. G., & Moore, C. H.
 13. Flight C_210, Frame B-4, April 15th, 1928, Courtesy of UCSB Library Geospatial Collection
 14. Flight PW_SB_17, Frame 17, April 15th, 2008, Courtesy of UCSB Library Geospatial Collection
 15. Friddell, Thunell, R. C., Guilderson, T. P., & Kashgarian, M. (2003). Increased northeast Pacific climatic variability during the warm middle Holocene. *Geophysical Research Letters*, 30(11), 1560–n/a. <https://doi.org/10.1029/2002GL016834>
 16. Goetschl, Dietzel, M. Purgstaller, B., Grengg, C., & Μαυρομάτης, Βασίλειος. (2021). Control of MgSO₄(aq) on the transformation of amorphous calcium carbonate to high-Mg calcite and long-term reactivity of the crystalline solid. *Geochimica et Cosmochimica Acta*, 312, 357-374. <https://doi.org/10.1016/j.gca.2021.07.026>
 17. Goto, Gray, S., Keller, E., & Clarke, K. (2021). Evacuation choice before and after major debris flows: The case of Montecito, CA. *International Journal of Disaster Risk Reduction*, 62, 102400–. <https://doi.org/10.1016/j.ijdr.2021.102400>
 18. Gregg, Bish, D. L., Kaczmarek, S. E., & Machel, H. G. (2015). Mineralogy, nucleation and growth of dolomite in the laboratory and sedimentary environment: A review. *Sedimentology*, 62(6), 1749–1769. <https://doi.org/10.1111/sed.12202>
 19. Gurrola, Keller, E. A., Chen, J. H., Owen, L. A., & Spencer, J. Q. (2014). Tectonic geomorphology of marine terraces; Santa Barbara fold belt, California. *Geological Society of America Bulletin*, 126(1-2), 219–233. <https://doi.org/10.1130/B30211.1>
 20. Harris, P. Kendall, C, Lerche, I (1985). Carbonate Cementation - A Brief Overview. *The Society of Economic Paleontologists and Mineralogists*. 79-95.
 21. Heusser, Hendy, I. L., & Barron, J. A. (2015). Vegetation response to southern California drought during the Medieval Climate Anomaly and early Little Ice Age (AD 800–1600). *Quaternary International*, 387, 23–35. <https://doi.org/10.1016/j.quaint.2014.09.032>
 22. Hiner, Kirby, M. E., Bonuso, N., Patterson, W. P., Palermo, J., & Silveira, E. (2016). Late Holocene hydroclimatic variability linked to Pacific forcing: evidence from Abbott Lake, coastal central California. *Journal of Paleolimnology*, 56(4), 299–313. <https://doi.org/10.1007/s10933-016-9912-4>

23. Holmquist, Reynolds, L., Brown, L. N., Southon, J. R., Simms, A. R., & MacDonald, G. M. (2015). Marine Radiocarbon Reservoir Values in Southern California Estuaries: Interspecies, Latitudinal, and Interannual Variability. *Radiocarbon*, 57(3), 449–458. https://doi.org/10.2458/azu_rc.57.18389
24. Hood-Nowotny, & Knols, B. G. . (2007). Stable isotope methods in biological and ecological studies of arthropods. *Entomologia Experimentalis et Applicata*, 124(1), 3–16. <https://doi.org/10.1111/j.1570-7458.2007.00572.x>
25. Irwin, H., Curtis, C. (1977). Isotopic evidence for source of diagenetic carbonates formed during burial of organic-rich sediments. *Nature*, 269, 209-213.
26. Jackson, & Yeats, R. S. (1982). Structural evolution of Carpinteria Basin, western Transverse Ranges, California. *AAPG Bulletin*, 66(7), 805-829. <https://doi.org/10.1306/03B5A33B-16D1-11D7-8645000102C1865D>
27. Jones & Stokes Associates, Inc. (1999). Management Plan for the Campus Lagoon at the University of California, Santa Barbara.
28. Keller, E. A. (2000). *Final Report, July 2000 Earthquake Hazard of the Santa Barbara Fold Belt, California*.
29. Keller, & Keller, V. R. (2011). Santa Barbara, land of dynamic beauty: a natural history. Santa Barbara Museum of Natural History.
30. King, B., Simms, A., Simkins, L. (2019). The Stratigraphic Architecture of Small Incised Valleys Along an Active Margin: Examples from the Oceanside Littoral Cell of the Southern California Coast. *Society for Sedimentary Geology*, 78-86. ISBN 978-565760-354-8.
31. Kirby, Poulsen, C. J., Lund, S. P., Patterson, W. P., Reidy, L., & Hammond, D. E. (2004). Late Holocene lake level dynamics inferred from magnetic susceptibility and stable oxygen isotope data: Lake Elsinore, southern California (USA). *Journal of Paleolimnology*, 31(3), 275–293. <https://doi.org/10.1023/B:JOPL.0000021710.39800.f6>
32. Kirby, Lund, S. P., Anderson, M. A., & Bird, B. W. (2007). Insolation forcing of Holocene climate change in Southern California: a sediment study from Lake Elsinore. *Journal of Paleolimnology*, 38(3), 395–417. <https://doi.org/10.1007/s10933-006-9085-7>
33. Kirby, Lund, S. P., Patterson, W. P., Anderson, M. A., Bird, B. W., Ivanovici, L., Monarrez, P., & Nielsen, S. (2010). A Holocene record of Pacific Decadal Oscillation (PDO)-related hydrologic variability in Southern California (Lake Elsinore, CA). *Journal of Paleolimnology*, 44(3), 819–839. <https://doi.org/10.1007/s10933-010-9454-0>

34. Kirby, Zimmerman, S. R. H., Patterson, W. P., & Rivera, J. J. (2012). A 9170-year record of decadal-to-multi-centennial scale pluvial episodes from the coastal Southwest United States: a role for atmospheric rivers? *Quaternary Science Reviews*, 46, 57–65. <https://doi.org/10.1016/j.quascirev.2012.05.008>
35. Kirby, Feakins, S. J., Hiner, C. A., Fantozzi, J., Zimmerman, S. R. H., Dingemans, T., & Mensing, S. A. (2014). Tropical Pacific forcing of Late-Holocene hydrologic variability in the coastal southwest United States. *Quaternary Science Reviews*, 102, 27–38. <https://doi.org/10.1016/j.quascirev.2014.08.005>
36. Kirby, Knell, E. J., Anderson, W. T., Lachniet, M. S., Palermo, J., Eeg, H., Lucero, R., Murrieta, R., Arevalo, A., Silveira, E., & Hiner, C. A. (2015). Evidence for insolation and Pacific forcing of late glacial through Holocene climate in the Central Mojave Desert (Silver Lake, CA). *Quaternary Research*, 84(2), 174–186. <https://doi.org/10.1016/j.yqres.2015.07.003>
37. Kirkels, De Boer, H. J., Concha Hernández, P., Martes, C. R. T., Van Der Meer, M. T. J., Basu, S., Usman, M. O., Peterse, F., Organic geochemistry, Global Ecology and Sustainability, Environmental Sciences, & Organic geochemistry & molecular biogeology. (2022). Carbon isotopic ratios of modern C3 and C4 vegetation on the Indian peninsula and changes along the plant–soil–river continuum – implications for vegetation reconstructions. *Biogeosciences*, 19(17), 4107–4127. <https://doi.org/10.5194/bg-19-4107-2022>
38. Kohn, & Cerling, T. E. (2002). Stable isotope compositions of biological apatite. *Reviews in Mineralogy and Geochemistry*, 48(1), 455–488. <https://doi.org/10.2138/rmg.2002.48.12>
39. Lambeck, Rouby, H., Purcell, A., Sun, Y., & Sambridge, M. (2014). Sea level and global ice volumes from the Last Glacial Maximum to the Holocene. *Proceedings of the National Academy of Sciences - PNAS*, 111(43), 15296–15303. <https://doi.org/10.1073/pnas.1411762111>
40. Lee, T., Rand, D., Lisiecki, L. E., Gebbie, G., and Lawrence, C.: Bayesian age models and stacks: combining age inferences from radiocarbon and benthic $\delta^{18}\text{O}$ stratigraphic alignment, *Clim. Past*, 19, 1993–2012, <https://doi.org/10.5194/cp-19-1993-2023>, 2023.
41. Lenders, Dey, A., Bomans, P.H. H., Spielmann, J., Hendrix, M. M. R. M., de With, G., Meldrum, F. C., Harder, S., & Sommerdijk, N. A. J. M. (2012). High-Magnesian Calcite Mesocrystals: A Coordination Chemistry Approach. *Journal of the American Chemical Society*, 134(2), 1367–1373. <https://doi.org/10.1021/ja210791p>

42. Machel. (2004). Concepts and models of dolomitization: a critical reappraisal. *The Geometry and Petrogenesis of Dolomite Hydrocarbon Reservoirs*, 235(1), 7–63. <https://doi.org/10.1144/GSL.SP.2004.235.01.02>
43. Masson-Delmotte, V. M. Schulz, A. Abe-Ouchi, J. Beer, A. Ganopolski, J.F. González Rouco, E. Jansen, K. Lambeck, J. Luterbacher, T. Naish, T. Osborn, B. Otto-Bliesner, T. Quinn, R. Ramesh, M. Jojas, X. Shao and A. Timmermann, 2013: Information from Paleoclimate Archives. In: *Climate Change 2013: The Physical Science Basis. Contribution of Working Group I to the Fifth Assessment Report of the Intergovernmental Panel on Climate Change* [Stocker, T.F., D. Qin, G.-K. Plattner, M. Tignor, S.K. Allen, J. Boshung, A. Nauels, Y. Xia, V. Bex and P.M. Midgley (eds.)]. Cambridge University Press, Cambridge, United Kingdom and New York, NY, USA.
44. Masters. (2006). Holocene sand beaches of southern California: ENSO forcing and coastal processes on millennial scales. *Palaeogeography, Palaeoclimatology, Palaeoecology*, 232(1), 73–95. <https://doi.org/10.1016/j.palaeo.2005.08.010>
45. Mensing, Sharpe, S. E., Tunno, I., Sada, D. W., Thomas, J. M., Starratt, S., & Smith, J. (2013). The Late Holocene Dry Period: multiproxy evidence for an extended drought between 2800 and 1850 cal yr BP across the central Great Basin, USA. *Quaternary Science Reviews*, 78, 266–282. <https://doi.org/10.1016/j.quascirev.2013.08.010>
46. Meyers. (1994). Preservation of elemental and isotopic source identification of sedimentary organic matter. *Chemical Geology*, 114(3), 289–302. [https://doi.org/10.1016/0009-2541\(94\)90059-0](https://doi.org/10.1016/0009-2541(94)90059-0)
47. Morel, Morell, K. D., Keller, E. A., & Rittenour, T. M. (2021). Quaternary chronology and rock uplift recorded by marine terraces, Gaviota Coast, Santa Barbara County, California, USA. *Geological Society of America Bulletin*. <https://doi.org/10.1130/B35609.1>
48. Moy, Seltzer, G. O., Rodbell, D. T., & Anderson, D. M. (2002). Variability of El Niño/Southern Oscillation activity at millennial timescales during the Holocene epoch. *Nature (London)*, 420(6912), 162–165. <https://doi.org/10.1038/nature01194>
49. Nelson, A. R. (1992). Holocene Tidal-Marsh Stratigraphy in South-Central Oregon—Evidence for Localized Sudden Submergence in the Cascadia Subduction Zone. *Quaternary Coasts of the United States: Marine and Lacustrine Systems*.
50. Nelson, Shennan, I., & Long, A. J. (1996). Identifying coseismic subsidence in tidal-wetland stratigraphic sequences at the Cascadia subduction zone of western North America. *Journal of Geophysical Research*, 101(B3), 6115–6135. <https://doi.org/10.1029/95JB01051>

51. Nelson, Ota, Y., Umitsu, M., Kashima, K., & Matsushima, Y. (1998). Seismic or hydrodynamic control of rapid late-Holocene sea-level rises in southern coastal Oregon, USA? *Holocene (Sevenoaks)*, 8(3), 287–299. <https://doi.org/10.1191/095968398668600476>
52. Nelson. (2018). *Late Pleistocene to Holocene environmental history of Devereux Slough*. ProQuest Dissertations Publishing.
53. O’Leary. (1988). Carbon isotopes in photosynthesis. *Bioscience*, 38(5), 328–336. <https://doi.org/10.2307/1310735>
54. Osleger. (2018). *Estuarine Response to Disturbance: A Holocene Record of Storm Episodes and Seismicity as Preserved in Coastal Systems*. ProQuest Dissertations Publishing.
55. Paul, Wronkiewicz, D. J., & Mormile, M. R. (2017). Impact of elevated CO₂ concentrations on carbonate mineral precipitation ability of sulfate-reducing bacteria and implications for CO₂ sequestration. *Applied Geochemistry*, 78(C), 250–271. <https://doi.org/10.1016/j.apgeochem.2017.01.010>
56. P. R. Vail, R. M. Mitchum, Jr., S. Thompson, III, 1977. "Seismic Stratigraphy and Global Changes of Sea Level, Part 3: Relative Changes of Sea Level from Coastal Onlap", *Seismic Stratigraphy — Applications to Hydrocarbon Exploration*, Charles E. Payton
57. Purgstaller, Mavromatis, V., Goetschl, K. E., Steindl, F. R., & Dietzel, M. (2021). Effect of temperature on the transformation of amorphous calcium magnesium carbonate with near-dolomite stoichiometry into high Mg-calcite. *CrystEngComm*, 23(9), 1969–1981. <https://doi.org/10.1039/d0ce01679a>
58. Rein, Lückge, A., Reinhardt, L., Sirocko, F., Wolf, A., & Dullo, W.-C. (2005). El Niño variability off Peru during the last 20,000 years. *Paleoceanography*, 20(4), PA4003–n/a. <https://doi.org/10.1029/2004PA001099>
59. Reis, Erhardt, A. M., McGlue, M. M., & Waite, L. (2019). Evaluating the effects of diagenesis on the $\delta^{13}\text{C}$ and $\delta^{18}\text{O}$ compositions of carbonates in a mud-rich depositional environment: A case study from the Midland Basin, USA. *Chemical Geology*, 524, 196–212. <https://doi.org/10.1016/j.chemgeo.2019.06.021>
60. Reynolds, & Simms, A. R. (2015). Late Quaternary relative sea level in Southern California and Monterey Bay. *Quaternary Science Reviews*, 126, 57–66. <https://doi.org/10.1016/j.quascirev.2015.08.003>
61. Reynolds, Simms, A. R., Rockwell, T. K., Yokoyama, Y., Miyairi, Y., & Hangsterfer, A. (2022). Sedimentary response of a structural estuary to Holocene coseismic

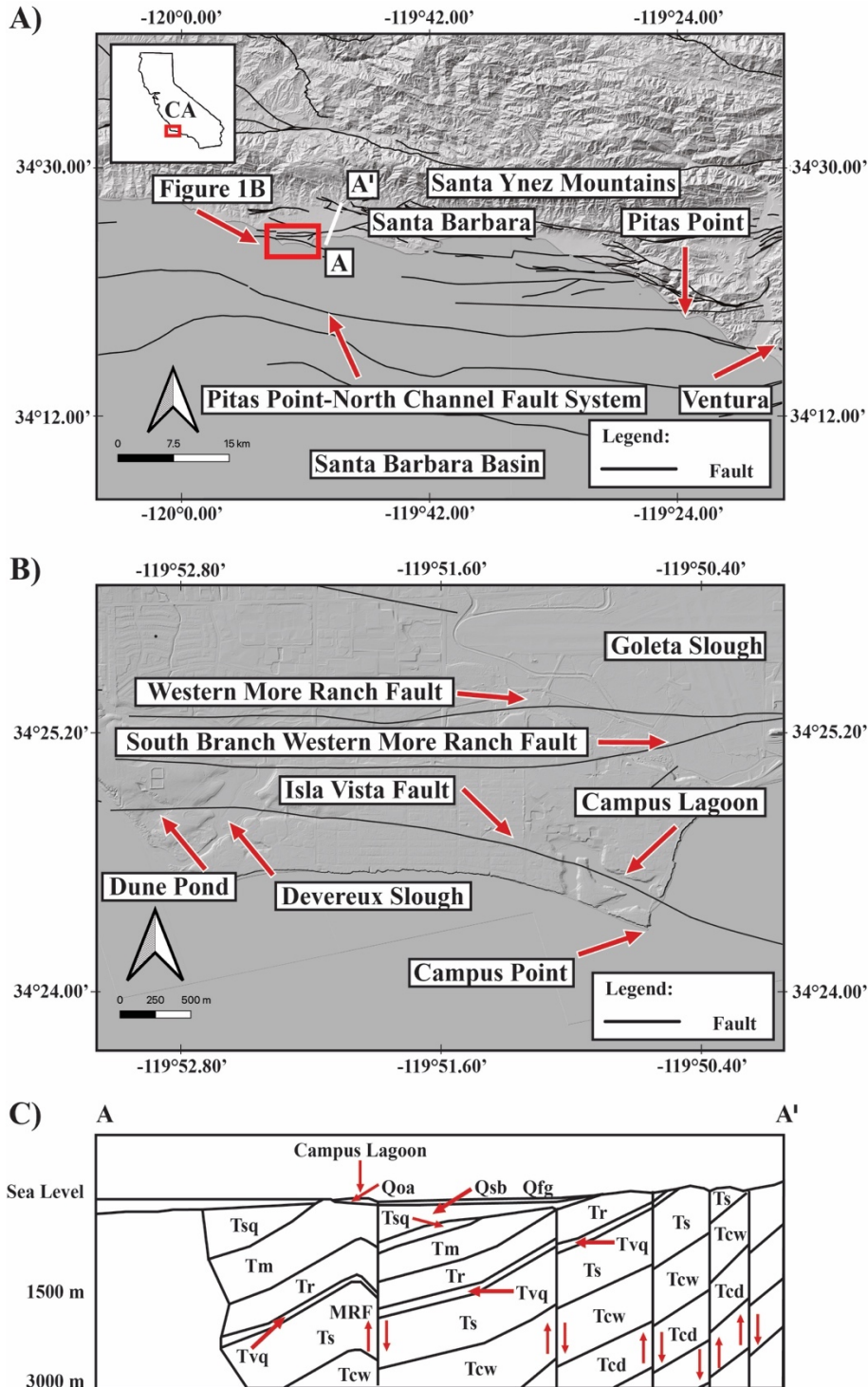
- subsidence. *Geological Society of America Bulletin*, 134(7-8), 2037–2050.
<https://doi.org/10.1130/B35827.1>
62. Ries, Ghazaleh, M. N., Connolly, B., Westfield, I., & Castillo, K. D. (2016). Impacts of seawater saturation state ($\Omega_A=0.4-4.6$) and temperature (10, 25°C) on the dissolution kinetics of whole-shell biogenic carbonates. *Geochemica et Cosmochimica Acta*, 192, 318-337. <https://doi.org/10.1016/j.gca.2016.07.001>
63. R. M. Mitchum, Jr., P. R. Vail, J. B. Sangree, 1977. “Seismic Stratigraphy and Global Changes of Sea Level, Part 6: Stratigraphic Interpretation of Seismic Reflection Patterns in Depositional Sequences”. *Seismic Stratigraphy— Applications to Hydrocarbon Exploration*, Charles E. Payton
64. Robert L. Folk. (1974). The Natural History Of Crystalline Calcium Carbonate: Effect of Magnesium Content And Salinity. *Journal of Sedimentary Research*, 44. <https://doi.org/10.1306/74D72973-2B21-11D7-8648000102C1865D>
65. Rockwell, T. K., Johnson, D. J., & Patterson, R. H. (1992). Ages and Deformation of Marine Terraces Between Point Conception and Gaviota, Western Transverse Ranges, California. *Society for Sedimentary Geology*, 48.
66. Rockwell, Clark, K., Gamble, L., Oskin, M. E., Haaker, E. C., & Kennedy, G. L. (2016). Large Transverse Range earthquakes cause coastal upheaval near Ventura, Southern California. *Bulletin of the Seismological Society of America*, 106(6), 2706–2720. <https://doi.org/10.1785/0120150378>
67. Roman, A. (2014). Holocene environmental history of Campus Lagoon, UC Santa Barbara. Undergraduate senior thesis.
68. Sandweiss, Richardson, J. B., Reitz, E. J., Rollins, H. B., & Maasch, K. A. (1996). Geoarchaeological Evidence from Peru for a 5000 Years B.P. Onset of El Niño. *Science (American Association for the Advancement of Science)*, 273(5281), 1531–1533. <https://doi.org/10.1126/science.273.5281.1531>
69. Santa Barbara South Coast Chamber of Commerce.
<https://sbscchamber.com/community/community-profile/>
70. SCEDC (2013): Southern California Earthquake Center. Caltech. Dataset.
doi:10.7909/C3WD3xH1
71. Shennan, Garrett, E., & Barlow, N. (2016). Detection limits of tidal-wetland sequences to identify variable rupture modes of megathrust earthquakes. *Quaternary Science Reviews*, 150, 1-30. <https://doi.org/10.1016/j.quascirev.2016.08.003>
72. Simms, Reynolds, L. C., Bentz, M., Roman, A., Rockwell, T., & Peters, R. (2016). Tectonic Subsidence of California Estuaries Increases Forecasts of Relative Sea-

- Level Rise. *Estuaries and Coasts*, 39(6), 1571–1581. <https://doi.org/10.1007/s12237-016-0105-1>
73. Sperazza, Moore, J. N., & Hendrix, M. S. (2004). High-resolution particle size analysis of naturally occurring very fine-grained sediment through laser diffractometry. *Journal of Sedimentary Research*, 74(5), 736–743. <https://doi.org/10.1306/031104740736>
74. Stine. (1990). Late holocene fluctuations of Mono Lake, eastern California. *Paleogeography, Palaeoclimatology, Palaeoecology*, 78(3), 333-381. [https://doi.org/10.1016/0031-0182\(90\)90221-R](https://doi.org/10.1016/0031-0182(90)90221-R)
75. Stine. (1994). Extreme and persistent drought in California and Patagonia during mediaeval time. *Nature (London)*, 369(6481), 546-549. <https://doi.org/10.1038/369546a0>
76. Stiros, Arnold, M., Pirazzoli, P. A., Laborel, J., Laborel, F., & Papageorgiou, S. (1992). Historical coseismic uplift on Euboea Island, Greece. *Earth and Planetary Science Letters*, 108(1), 109–117. [https://doi.org/10.1016/0012-821X\(92\)90063-2](https://doi.org/10.1016/0012-821X(92)90063-2)
77. Stuiver, & Reimer, P. J. (1993). Extended 14C Data Base and Revised CALIB 3.0 14C Age Calibration Program. *Radiocarbon*, 35(1), 215-230. <https://doi.org/10.1017/S0033822200013904>
78. Swart. (2015). The geochemistry of carbonate diagenesis: The past, present and future. *Sedimentology*, 62(5), 1233–1304. <https://doi.org/10.1111/sed.12205>
79. Washington Department of Fish and Wildlife. (2023). Native littleneck clam. <https://wdfw.wa.gov/species-habitats/species/leukoma-staminea>.
80. Wells, & Coppersmith, K. J. (1994). New empirical relationships among magnitude, rupture length, rupture width, rupture area, and surface displacement. *Bulletin of the Seismological Society of America*, 84(4), 974–1002.
81. Woodroffe, Beech, M. R., & Gagan, M. K. (2003). Mid-late Holocene El Niño variability in the equatorial Pacific from coral microatolls. *Geophysical Research Letters*, 30(7), 1358–n/a. <https://doi.org/10.1029/2002GL015868>
82. Zhou, & Chafetz, H. S. (2010). Pedogenic carbonates in Texas: stable-isotope distributions and their implications for reconstructing region-wide paleoenvironments. *Journal of Sedimentary Research*, 80(2), 137-150. <https://doi.org/10.2110/jsr.2010.018>

REMOTE SENSING CITATIONS:

1. Source for USGS Quaternary Faults used in ArcGIS (<https://www.arcgis.com/apps/webappviewer/index.html?id=5a6038b3a1684561a9b0aadf88412fcf>).
2. Source for CA state border outline: United States. Bureau of Transportation Statistics. United States. Bureau of the Census. Geography Division. (2014). State Boundaries: United States and Territories, 2012. [Shapefile]. United States. Bureau of Transportation Statistics. Retrieved from <https://earthworks.stanford.edu/catalog/stanford-vt021tk4894>
3. Source for digital elevation models: United States Geological Survey National Map 3DEM.

8. FIGURES



(A) Map of Santa Barbara coastal plain, (B) close-up of Campus Lagoon region, and (C) generalized geologic cross section of the Santa Barbara region modified after Dibblee (1966). Labeled Units / Faults: Qsb (Santa Barbara Formation), Qfg (Fanglomerate Formation), Qoa (Quaternary Marine Terrace), MRF (More Ranch Fault), Tsq (Sisquoc Formation), Tm (Monterey Formation), Tr (Rincon Formation), Tvq (Vaqueros Formation), Ts (Sespe Formation), Tcw (Coldwater Formation), Tcd (Cozy Del Shale).

Figure 1: (A-C) Geologic overview of Santa Barbara region.



Figure 2: Views of Campus Lagoon towards the (A) north, (B) southeast, and (C) south.

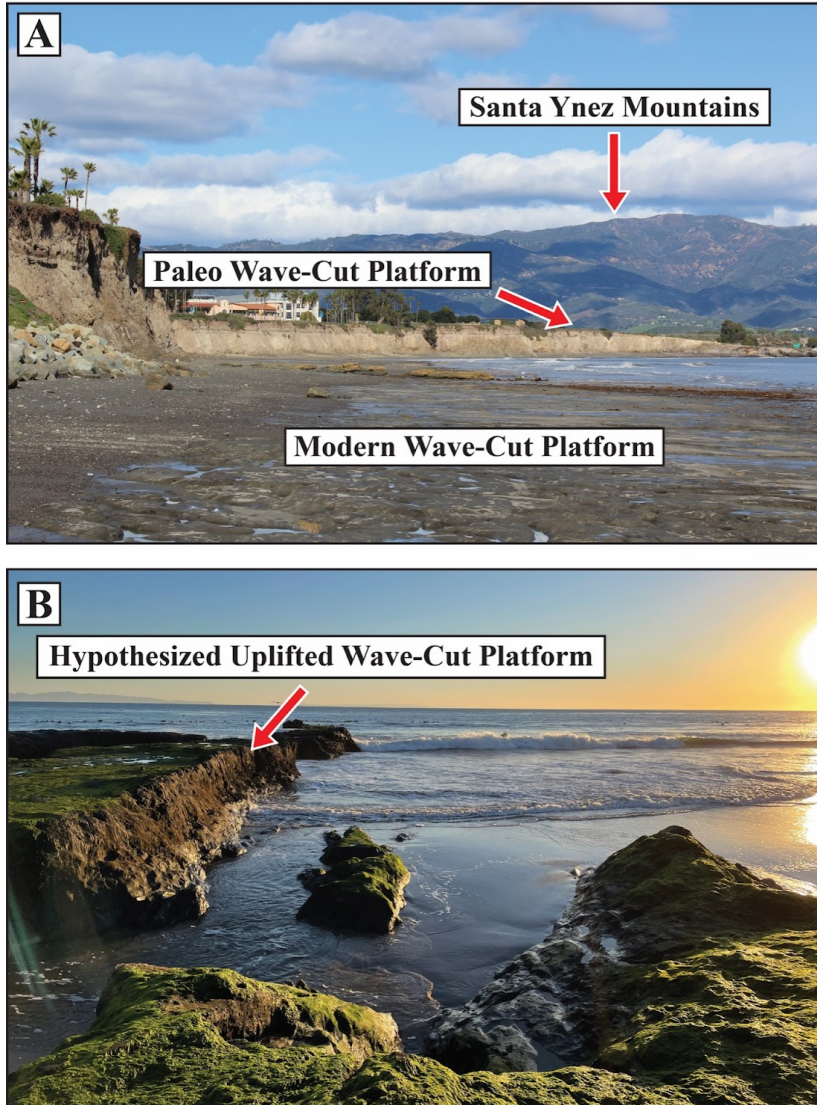
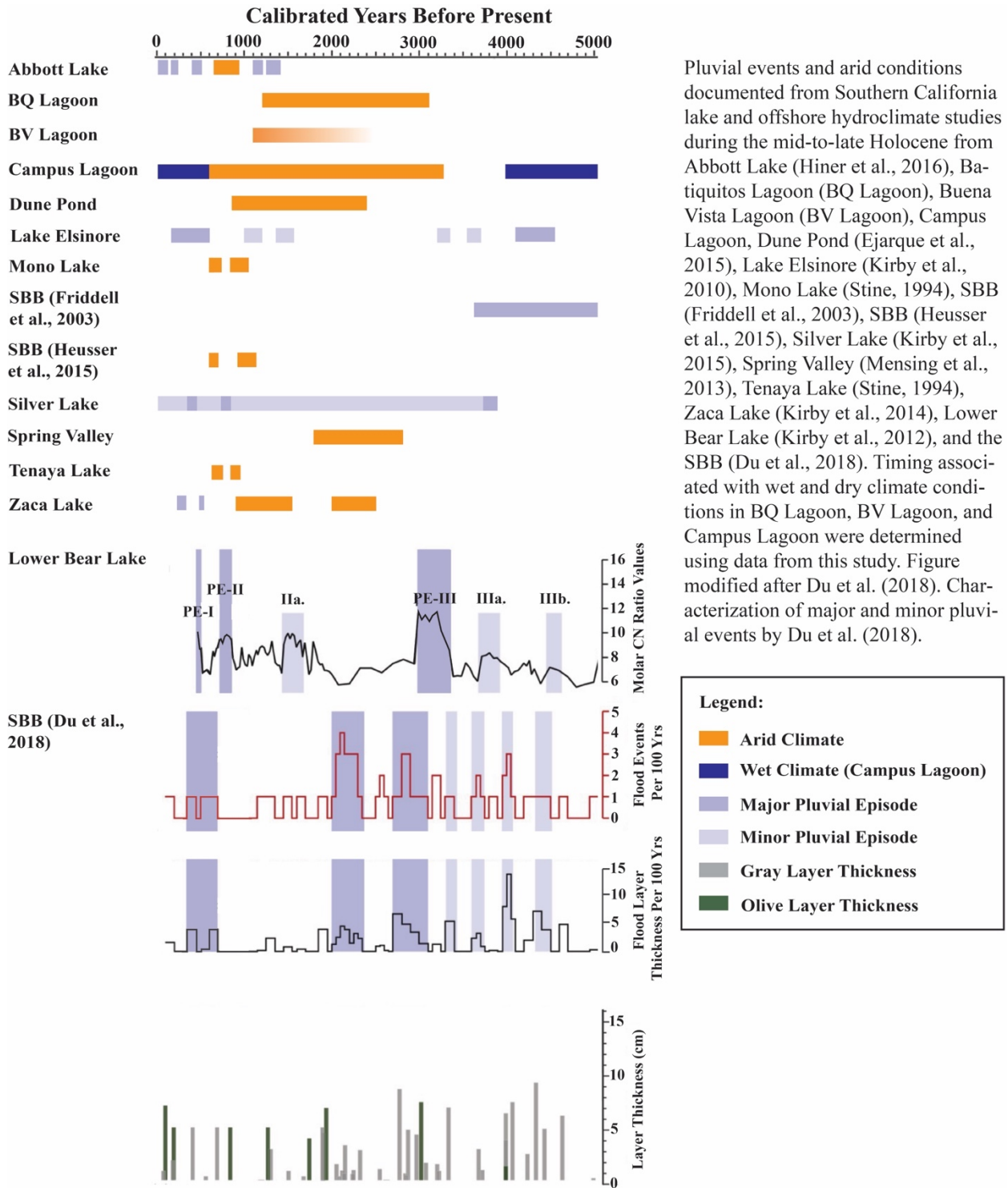


Figure 3: (A) Marine terrace at the UCSB campus, and (B) a ~2 m high wave-cut platform at the southern edge of the UCSB Campus (Campus Point), which is also adjacent to Campus Lagoon. Gurrola et al. (2014) hypothesized the wave-cut platform at Campus Point was possibly uplifted by a large magnitude earthquake.



Pluvial events and arid conditions documented from Southern California lake and offshore hydroclimate studies during the mid-to-late Holocene from Abbott Lake (Hiner et al., 2016), Batiqitos Lagoon (BQ Lagoon), Buena Vista Lagoon (BV Lagoon), Campus Lagoon, Dune Pond (Ejarque et al., 2015), Lake Elsinore (Kirby et al., 2010), Mono Lake (Stine, 1994), SBB (Friddell et al., 2003), SBB (Heusser et al., 2015), Silver Lake (Kirby et al., 2015), Spring Valley (Mensing et al., 2013), Tenaya Lake (Stine, 1994), Zaca Lake (Kirby et al., 2014), Lower Bear Lake (Kirby et al., 2012), and the SBB (Du et al., 2018). Timing associated with wet and dry climate conditions in BQ Lagoon, BV Lagoon, and Campus Lagoon were determined using data from this study. Figure modified after Du et al. (2018). Characterization of major and minor pluvial events by Du et al. (2018).

Figure 4: Hydroclimate studies from the western United States using lake records and offshore marine sediment cores.

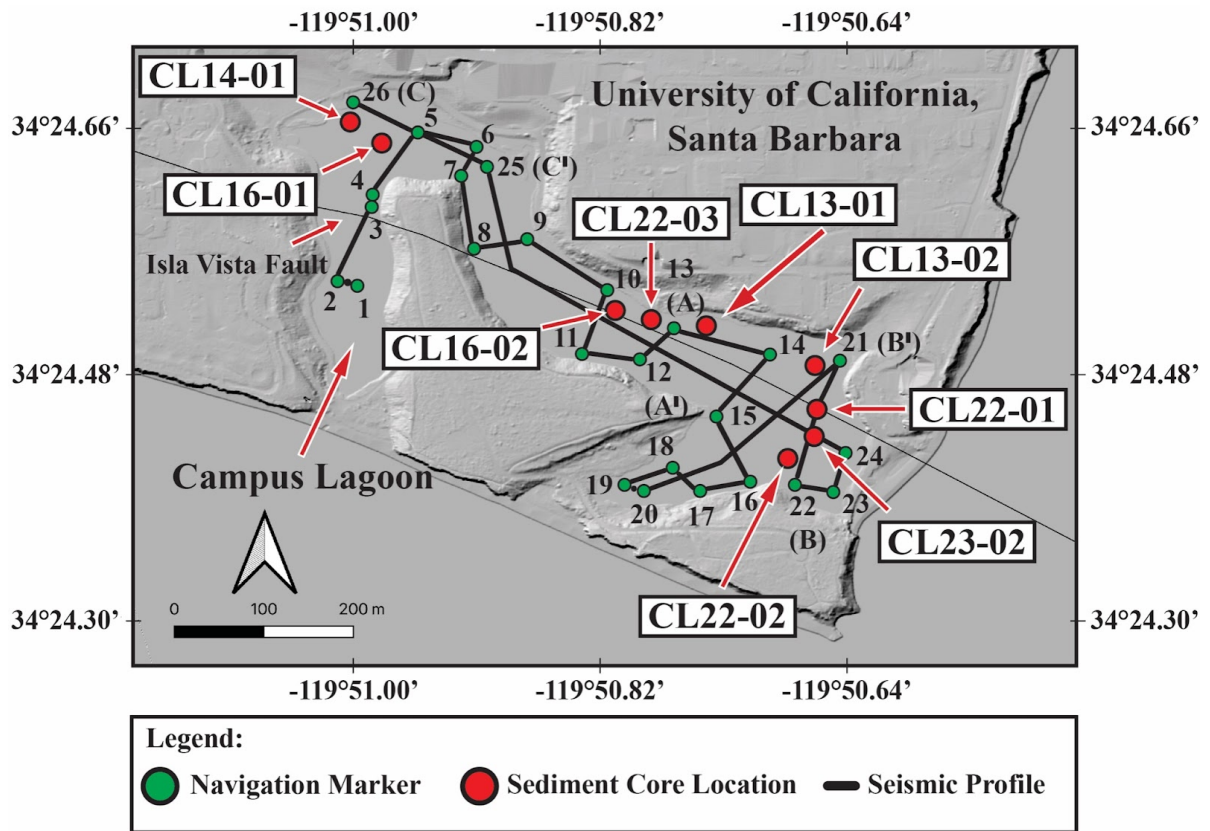


Figure 5: Map showing seismic survey conducted within Campus Lagoon and locations of sediment cores used within this study.

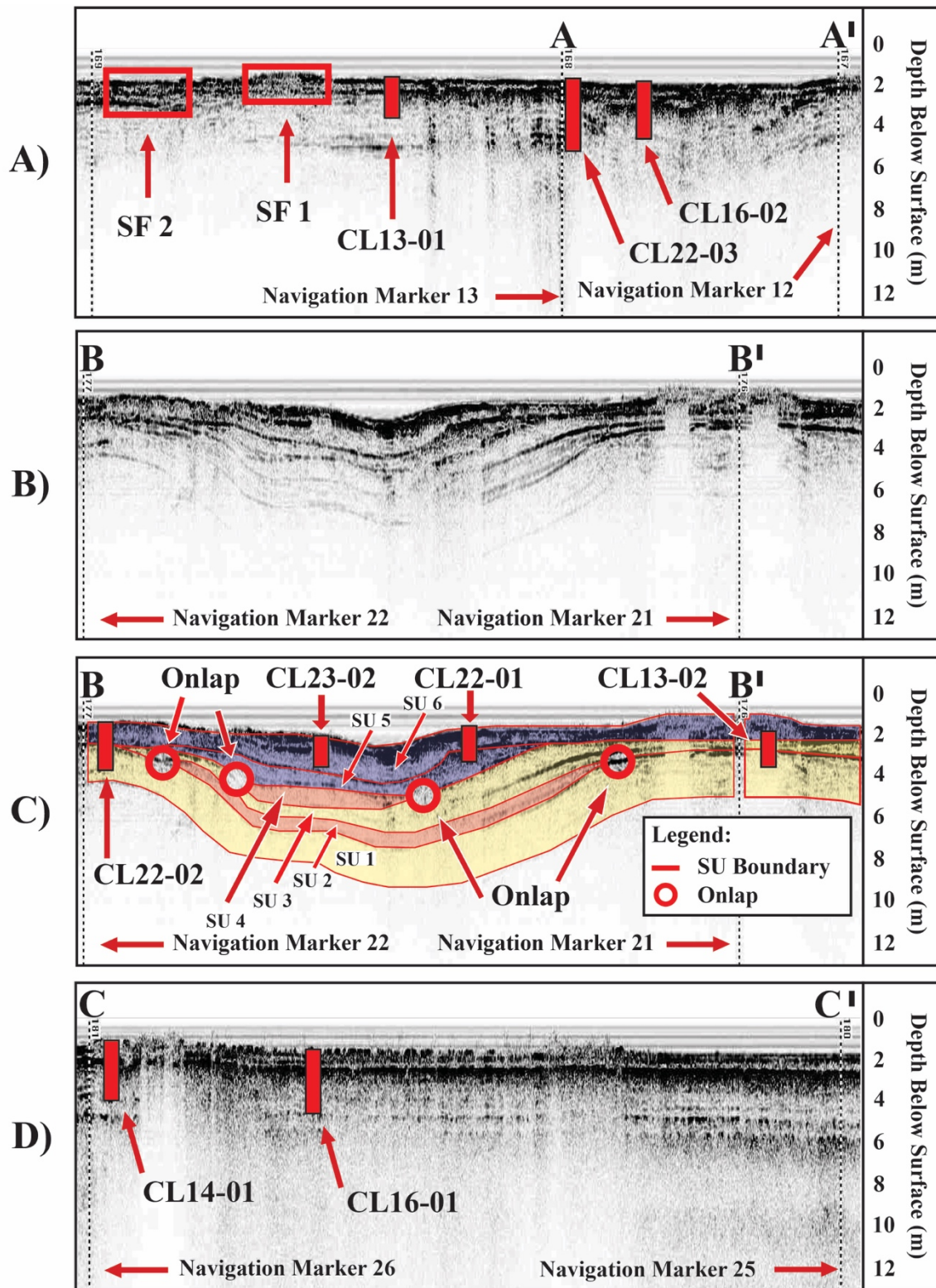
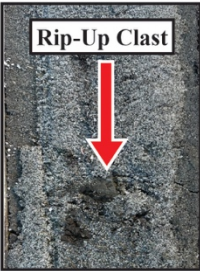




Figure 6: (A-D) Seismic profiles with sediment cores, (A) seismic facies (SF), (B) uninterpreted seismic profile showing region with downward shift in onlap, and (C) labeled seismic units (SU).

Facies	Facies Photograph	Description	Interpretation
A) Gray Sand (GS)		Coarse grained gray colored sand. Pebbles, rip-up clasts, and small shell fragments common. Organic material rare.	Intertidal region between lagoon and open-ocean. Pebbles and rip-up clasts indicate high energy environment.
B) Clayey Silt - Evaporite (CS-E)		Fine grained clayey silt gypsum lamina / displacive growth, carbonate beds, and lack of shells.	Mudflat / lower supratidal environment with limited connectivity with the open-ocean.
C) Clayey Silt (CS)		Clayey silt without evaporites. Occurs throughout UCSB Campus Lagoon. Bioturbation present in lower half of CL22-03. Ostracods commonly present within CS facies.	Mudflat / lower supratidal environment with limited connectivity with the open-ocean. Bioturbation within CS facies between 260 and 290 cm may represent central basin lagoon environment.

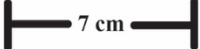





Figure 7: Sedimentary facies within sediment cores from Campus Lagoon.

Facies	Facies Photograph	Description	Interpretation
A) Clayey Silt-Shell Fragments (CS-SF)		Fine grained clayey silt matrix with fragmented shell material. Seen within CL16-01 and CL16-02.	Central basin lagoon environment.
B) Sandy Silt (SASL)		Well sorted brown / gray sands. Commonly occurs within the CS and CS-E facies. Lacks rip-up clasts, shell fragments, and small rocks. Organic material more common relative to the GS facies. Occurs in the upper 143 cm of CL22-03.	Distal sands associated with GS facies.
C) Laminated Sandy Silt (LSS)		Medium to fine grained laminated sandy silt. Lacks rip-up clasts, shell fragments, and pebbles. Contains more charcoal and wood fragments than other sand facies. Occurs solely in CL14-01.	Terrestrial input from overland flow from the northwest region of Campus Lagoon.

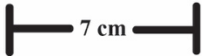


Figure 8: Sedimentary facies within sediment cores from Campus Lagoon.

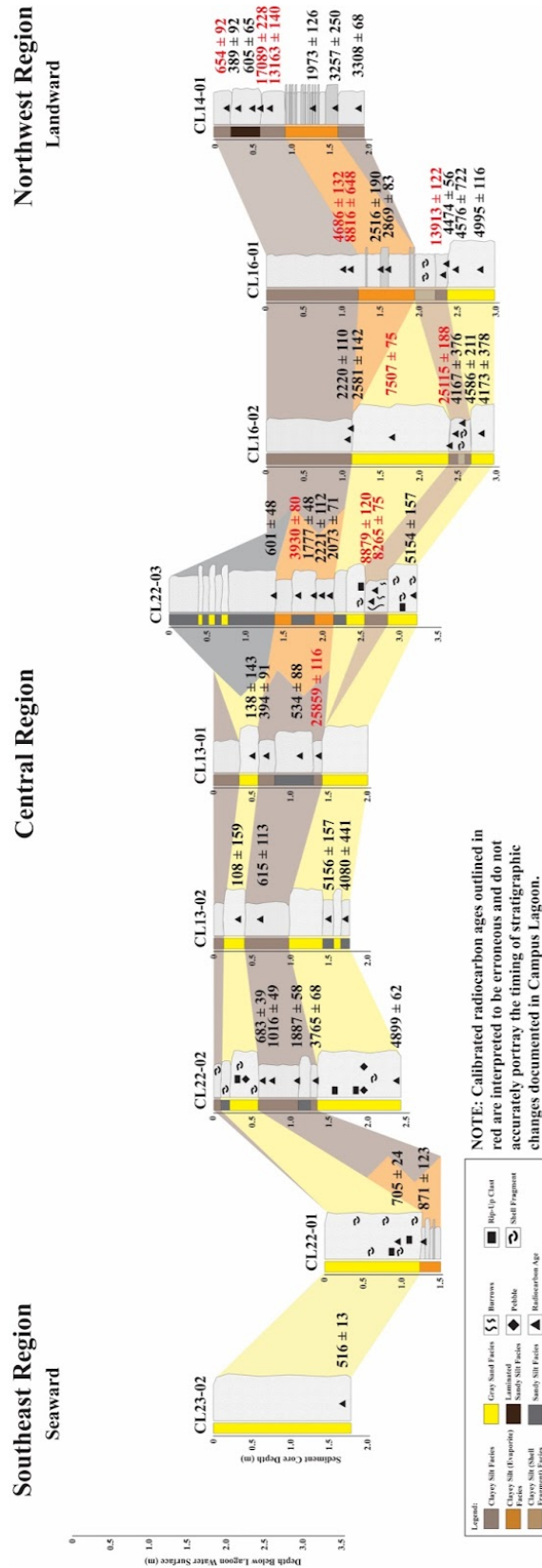


Figure 9: Correlation of sediment cores from Campus Lagoon.

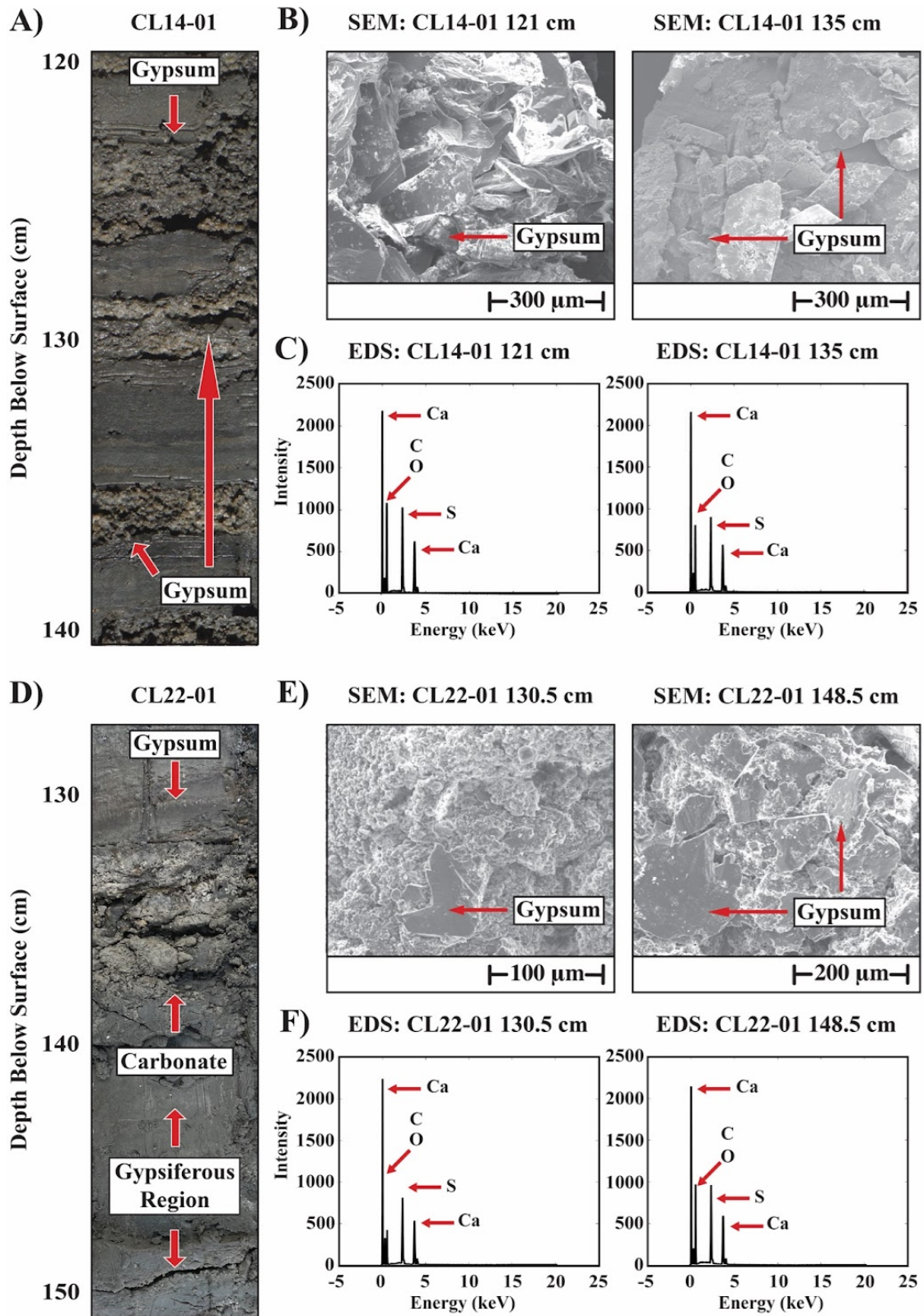


Figure 10: (A and D) Sediment core photographs and (B-C and E-F) SEM images and EDS data of gypsum lamina within CL14-01 and CL22-01.

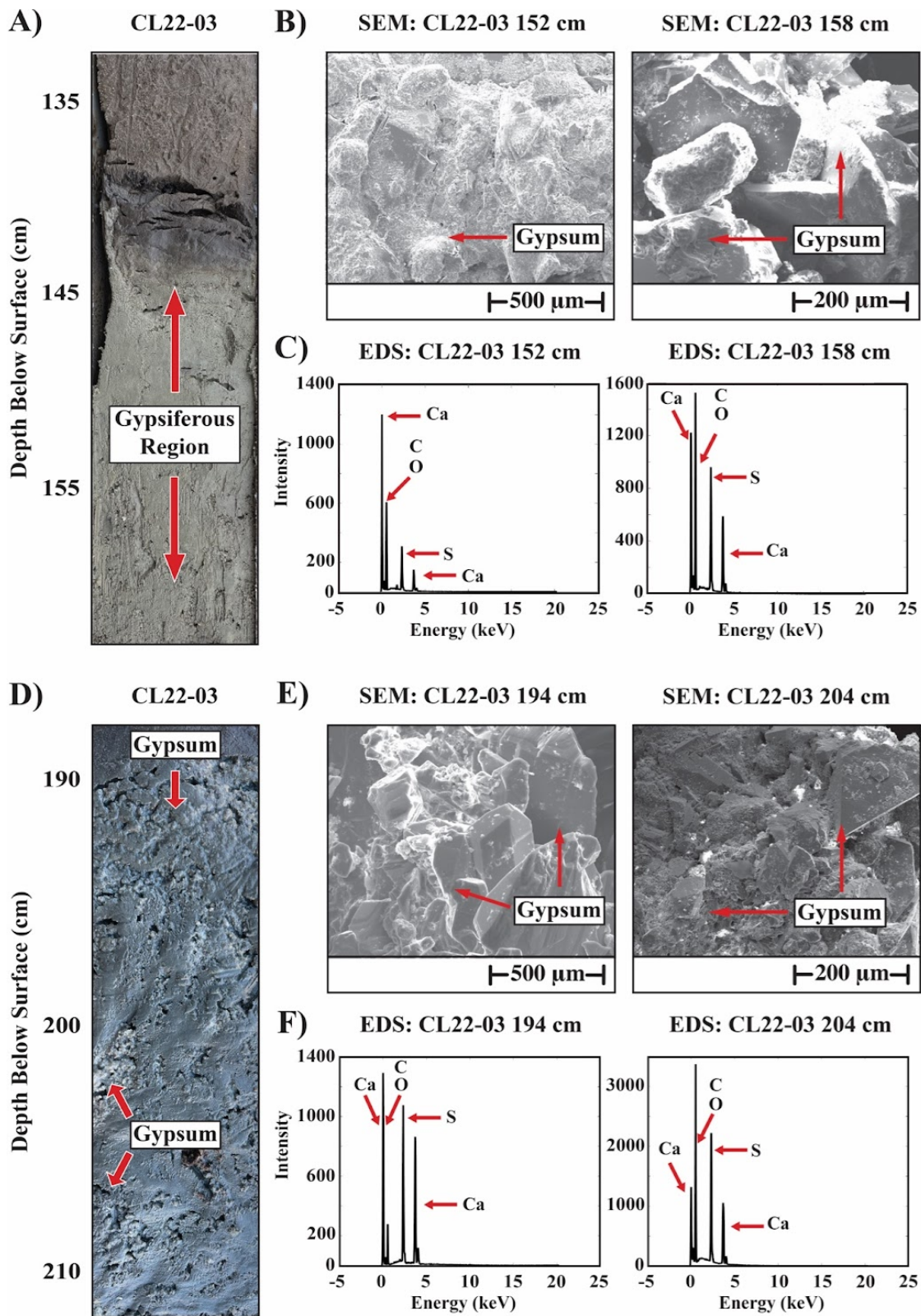


Figure 11: (A and D) Sediment core photographs and (B-C and E-F) SEM images and EDS data of gypsiferous regions within CL22-03.

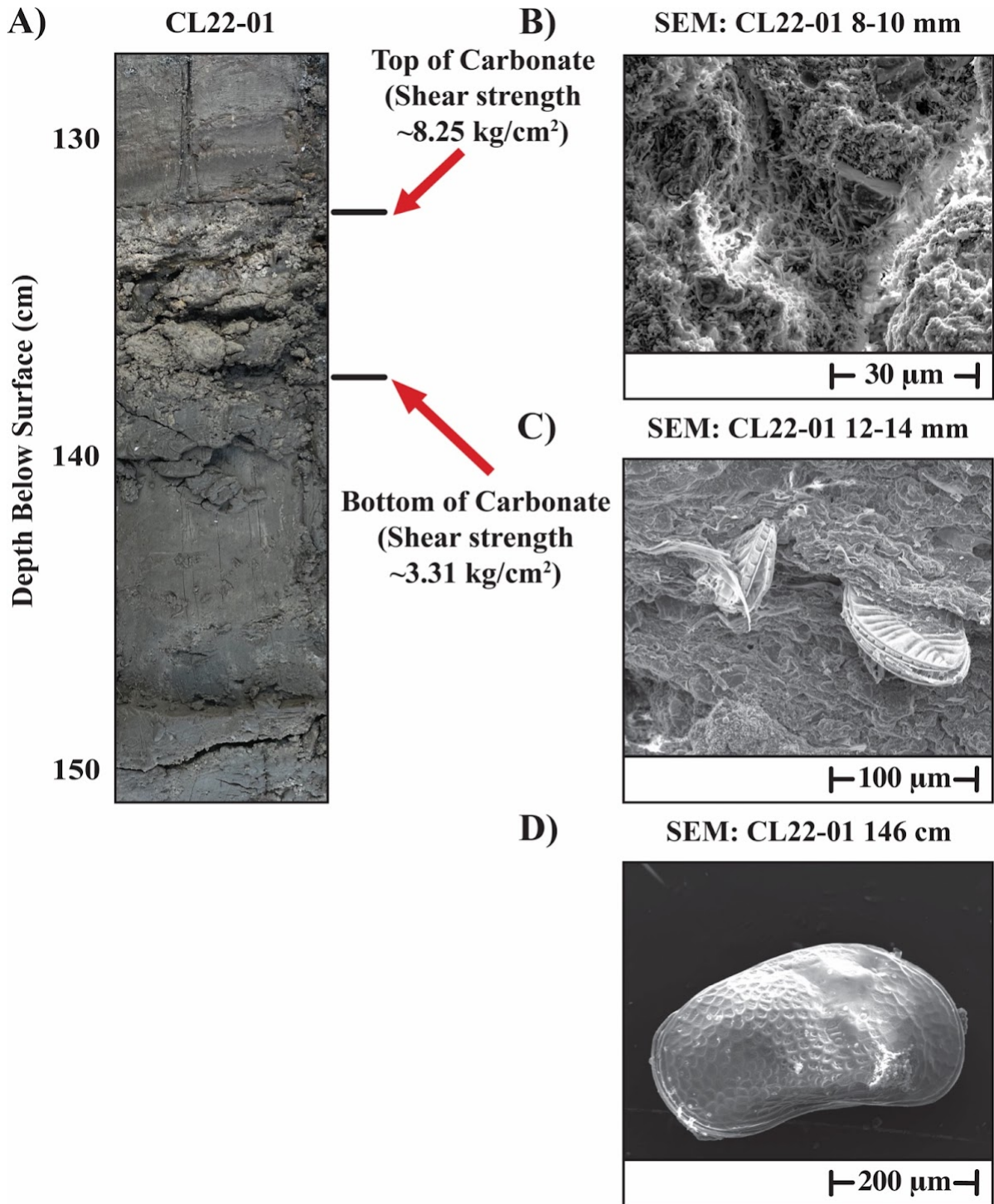


Figure 12: (A) Carbonate bed within CL22-01 and shear strength, (B) SEM image of carbonate in CL22-01 shows possible fibrous microcrystalline calcite, (C) diatoms encrusted within the carbonate bed, and (D) shows ostracod microfossil found within CS-E facies of CL22-01.

UCIAMS / D-AMS #	Sample Name	Sample Material	¹⁴ C age (BP)	±	Calibrated Years (BP)	±	Source
UCIAMS-200624	CL13-01 50 cm	Charcoal	145	30	138	143	Osleger (2018)
UCIAMS-200625	CL13-01 67 cm	Charcoal	305	20	394	91	Osleger (2018)
UCIAMS-200626	CL13-01 115 cm	Charcoal	520	25	534	88	Osleger (2018)
UCIAMS-281134	CL13-01 138 cm	Charcoal	21540	70	25859	116	This Study
D-AMS 005757	CL13-02 36 cm	Wood	117	23	108	159	Roman (2014)
UCIAMS-186414	CL13-02 60 cm	Charcoal	650	90	615	113	Osleger (2018)
UCIAMS-200629	CL13-02 150 cm	Charcoal	4530	25	5156	157	Osleger (2018)
D-AMS 005756	CL13-02 180 cm	Shell	4358	29	4080	441	Simms et al., (2016)
UCIAMS-191118	CL14-01 17 cm	Charcoal	690	30	654	92	Osleger (2018)
UCIAMS-191112	CL14-01 31 cm	Charcoal	305	30	389	92	Osleger (2018)
UCIAMS-200632	CL14-01 50 cm	Charcoal	580	20	605	65	Osleger (2018)
UCIAMS-281135	CL14-01 59 cm	Wood	14055	30	17089	228	This Study
UCIAMS-191115	CL14-01 75 cm	Charcoal	11260	70	13163	140	Osleger (2018)
UCIAMS-191116	CL14-01 131 cm	Charcoal	2035	30	1973	126	Osleger (2018)
UCIAMS-191117	CL14-01 160 cm	Charcoal	3060	80	3257	250	Osleger (2018)
UCIAMS-281136	CL14-01 194 cm	Wood	3100	20	3308	68	This Study
UCIAMS-281137	CL16-01 100 cm	Charcoal	4140	15	4686	132	This Study
UCIAMS-183702	CL16-01 115 cm	Charcoal	7930	260	8816	648	Osleger (2018)
UCIAMS-200631	CL16-01 150 cm	Charcoal	2445	45	2516	190	Osleger (2018)
UCIAMS-281138	CL16-01 162 cm	Wood	2775	20	2869	83	This Study
UCIAMS-281139	CL16-01 237 cm	Wood	11985	25	13913	122	This Study
UCIAMS-183700	CL16-01 238 cm	Charcoal	4030	15	4474	56	Osleger (2018)
UCIAMS-191111	CL16-01 250 cm	Charcoal	4080	250	4576	722	Osleger (2018)
UCIAMS-281140	CL16-01 282 cm	Wood	4415	15	4995	116	This Study
UCIAMS-281141	CL16-02 104 cm	Wood	2235	15	2220	110	This Study

Table 1: Radiocarbon (¹⁴C) age data from Campus Lagoon.

UCIAMS / D-AMS #	Sample Name	Sample Material	¹⁴ C age (BP)	±	Calibrated Years (BP)	±	Source
UCIAMS-183697	CL16-02 110 cm	Charcoal	2510	15	2581	142	Osleger (2018)
UCIAMS-200630	CL16-02 160 cm	Charcoal	6620	35	7507	75	Osleger (2018)
UCIAMS-281142	CL16-02 243 cm	Wood	20860	70	25155	188	This Study
UCIAMS-200651	CL16-02 250 cm	Shell	4470	25	4167	376	Osleger (2018)
UCIAMS-281143	CL16-02 259 cm	Wood	4095	15	4586	211	This Study
UCIAMS-183690	CL16-02 285 cm	Shell	4475	15	4173	378	Osleger (2018)
UCIAMS-272997	CL22-01 96 cm	Wood	795	15	705	24	This Study
UCIAMS-281144	CL22-01 128 cm	Wood	915	15	871	123	This Study
UCIAMS-281145	CL22-02 66 cm	Wood	765	15	683	39	This Study
UCIAMS-272998	CL22-02 77 cm	Wood	1130	15	1016	49	This Study
UCIAMS-272999	CL22-02 107 cm	Wood	1960	15	1887	58	This Study
UCIAMS-281146	CL22-02 134 cm	Wood	3495	15	3765	68	This Study
UCIAMS-281147	CL22-02 245 cm	Wood	4340	20	4899	62	This Study
UCIAMS-273000	CL22-03 138 cm	Wood	620	15	601	48	This Study
UCIAMS-281148	CL22-03 169 cm	Wood	3620	15	3930	80	This Study
UCIAMS-281149	CL22-03 188 cm	Wood	1870	15	1777	48	This Study
UCIAMS-273001	CL22-03 201 cm	Wood	2240	15	2221	112	This Study
UCIAMS-281150	CL22-03 212 cm	Wood	2110	15	2073	71	This Study
UCIAMS-273002	CL22-03 269 cm	Wood	8000	20	8879	120	This Study
UCIAMS-281151	CL22-03 275 cm	Wood	7440	20	8265	75	This Study
UCIAMS-281152	CL22-03 323 cm	Wood	4530	15	5154	157	This Study
UCIAMS-281153	CL23-02 166 cm	Wood	475	15	516	13	This Study
UCIAMS-219849	BVL11-2 167 cm	Shell	1935	15	1109	306	This Study
UCIAMS-219850	BQL11-1 106 cm	Caliche	3745	20	3242	368	This Study
UCIAMS-219851	BQL11-1 140 cm	Shell	3780	15	3284	360	This Study
UCIAMS-219852	BQL11-1 316 cm	Shell	4065	15	3640	366	This Study

Table 2: Radiocarbon (¹⁴C) age data from Campus Lagoon, Batiquitos Lagoon, and Buena Vista Lagoon.

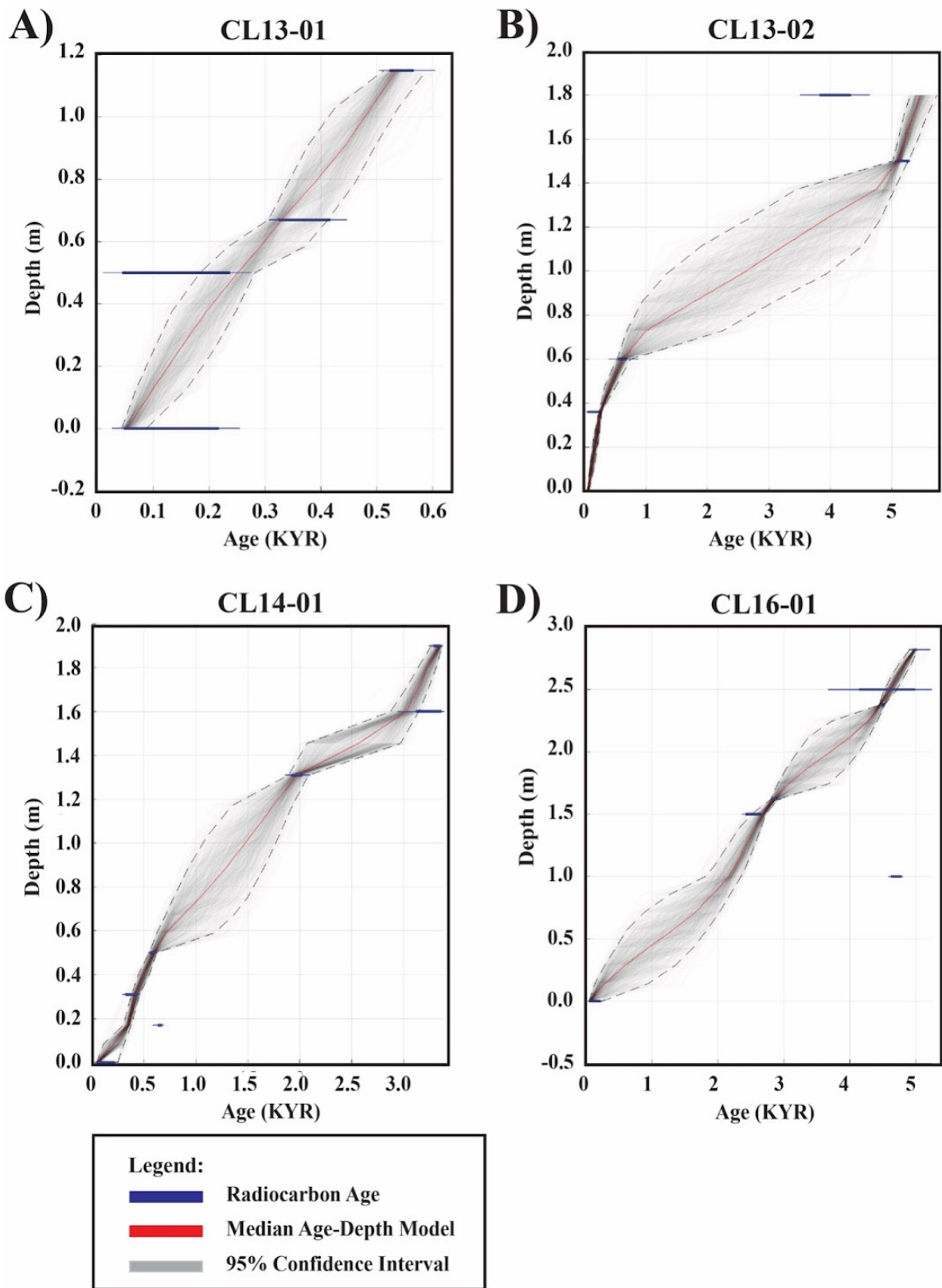


Figure 13: Age-depth models of (A) CL13-01, (B) CL13-02, (C) CL14-01, and (D) CL16-01.

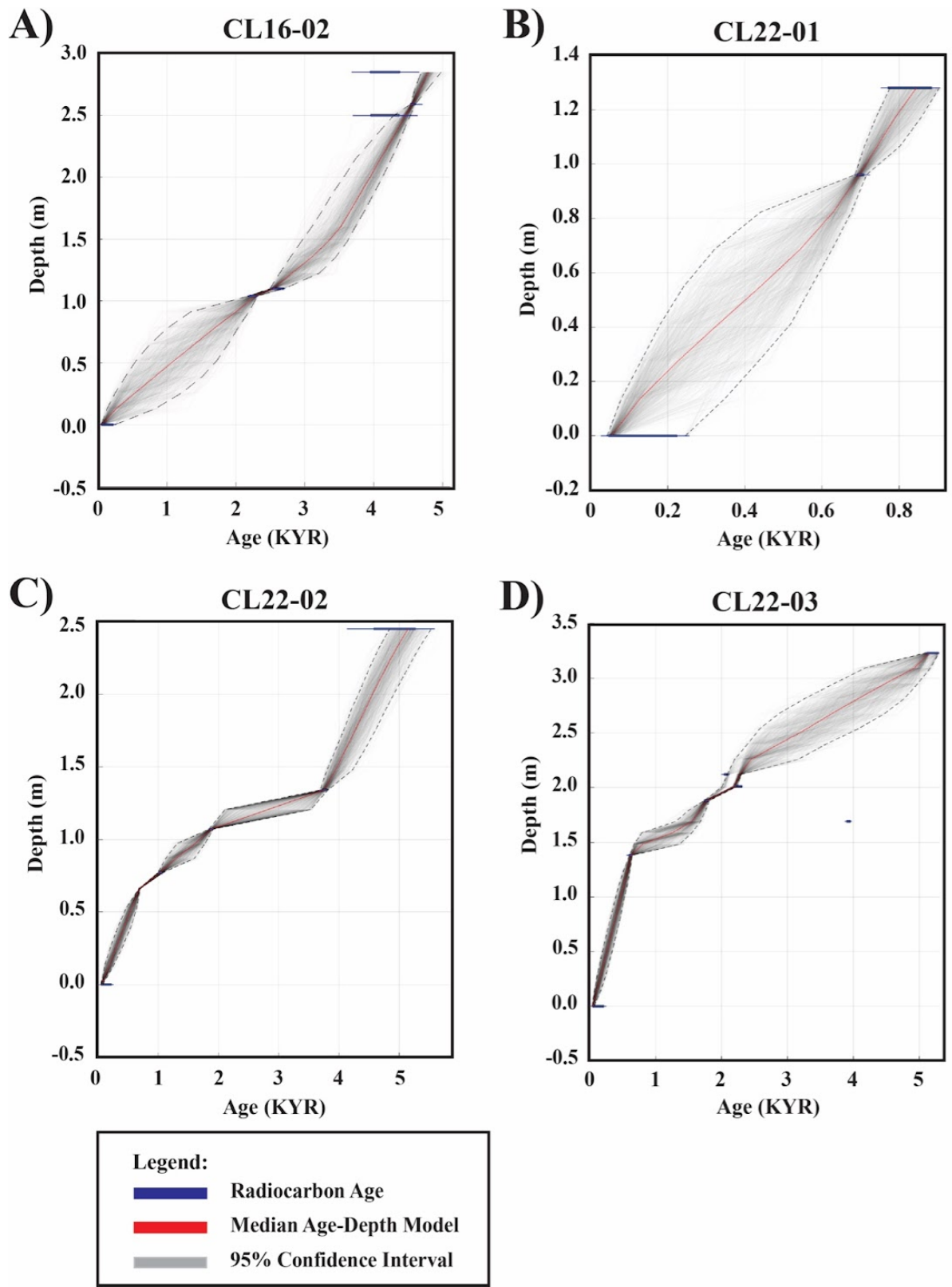


Figure 14: Age-depth models of (A) CL16-02, (B) CL22-01, (C) CL22-02, and (D) CL22-03.

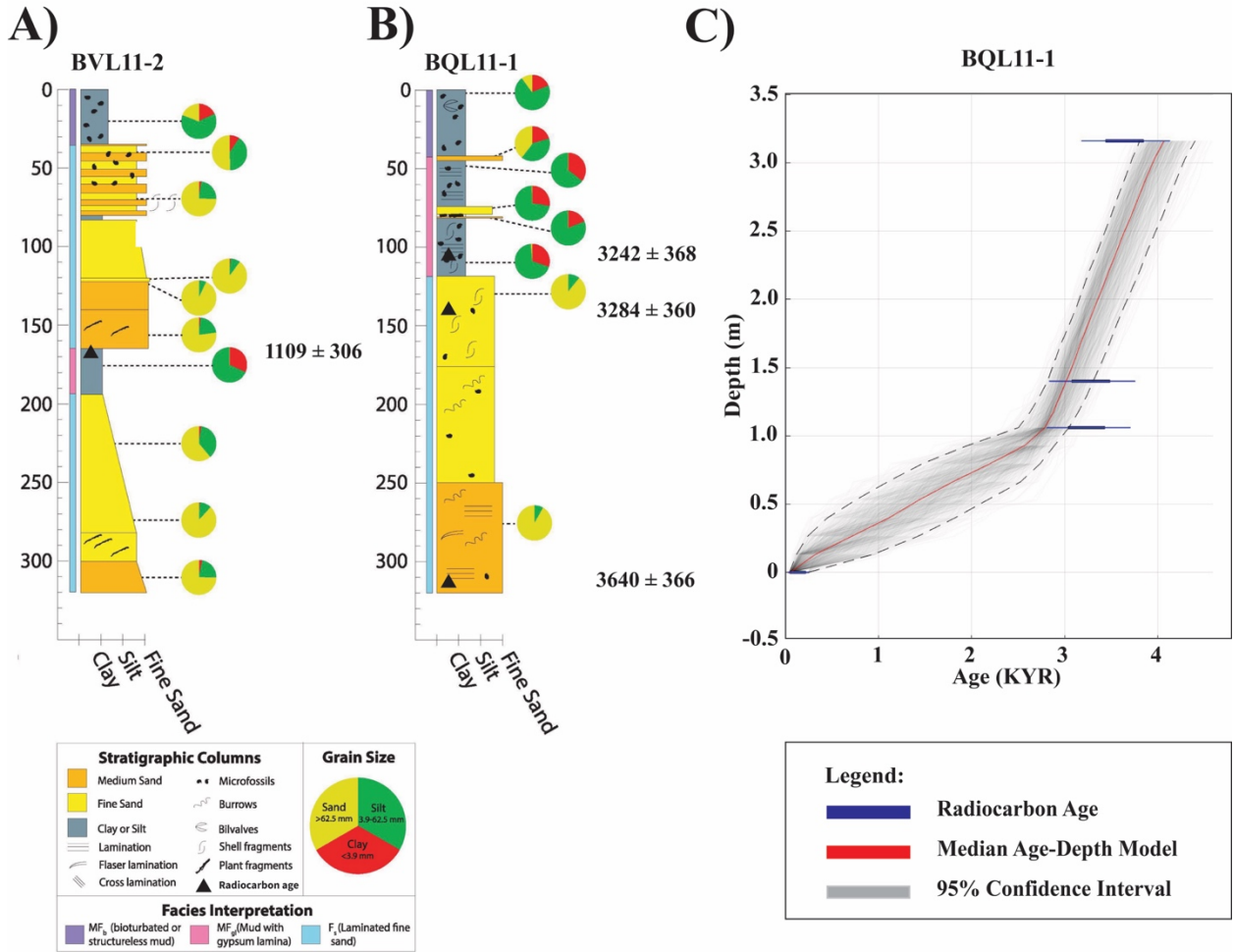


Figure 15: Sediment cores (A) BVL11-2, (B) BQL11-1, and (C) age-depth model for BQL11-1. Lithological descriptions of BVL11-2 and BQL11-1 from King et al. (2019).

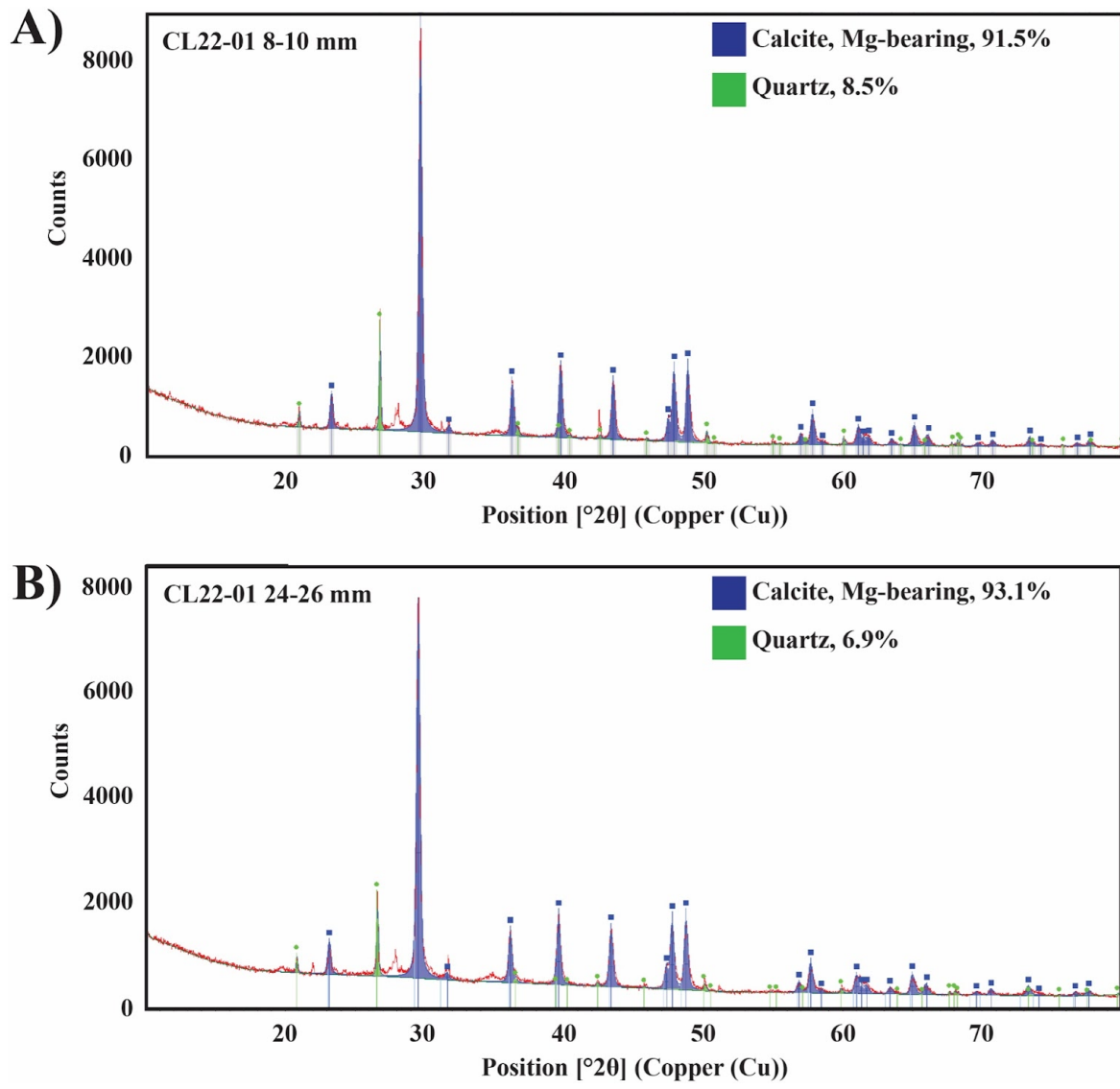


Figure 16: XRD data of (A) stratigraphic top and (B) stratigraphic bottom of carbonate bed from CL22-01.

Sample ID	Mg Wt%	Ca Wt%	Molar Ratio (Mg/Ca)	Mol% Mg	Mol% Ca	Weight Ratio (Mg)	$\delta^{18}\text{O}$ (% VPDB)	$\delta^{13}\text{C}$ (% VPDB)
CL22-01 Top	--	--	--	--	--	--	0.83	-15.44
CL 22-01 1 mm	3.03	28.26	0.18	15.18	84.82	10.62	1.62	-15.11
CL 22-01 3 mm	2.38	33.28	0.12	10.64	89.36	8.32	--	--
CL22-01 5 mm	2.27	31.91	0.12	10.61	89.39	7.95	0.94	-15.69
CL22-01 7 mm	2.21	31.39	0.12	10.52	89.48	7.75	--	--
CL22-01 9 mm	2.55	31.60	0.13	11.84	88.15	8.91	0.93	-16.07
CL22-01 11 mm	2.17	34.20	0.11	9.56	90.43	7.59	1.62	-15.86
CL22-01 17 mm	2.41	32.79	0.12	10.91	89.09	8.44	1.44	-16.02
CL22-01 19 mm	2.31	32.27	0.12	10.65	89.34	8.08	--	--
CL22-01 21 mm	2.24	32.64	0.11	10.28	89.72	7.85	1.64	-16.13
CL22-01 23 mm	2.51	33.77	0.12	11.04	88.96	8.80	--	--
CL22-01 25 mm	2.08	32.52	0.11	9.64	90.36	7.28	1.15	-16.24
CL22-01 27 mm	2.26	33.98	0.11	9.99	90.01	7.92	--	--
CL22-01 29 mm	2.51	31.42	0.13	11.74	88.26	8.78	1.35	-16.1
CL22-01 32 mm	--	--	--	--	--	--	1.35	-16.11
CL22-01 Bottom	--	--	--	--	--	--	1.14	-16.12

Table 3: Electron probe microanalysis (EPMA) data and stable isotopic ($\delta^{18}\text{O}$ and $\delta^{13}\text{C}$) signatures of CL22-01 calcite bed.

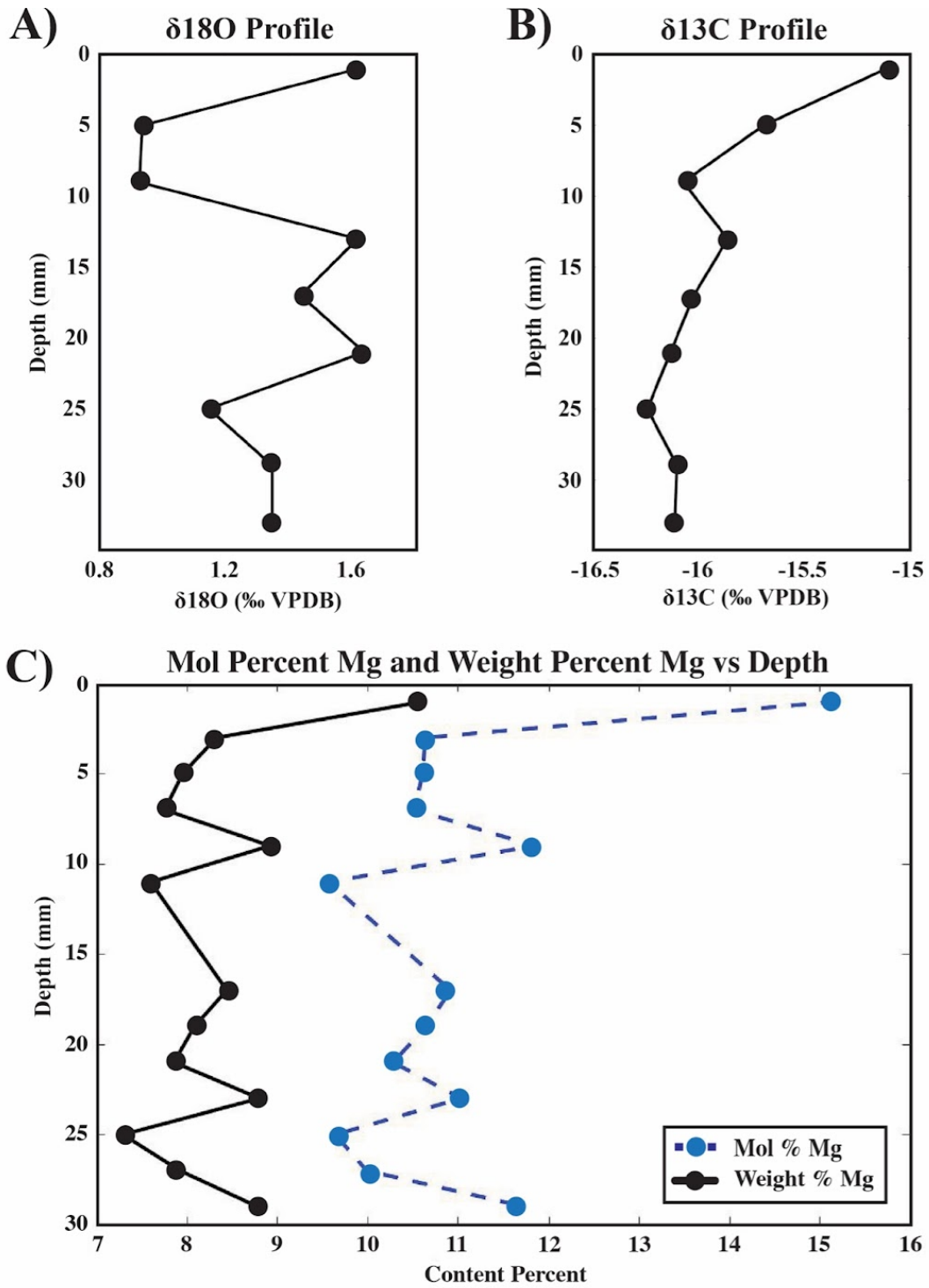


Figure 17: Stable isotope (A) $\delta^{18}\text{O}$ and (B) $\delta^{13}\text{C}$ profiles of calcite bed, and (C) EPMA (Mol% Mg and Weight% Mg) of CL22-01 calcite bed as a function of depth.

Sample ID	Amount (ug)	Nitrogen (vs Air)		Carbon (vs PDB)	
		$\delta^{15}\text{N}$	Wt.% N	$\delta^{13}\text{C}$	Wt.% C
CL22-03 211-212 cm	21636	8.74	0.17	-20.73	1.92
CL22-03 219-220 cm	60869	7.38	0.02	-21.91	0.22
CL22-03 220-221 cm	61610	8.56	0.02	-21.49	0.2
CL22-03 224-225 cm	31420	7.81	0.04	-21.15	0.41
CL22-03 229-230 cm	33201	7.51	0.05	-20.73	0.47
CL22-03 230-231 cm	57495	7.78	0.04	-20.18	0.4
CL22-03 234-235 cm	46451	7.69	0.03	-20.54	0.3
CL22-03 239-240 cm	50078	7.46	0.03	-20.66	0.27
CL22-03 240-241 cm	88395	7.63	0.02	-18.73	0.2
CL22-03 245-246 cm	94334	6.04	0.01	-17.94	0.12
CL22-03 250-251 cm	105259	4.36	0.01	-20.51	0.1
CL22-03 251-252 cm	97724	4.69	0.01	-21.86	0.07
CL22-03 257-258 cm	96106	7.9	0.01	-22.36	0.14
CL22-03 263-264 cm	21132	7.89	0.08	-21.69	0.74
CL22-03 273-274 cm	57554	7.57	0.11	-21.19	1

Table 4: Carbon and nitrogen isotope analysis ($\delta^{13}\text{C}$ and $\delta^{15}\text{N}$) and carbon and nitrogen weight percent (wt%) within CL22-03. Samples taken between the bioturbated CS facies and CS-E facies. Samples were analyzed on bulk samples following the removal of carbonate with HCl pretreatment.

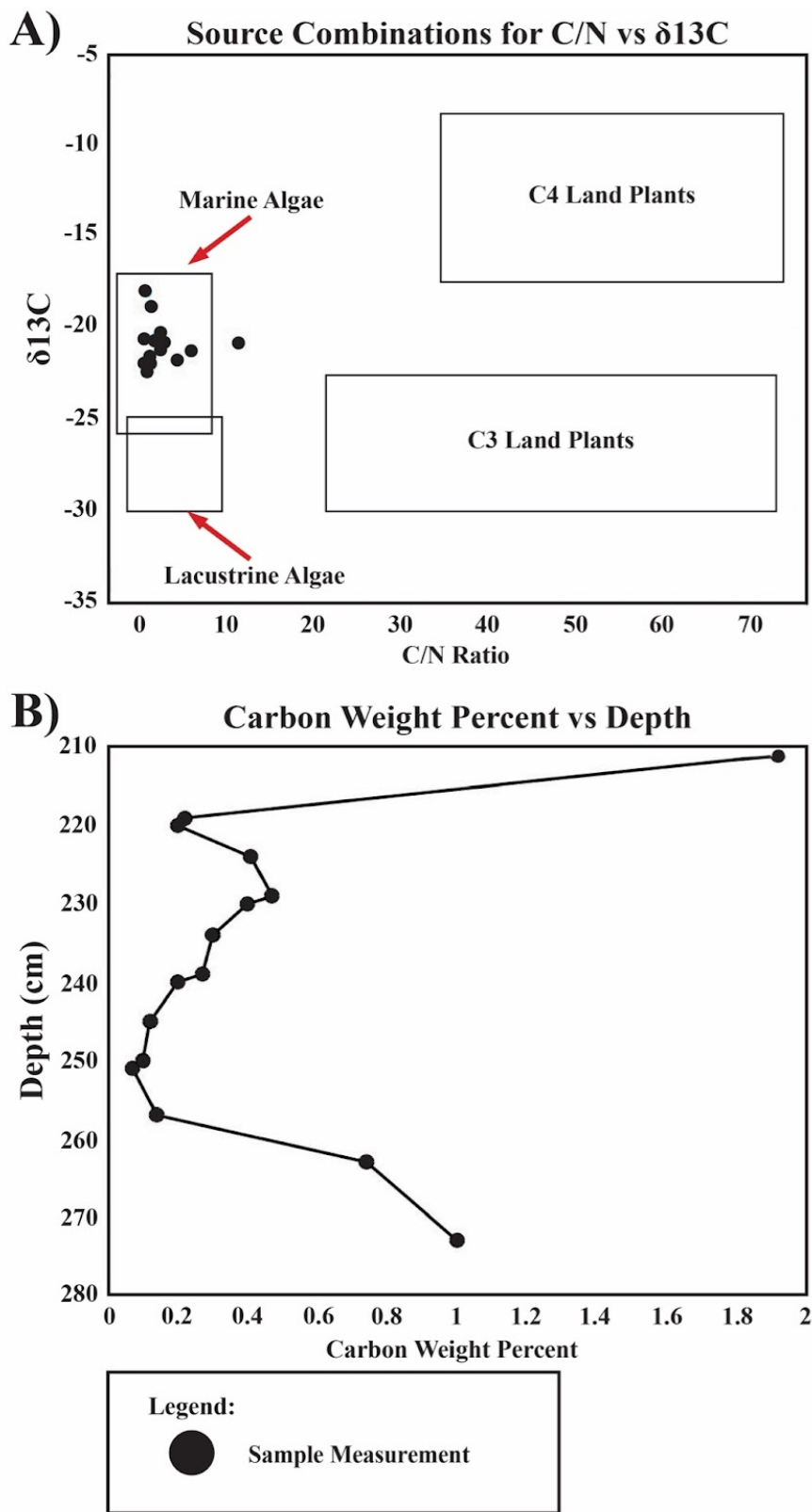


Figure 18: (A) Atomic C/N ratios vs $\delta^{13}C$ and (B) carbon weight percent vs depth across GS facies.

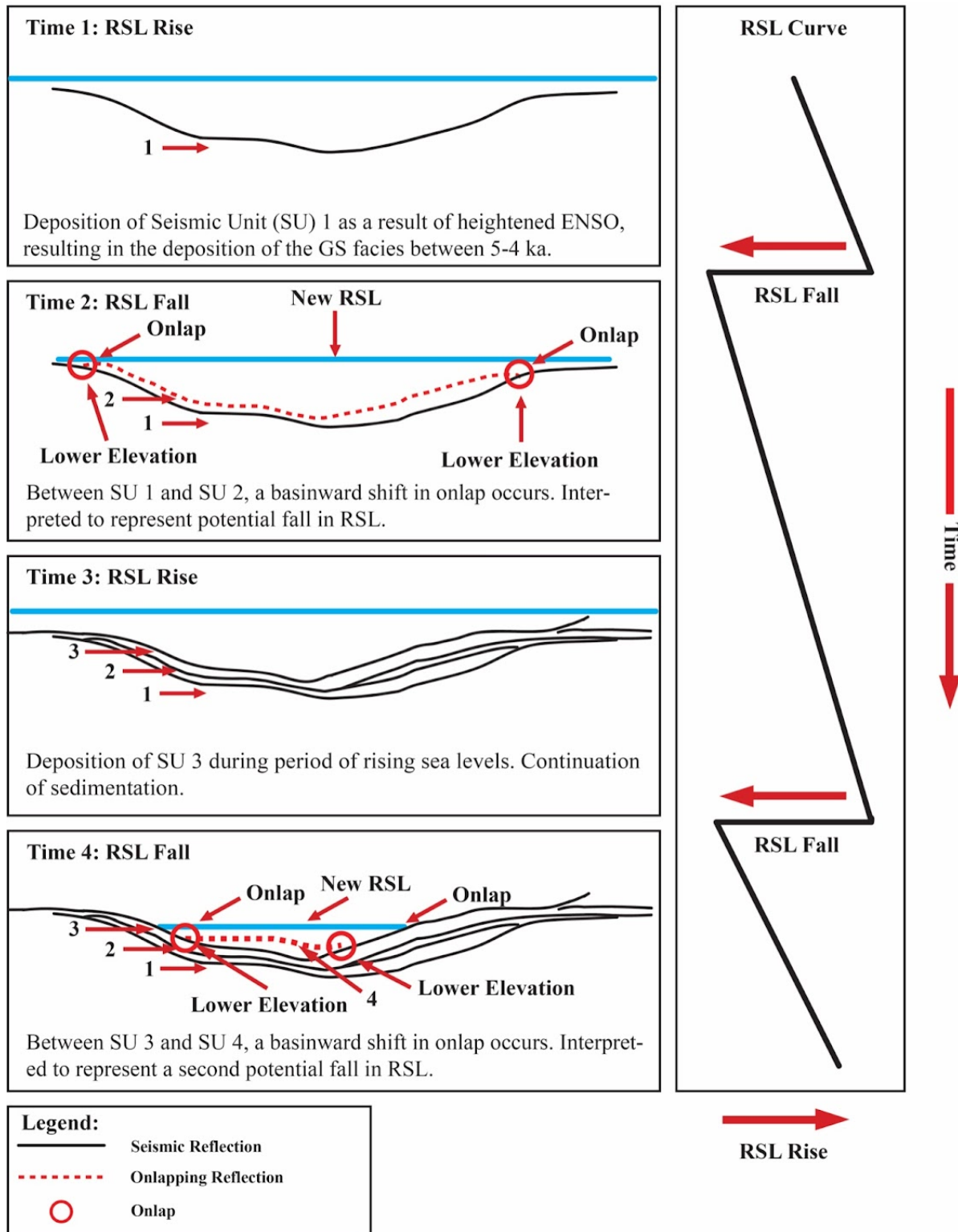


Figure 19: Reconstruction of onlapping geometry at mouth of Campus Lagoon in response to possible coseismic uplift. Two instances of possible RSL fall based on studies by Vail et al. (1977).

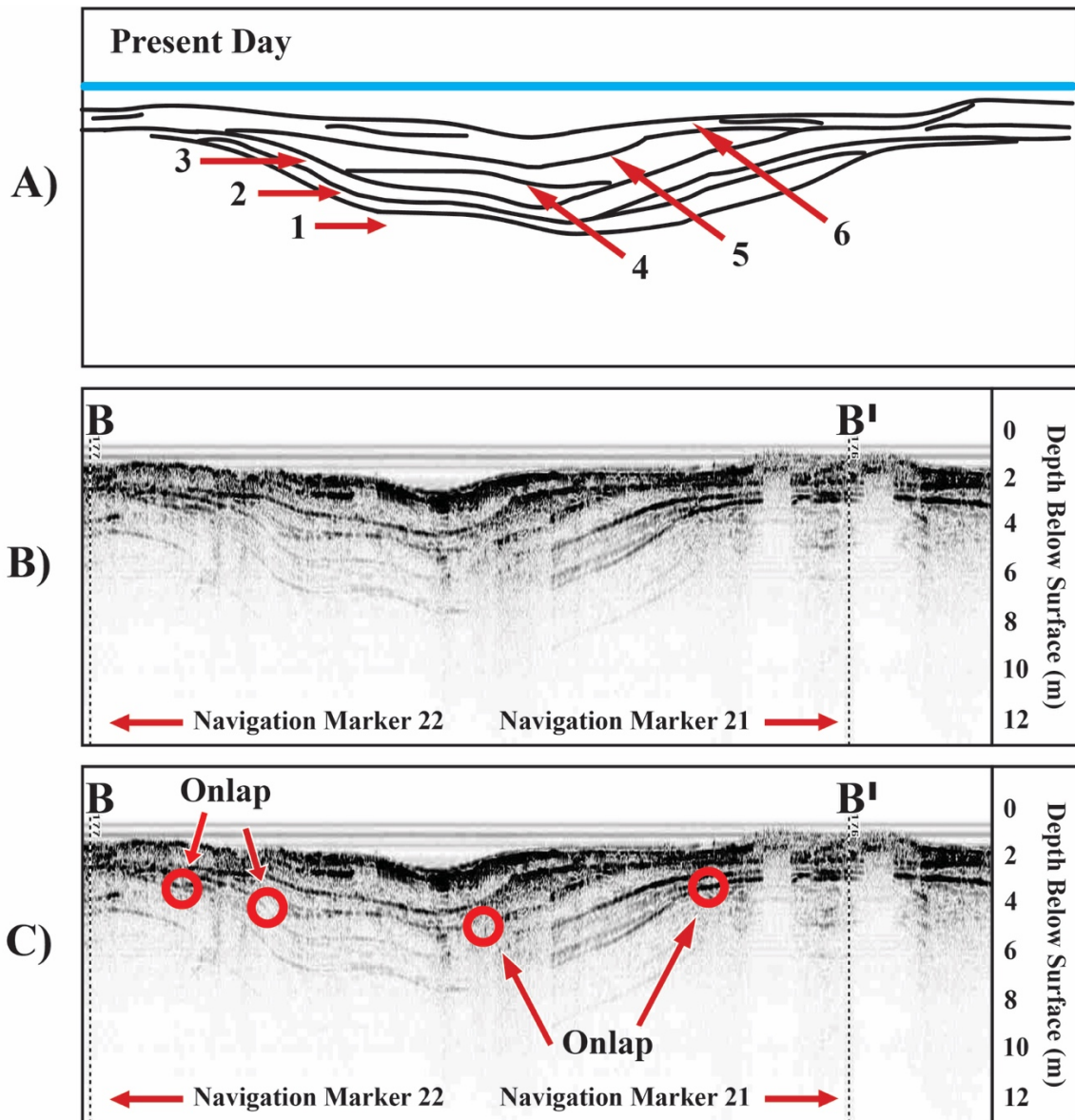


Figure 20: (A) Continuation of onlap reconstruction from mouth of Campus Lagoon where RSL rise is indicated by deposition of SU 5 through SU 6, (B) uninterpreted seismic profile, and (C) seismic profile highlights the regions of onlap.

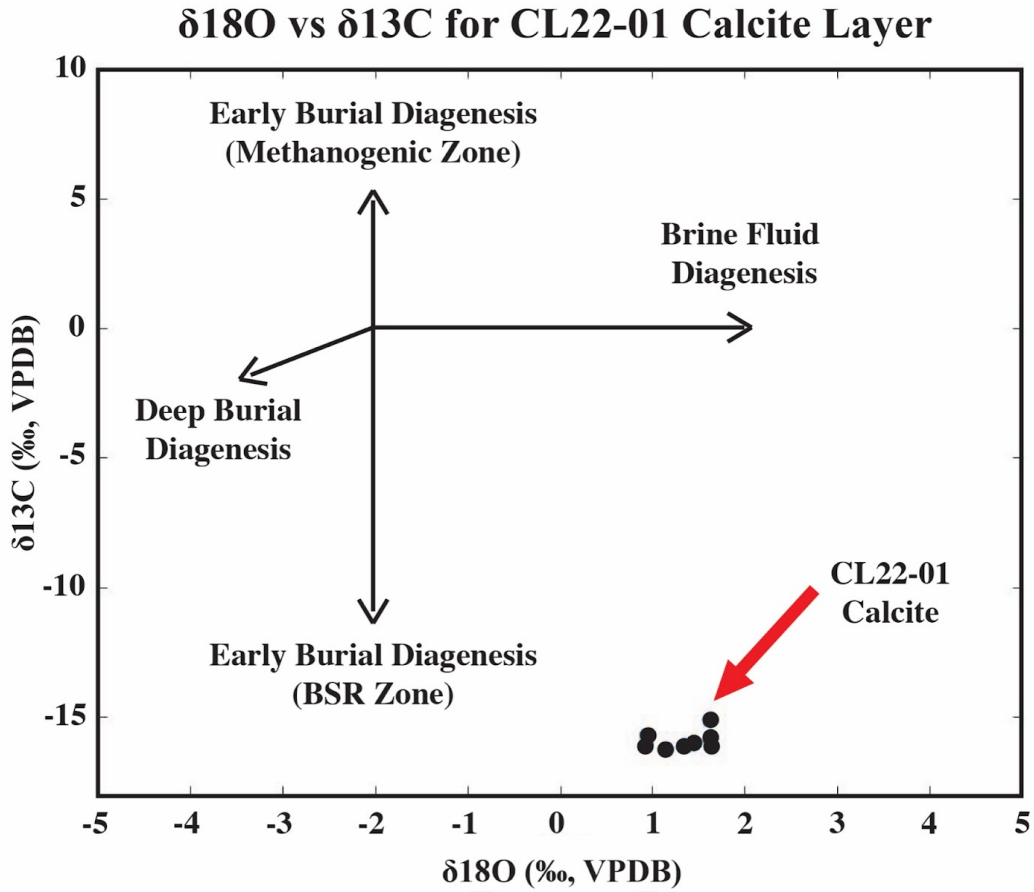


Figure 21: Plot showing $\delta^{18}\text{O}$ and $\delta^{13}\text{C}$ isotopic signatures of calcite bed from CL22-01. General trends of diagenesis adapted from Irwin and Curtis (1977), Machel (2004), Swart (2015), and Reis et al. (2019). Calcite formation within CL22-01 possibly caused by a combination of factors, such as brine fluid diagenesis and / or early burial diagenesis associated with the BSR Zone.

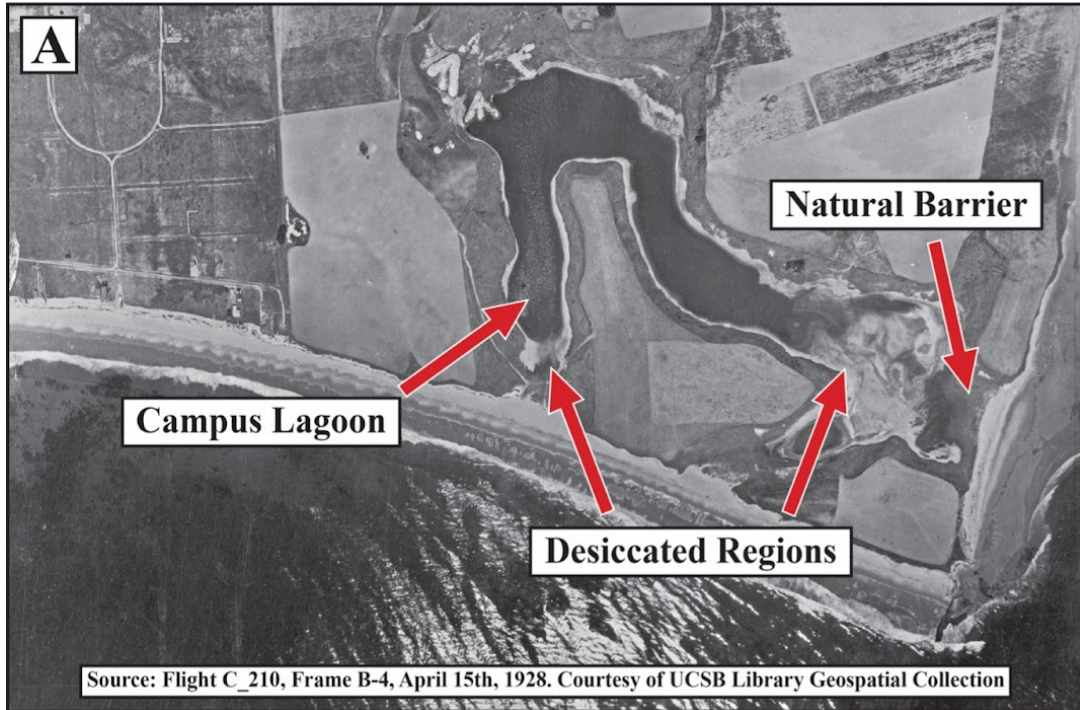


Figure 22: Aerial photograph of Campus Lagoon region from (A) 1928 and (B) 2008. In 1942, a revetment consisting of beach sand and cobbles was constructed across the opening of the southeast region of the lagoon, preventing tidal influence (Jones & Stokes Associates, Inc., 1999). Water levels within the lagoon are sustained by the discharge of seawater by operations related to UCSB Marine Science research (Jones & Stokes Associates, Inc., 1999).

9. APPENDIX

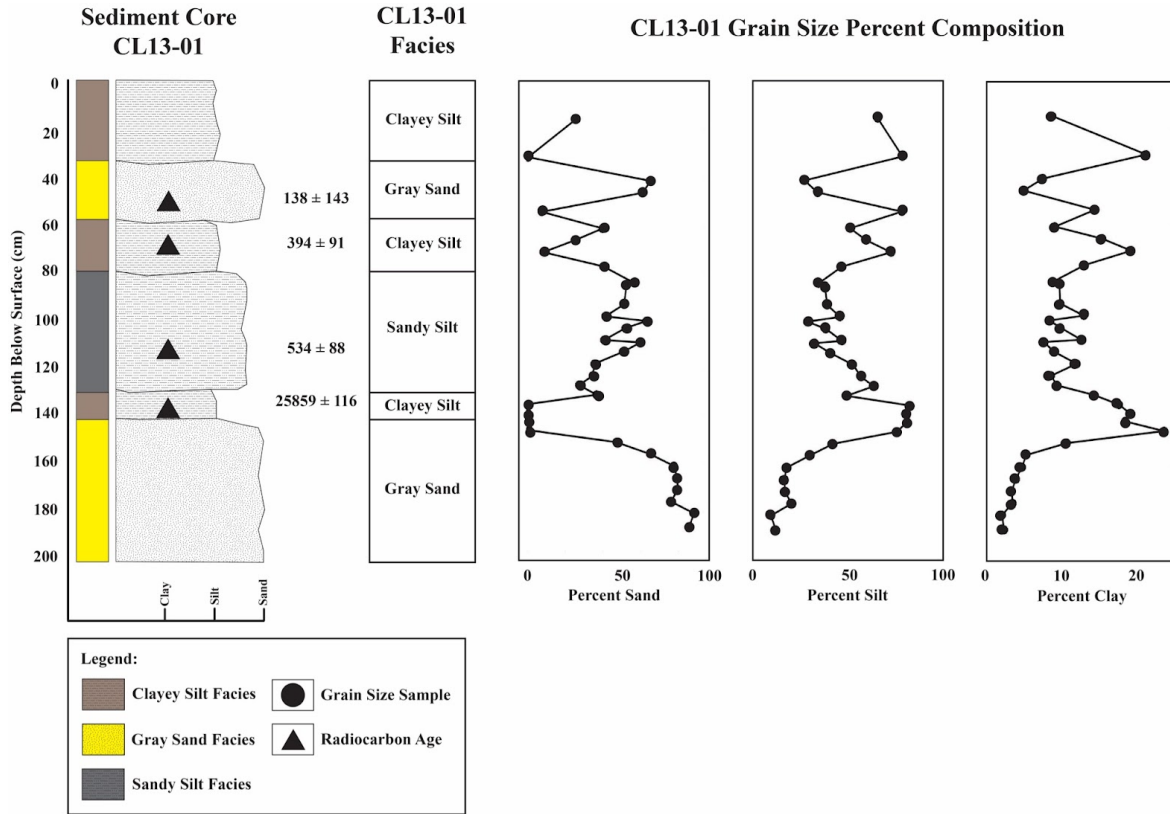


Figure A1: Sediment core CL13-01 and grain size percent composition.

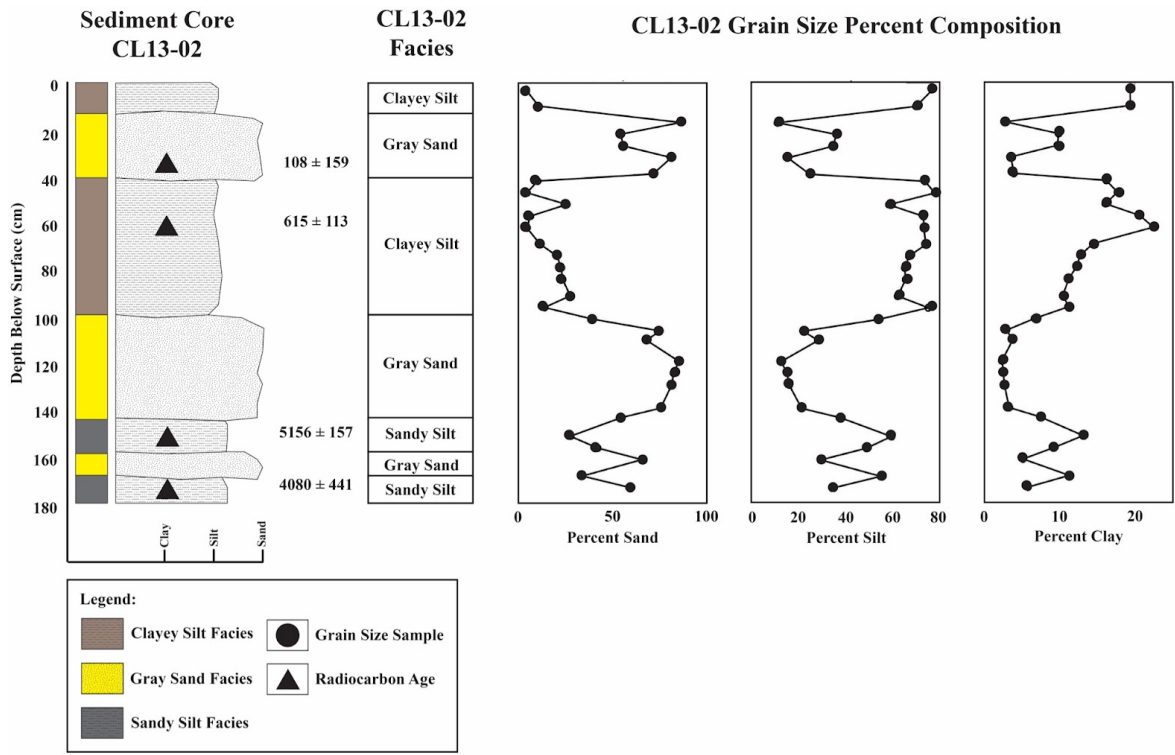


Figure A2: Sediment core CL13-02 and grain size percent composition.

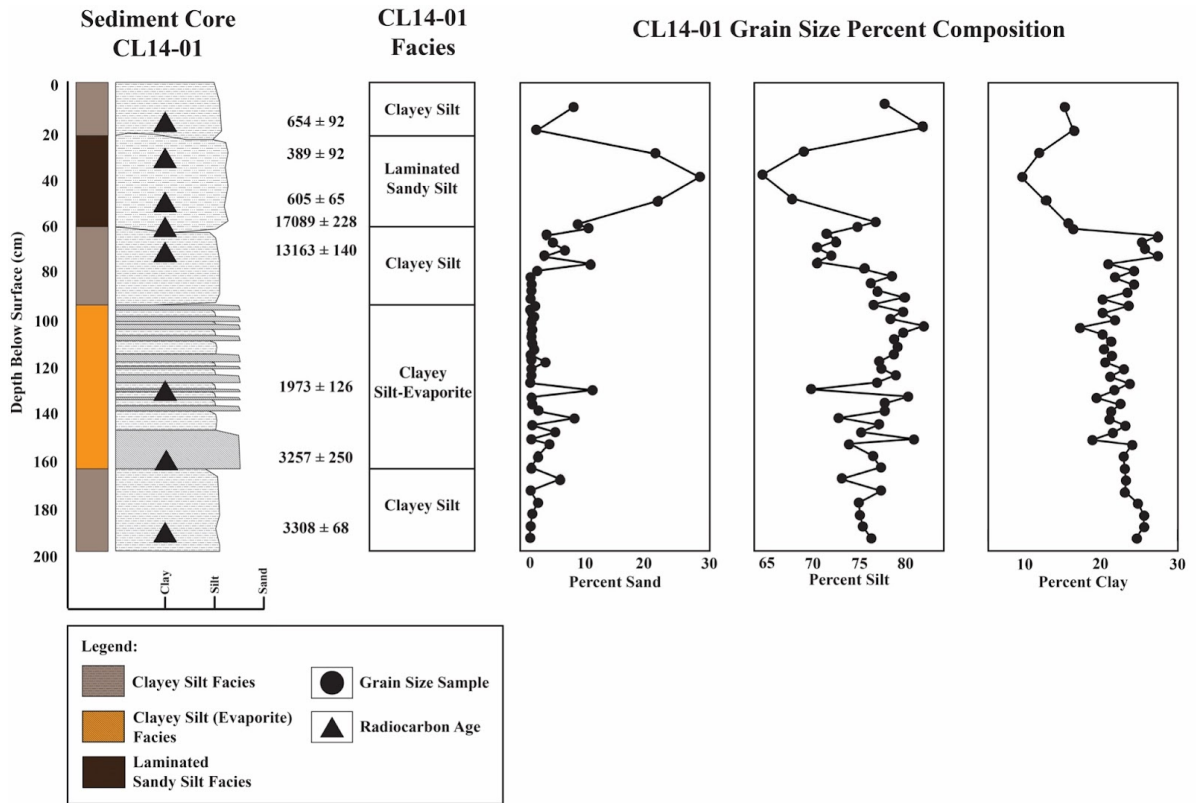


Figure A3: Sediment core CL14-01 and grain size percent composition.

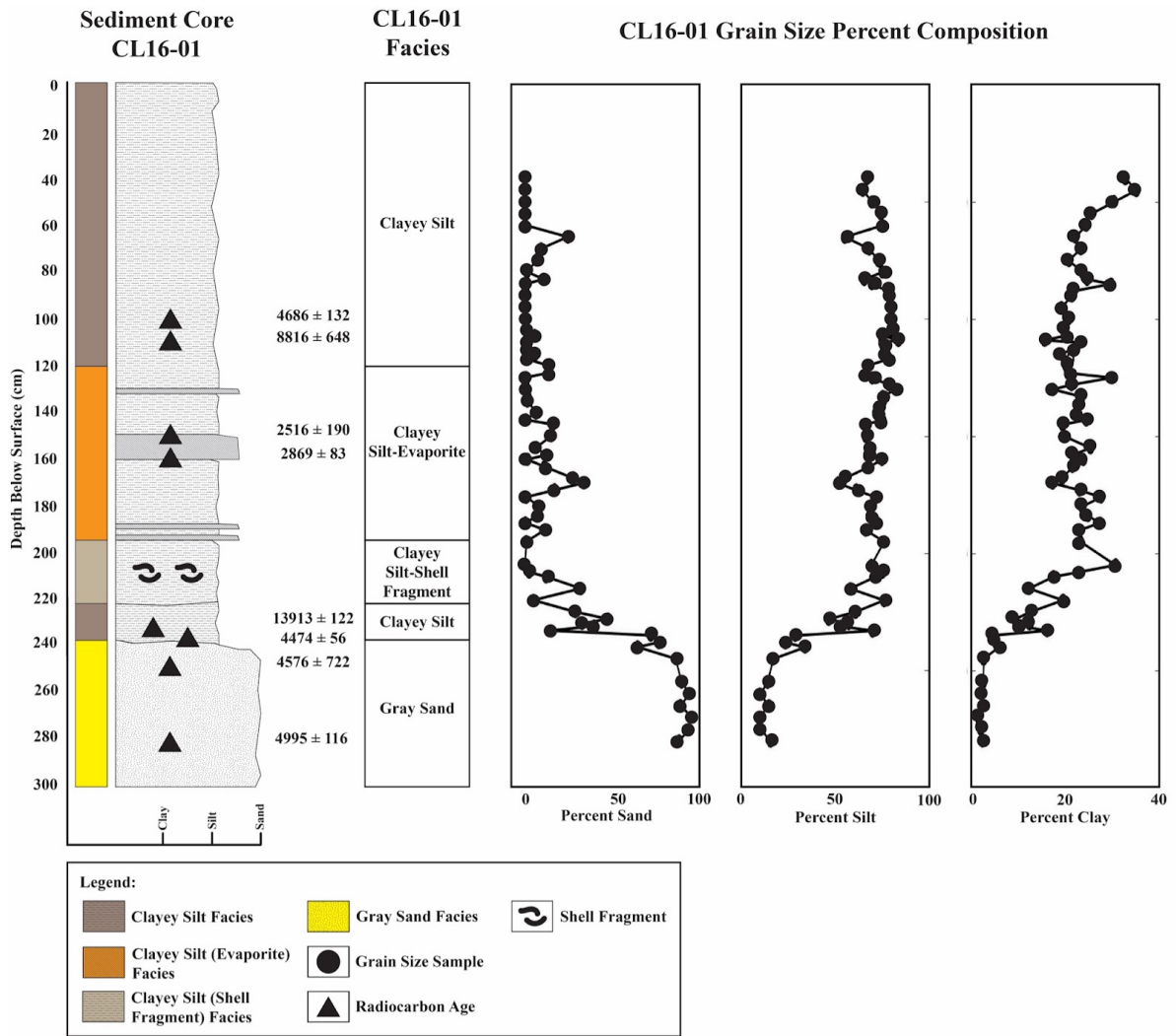


Figure A4: Sediment core CL16-01 and grain size percent composition.

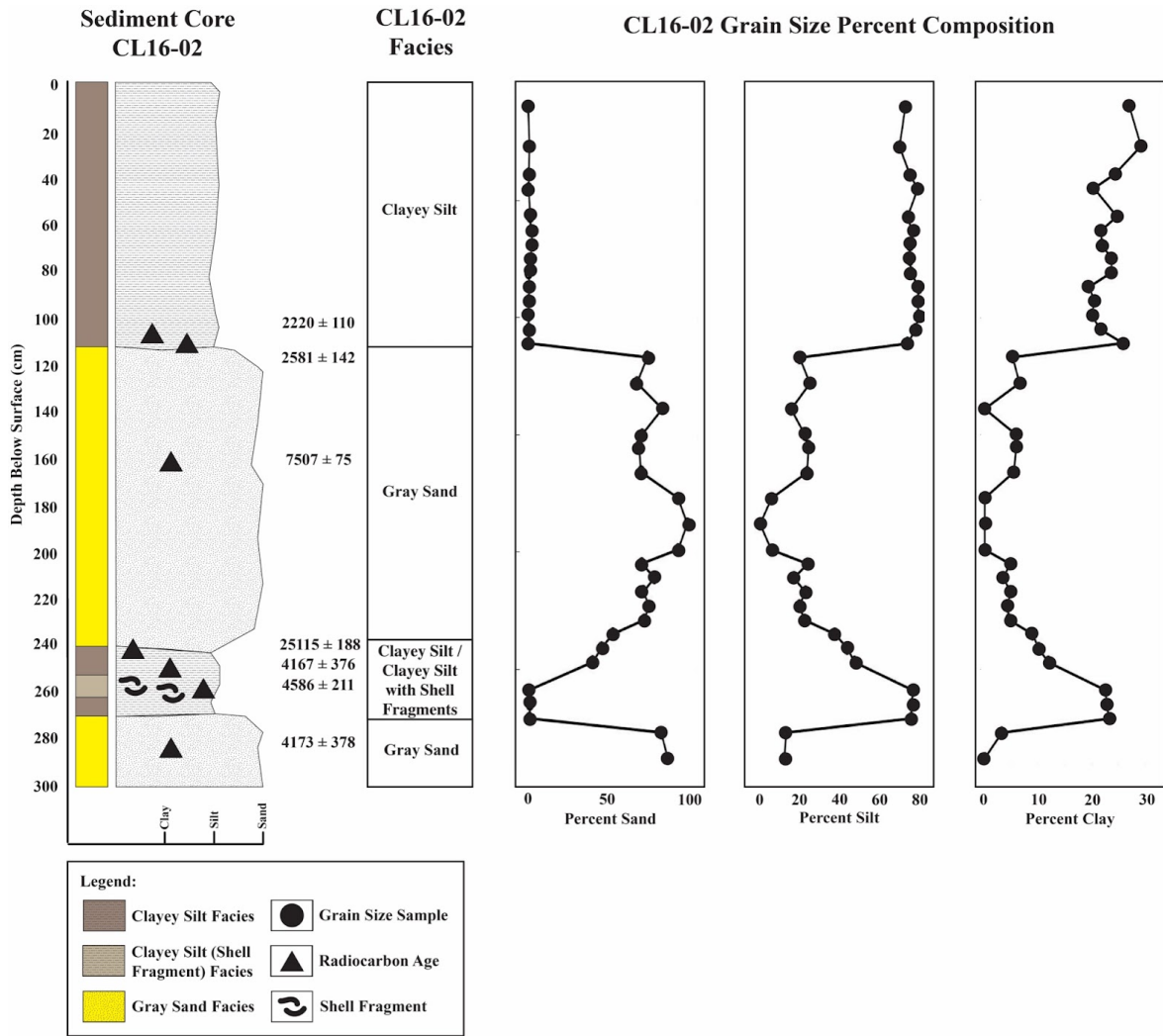


Figure A5: Sediment core CL16-02 and grain size percent composition.

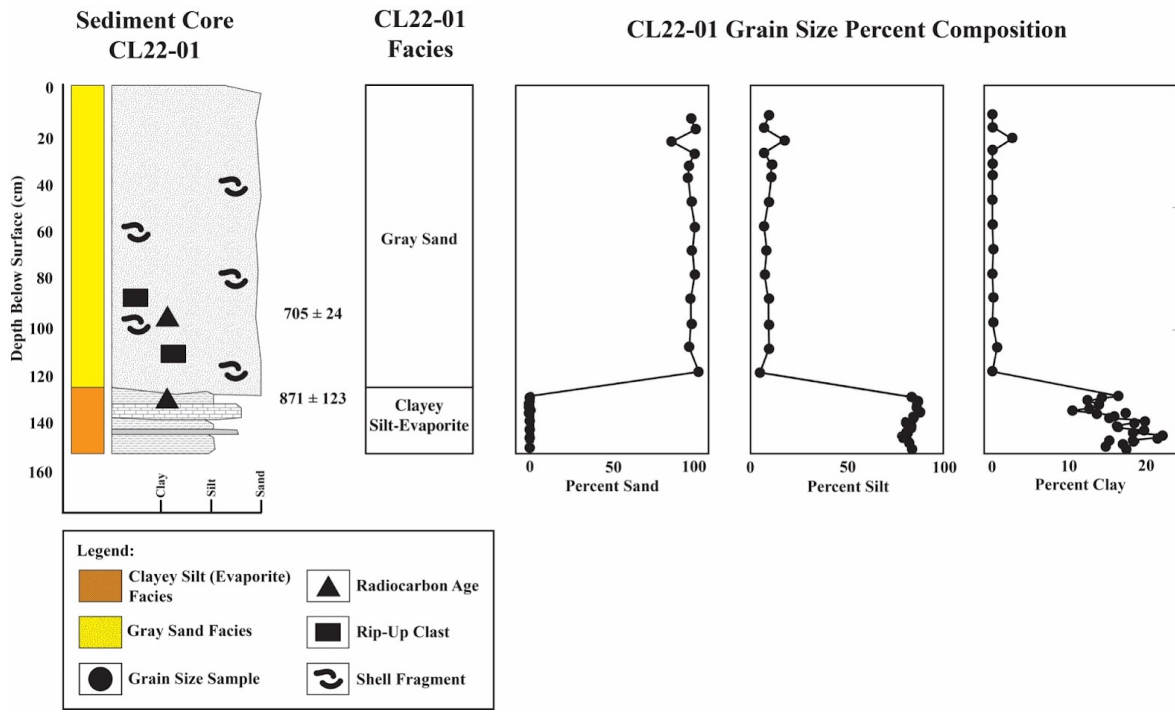


Figure A6: Sediment core CL22-01 and grain size percent composition.

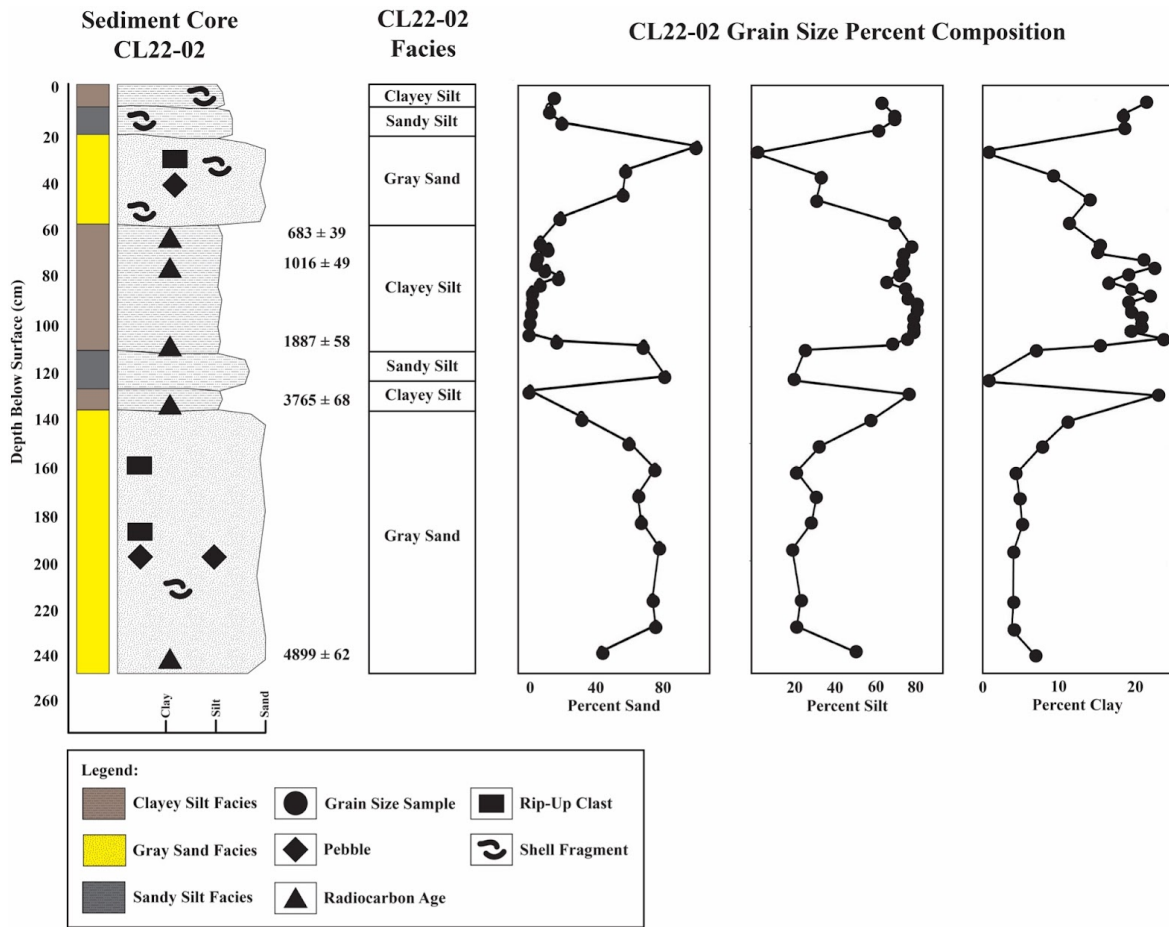


Figure A7: Sediment core CL22-02 and grain size percent composition.

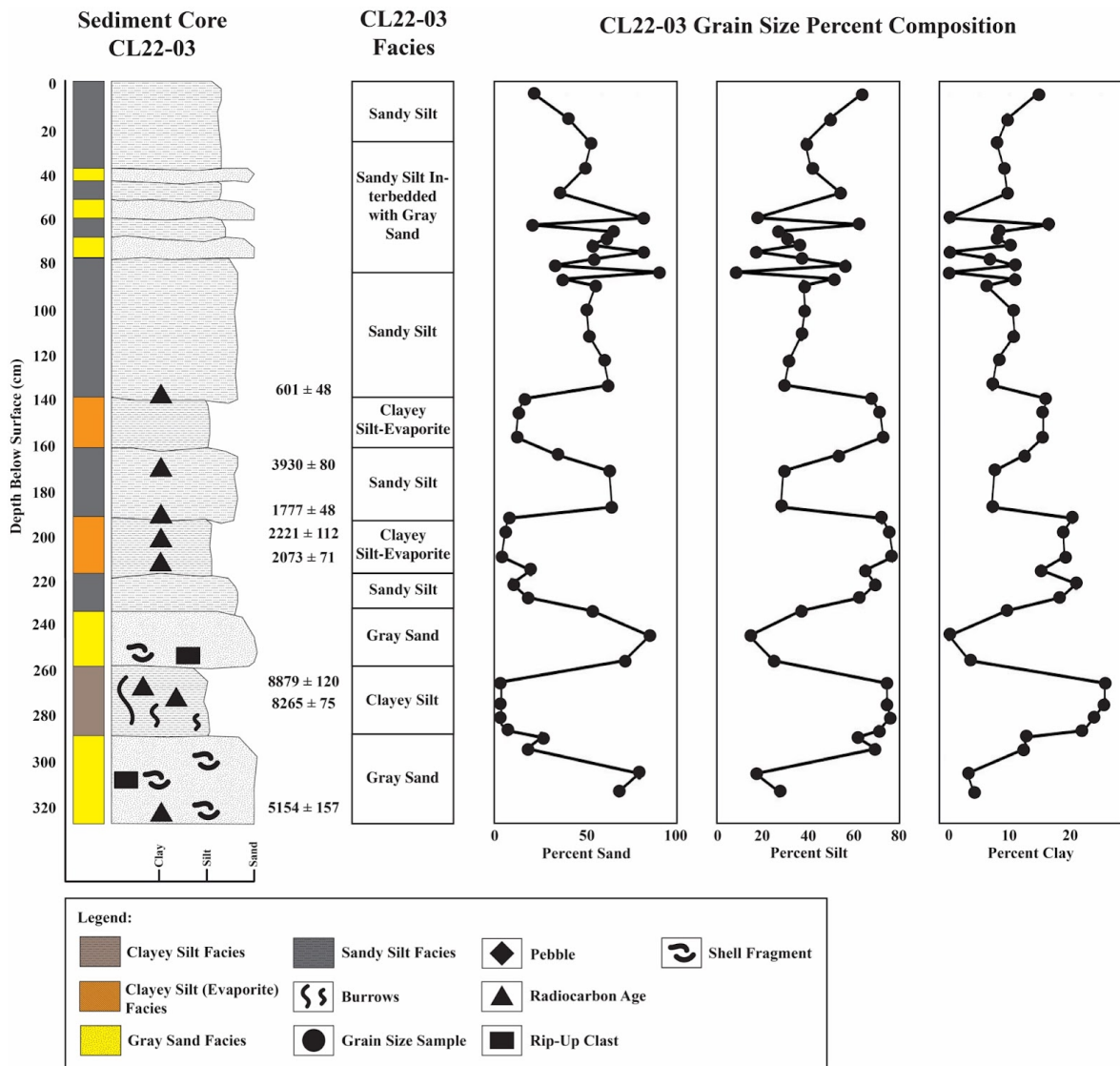


Figure A8: Sediment core CL22-03 and grain size percent composition.

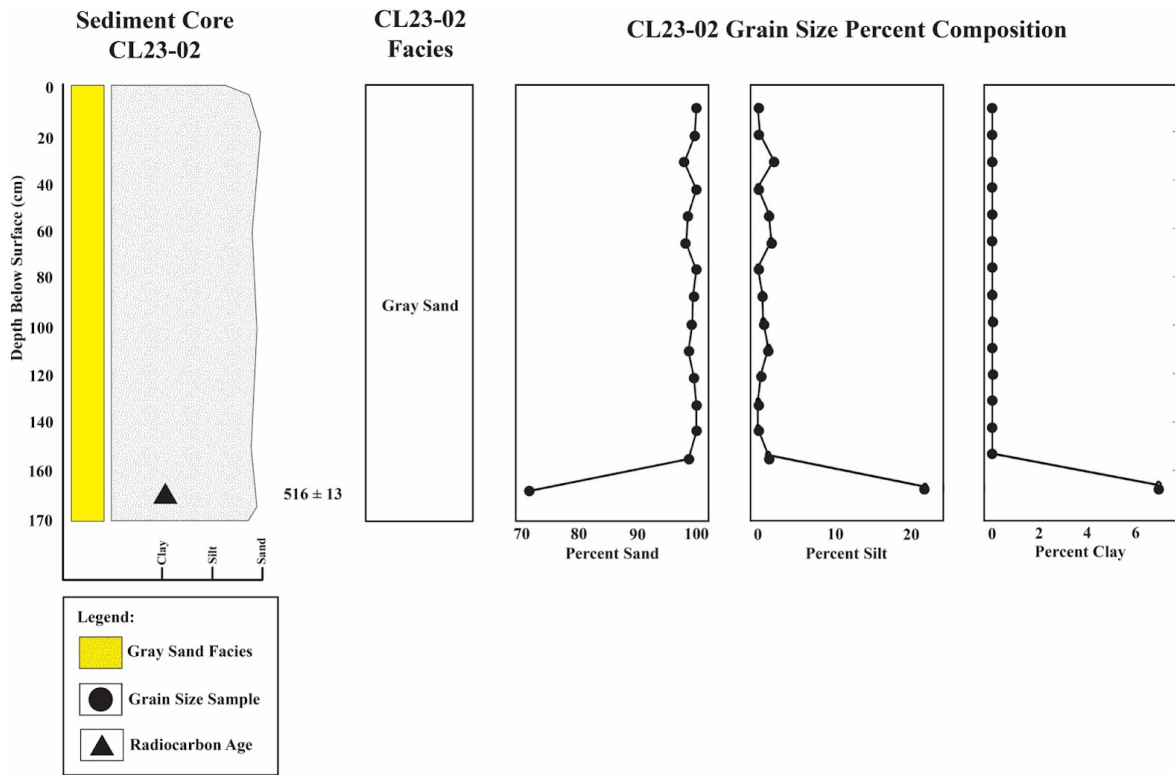


Figure A9: Sediment core CL23-02 and grain size percent composition.

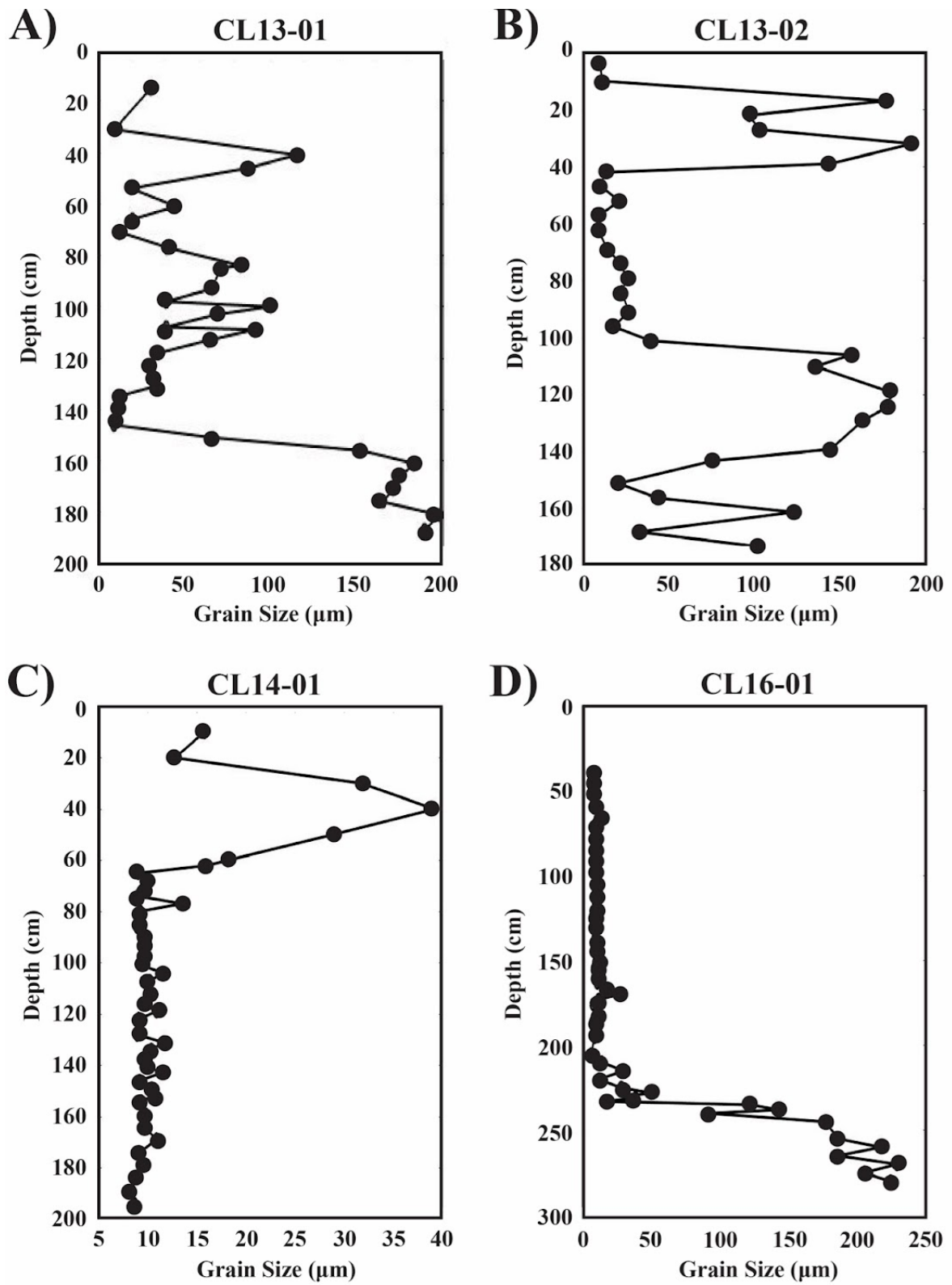


Figure A10: Median grain size vs depth of sediment cores (A) CL13-01, (B) CL13-02, (C) CL14-01, and (D) CL16-01 from Campus Lagoon.

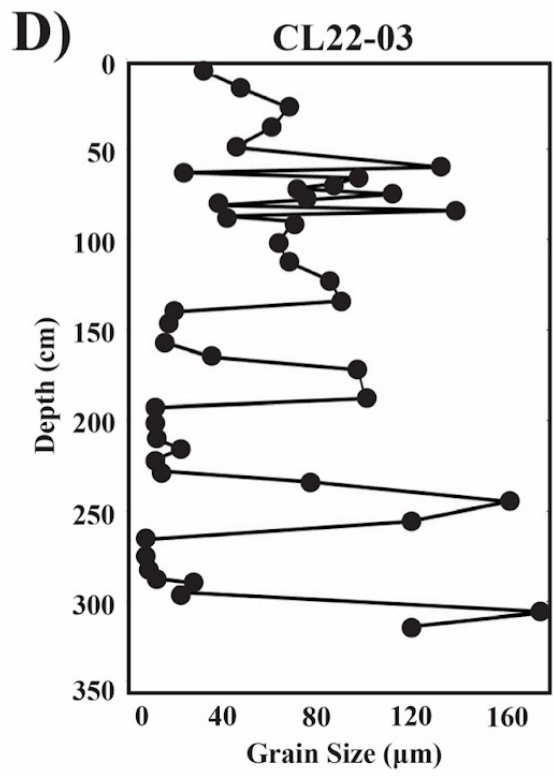
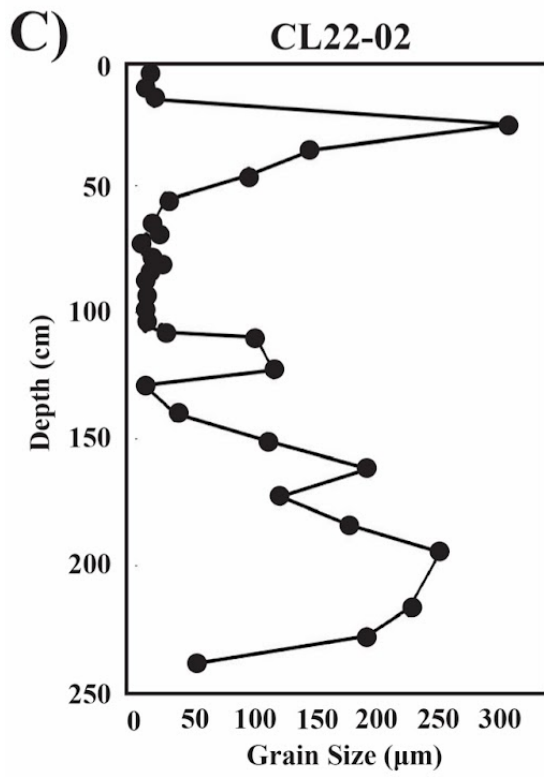
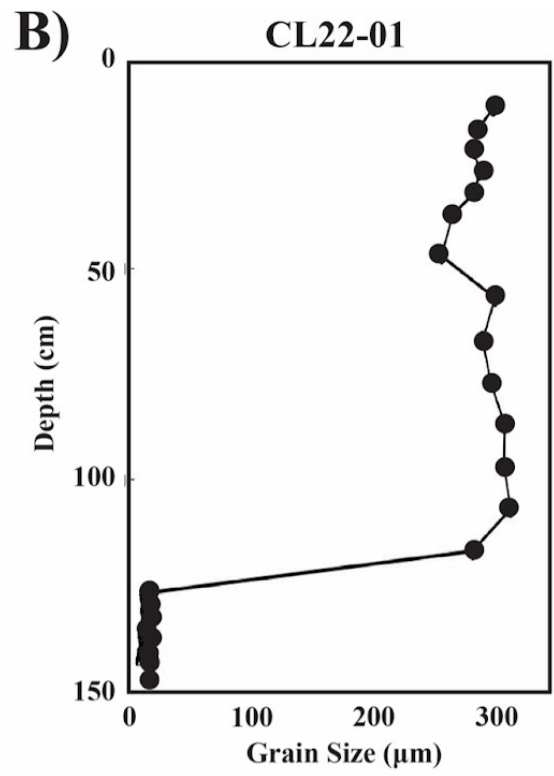
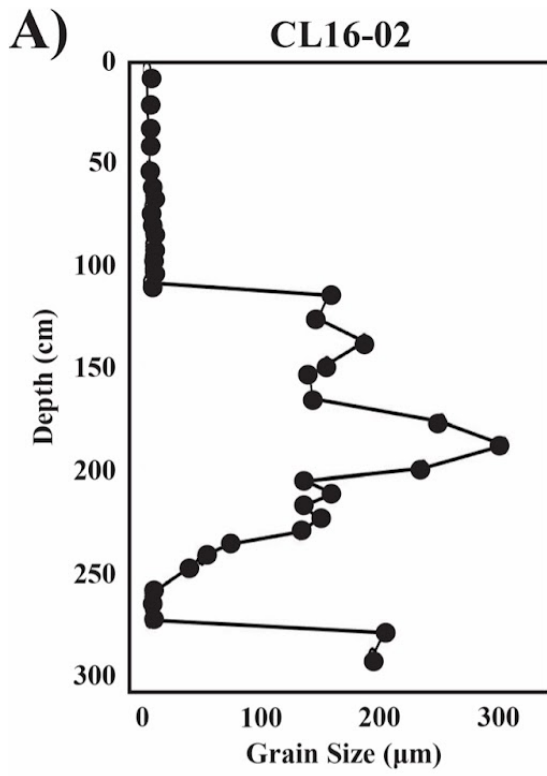


Figure A11: Median grain size vs depth of sediment cores (A) CL16-02, (B) CL22-01, (C) CL22-02, and (D) CL22-03 from Campus Lagoon.

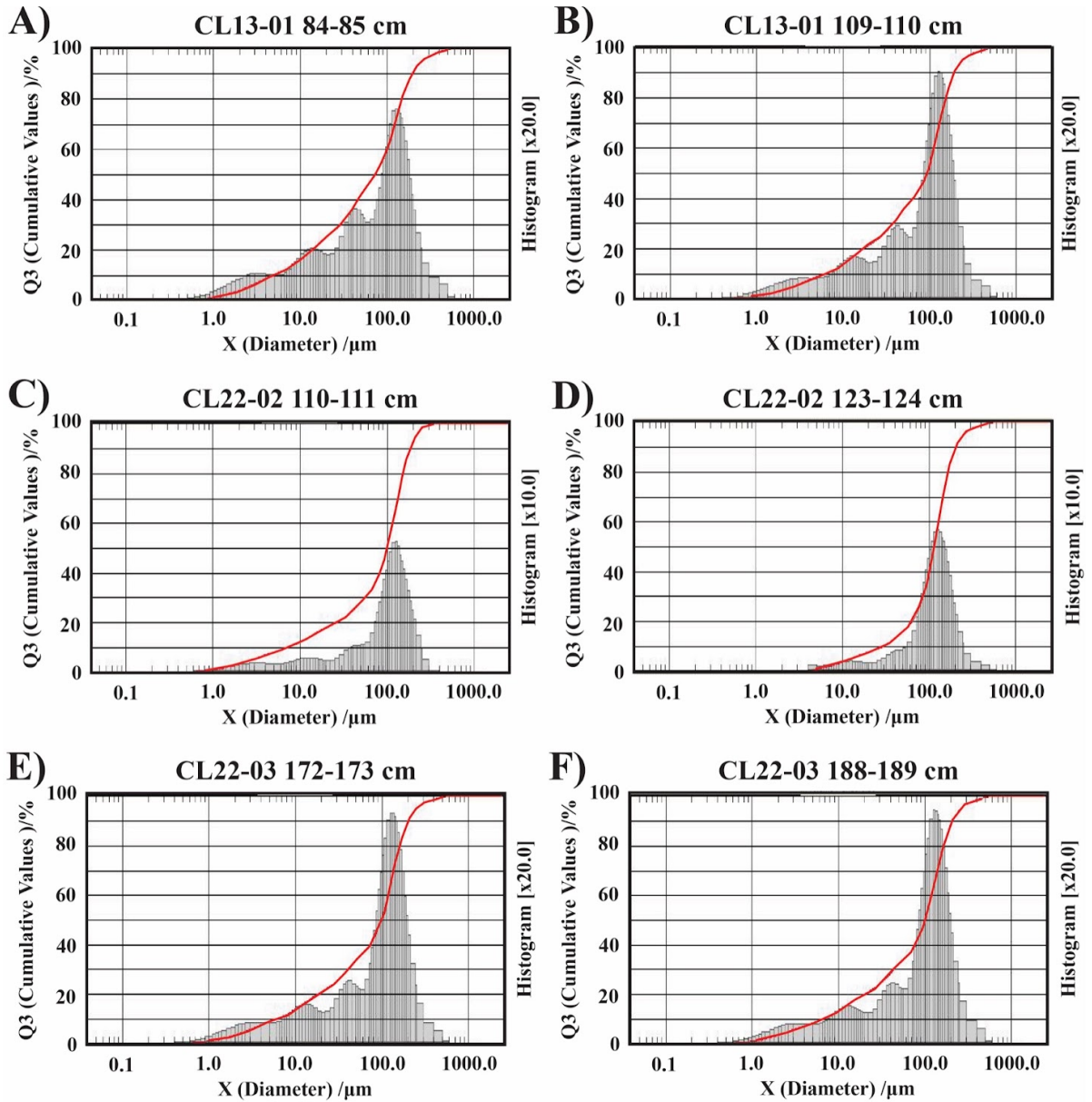


Figure A12: Grain size frequency curves for SASL facies (interbedded within CS-E / CS facies) exhibit a fine skew.